Kent Academic Repository

Full text document (pdf)

Citation for published version

Mahbas, Ali (2017) Challenges Imposed by User's Mobility in Future HetNet: Offloading and Mobility Management. Doctor of Philosophy (PhD) thesis, University of Kent,.

DOI

Link to record in KAR

http://kar.kent.ac.uk/62522/

Document Version

UNSPECIFIED

Challenges Imposed by User's Mobility in Future HetNet: Offloading and Mobility Management

A Thesis Submitted to The University of Kent

For The Degree of Doctor of Philosophy

In Electronic Engineering

By

ALI MAHBAS

APRIL, 2017

Supervisor

Professor Jiangzhou Wang

"Knowledge is superior to wealth. It guards you whereas you guard wealth ....."

Imam Ali

Dedication

To the cradle of the civilisation, Iraq

To those who firmly confront terrorism on behalf of the world, the Iraqi people

Acknowledgements

Firstly, I would like to thank Prof. Jiangzhou Wang for the motivation and immense knowledge as well as the continuous support of my PhD study and personal development. This thesis could not be achieved without his contributions and guidance.
I would like to thank Dr. Huiling Zhu for the support and the constructive comments to improve my research and the work of this thesis. I would like to thank my colleagues in the school for the support.

I would like to thank the Higher Committee for Education Development in Iraq (HCED) for the financial support.

I would like to thank my wife Katherine for her support and for accepting nothing less than excellence from me. Last but not the least, I would like to thank my family: my parents, sister, brother and son, and friends for supporting me spiritually throughout my studies and my life in general.

List of publications and submissions

1. A. Mahbas, H. Zhu, and J. Wang, "The Effect of Small Cells Overlapping on Mobility Management," *submitted to IEEE Transactions on Wireless Communication*, Apr. 2017

2. A. Mahbas, H. Zhu, and J. Wang, "Trio-Connectivity for Efficient Offloading in Future Cellular Systems," *submitted to IEEE Transactions on Vehicular Technology*, Apr. 2017

3. A. Mahbas, H. Zhu, and J. Wang, "The Role of Inter-Frequency Measurement in Offloading Traffic to Small Cells," *to appear in IEEE 85th Vehicular Technology Conference: VTC2017-Spring*, Jun. 2017

4. A. Mahbas, H. Zhu, and J. Wang, "The Optimum Rate of Inter-Frequency Scan in Inter-Frequency HetNets," *to appear in IEEE International Conference on Communications (ICC'17)*, May 2017

5. A. Mahbas, H. Zhu, and J. Wang, "Unsynchronized Small Cells with a Dynamic TDD System in a Two-Tier HetNet," *IEEE 83rd Vehicular Technology Conference: VTC2016-Spring*, pp. 1 – 6, May 2016

6. A. Mahbas, "Double Spectrum Small Cell (DSSC) for Discovering Inter-Frequency Small Cell in HetNet," *IEEE International Conference on Communications (ICC'15)*, pp. 3454–3459, Jun. 2015

Abstract

The users' mobility imposes challenges to mobility management and, the offloading process, which hinder the conventional heterogeneous networks (HetNets) in meeting the huge data traffic requirements of the future. In this thesis, a trio-connectivity (TC), which includes a control-plane (C-plane), a user-plane (U-plane) and an indication-plane (I-plane), is proposed to tackle these challenges. Especially, the I-plane is created as an indicator to help the user equipment (UE) identify and discover the small cells in the system prior to offloading her from the overloaded cells e.g. macro cells, to the cells with abundant resources e.g. small cells. In order to show the advantages of the proposed TC structure, a comparison between the TC and the dual-connectivity (DC) is presented in this thesis, in terms of uplink energy efficiency (ULEE) and energy consumption. Furthermore, the complexity of mobility management is addressed in this thesis as the HetNets will have to handle a large number of UEs and their frequent handoffs due to very dense small-footprint small cells. Considering an accurate mobility framework is essential not only to find the potential offloading to the small cells but also to show the mobility impact on the quality of service (QoS). This thesis presents a framework to model and derive the coverage of small cells, the cell sojourn time and the handoff rate in a multi-tier HetNet by taking into account the overlap coverage among the small cells.

The results show the effects of a number of parameters, including the density and the transmit power of the small cells and the power control factor, on the system performance. They also show that the TC can outperform the DC in dense HetNets in terms of energy efficiency and energy consumption.

Contents

List of Figures

List of Tables

Abbreviations

4G ..... Fourth Generation

BS ..... Base Station

CDF ..... Cumulative Distribution Function

CDMA ..... Code Division Multiple Access

CID ..... Cell Identification

cm-Wave .... Centimetre-Wave

C-plane ..... Control-Plane

CRLB ..... Cramer-Rao Lower Bound

D2D ..... Device-to-Device

DAS ..... Distributed Antenna System

dBm ..... Decibel-milliwatts

DL ..... Downlink

DC ..... Dual-Connectivity

eICIC ..... enhanced Inter-Cell Interference Coordination

FPC ..... Frictional Power Control

GHz ..... Giga Hertz

HetNet ..... Heterogeneous Network

i.i.d. ..... Independent and Identically Distributed

IAF ..... Intra-Frequency

IAH ..... Intra-Frequency Handoff

I-plane ..... Indication-Plane

IRF ..... Inter-Frequency

IRH ..... Inter-Frequency Handoff

IRWP ..... Improved Random Waypoint

LOS ..... Line of Sight

LTE ..... Long Term Evolution

MAC ..... Medium Access Control

MCBS ..... Macro Cell Base Station

MIMO ..... Multi-Input Multi-Output

mm-Wave ... Millimetre Wave

MPP ..... Marked Point Process

NLOS ..... Non-Line of Sight

NS-2 ..... Network Simulator-2

OFDMA .... Orthogonal Frequency-Division Multiple Access

PCF ..... Power Control Factor

PDCP ..... Packet Data Convergence Protocol

PDF ..... Probability Density Function

PGFL ..... Probability Generating Functional

PHY ..... Physical

PPP ..... Poison Point Process

QoS ..... Quality of Service

RLC ..... Radio Link Control

RRC ..... Radio Resources Control

RS ..... Reference Signal

RSS ..... Received Signal Strength

RWP ..... Random Waypoint

SCBS ..... Small Cell Base Station

SCD ..... Small Cell Discovery

SINR ..... Signal to Interference plus Noise Ratio

TDD ..... Time Division Duplex

TC ..... Trio-Connectivity

UE ..... User Equipment

UL ..... Uplink

ULEE ..... Uplink Energy Efficiency

U-plane ..... User-Plane

VTC ..... Voronoi Tessellation Cell

List of Symbols

$f_\tau(\tau)$ ..... PDF of the vertical distance τ.

α_k ..... Path-loss exponent of the kth tier.

$\bar{\lambda}_m$ ..... Density of the path points of the mth tier on $\mathcal{P}_0$.

$\bar{\Phi}_m$ ..... Crossed small cells by $\mathcal{U}_0$ process of the mth tier.

$\bar{\rho}_f$ ..... Received power at a reference point from a SCBS transmitting on F_f.

$\bar{C}_{mn}$ ..... Maximum path point inter-distance of any two overlapped small cells.

$\bar{f}(\mathfrak{x}, \mathfrak{y})$ ..... Spatial UE distribution between two waypoints.

$\bar{K}$ ..... Number of small cell tiers in the network.

$\bar{N}_0$ ..... Number of path points on $\mathcal{P}_0$.

$\bar{O}$ ..... Point where $\mathcal{P}_0$ receives the same power from two overlapped small cells.

$\bar{r}_f$ ..... Distance between a SCBS transmitting on F_f and a reference point.

$\bar{y}$ ..... Path points of one-tier small cell network on $\mathcal{P}_0$.

$\bar{z}$ ..... Path points of multi-tier small cell network on $\mathcal{P}_0$.

$\chi_{n \mapsto m}$ ..... Footage of a cell of the mth tier served by another of nth tier.

ϵ ..... UL power control factor.

$\Gamma(.)$ ..... Gamma function.

$\hat{q}_j$ ..... Distance between the jth interfering UE and its serving cell.

$\hat{t}_p$ ..... Optimum value of t_p.

ι ..... Threshold of the UL achievable data rate.

λ_k ..... BS density of the kth tier.

λ_u ..... UE density.

λ_w ..... Density of the waypoints.

$\mathbb{E}(.)$ ..... Expectation.

$\mathbb{P}(A \mid B)$ ..... A condition on B.

$\mathbb{P}(.)$ ..... Probability.

$\mathbb{P}_{\mathcal{S},m}$ ..... Probability of $\mathcal{U}_0$ at W_1 being served by the small cell of the mth tier.

$\mathbb{P}_{OL,mn}$ ..... Probability of a cell of the mth tier overlapping with another cell on $\mathcal{P}_0$.

$\mathbb{P}_m$ ..... Probability of any small cell of the mth tier being crossed by $\mathcal{U}_0$.

$\mathbb{R}^\delta$ ..... δ-dimensional Euclidean space.

$\mathbf{1}(.)$ ..... Indication function.

$\mathcal{A}_k$ ..... Probability of $\mathcal{U}_0$ associated to the kth tier.

$\mathcal{A}_{\bar{K}}$ ..... Probability of $\mathcal{U}_0$ associated to the small cells.

$\mathcal{F}$ ..... Number of high frequency channels deployed in the system.

$\mathcal{H}_{IA}$ ..... IAH rate.

$\mathcal{H}_{IR}$ ..... IRH rate.

$\mathcal{H}_T$ ..... Total handoff rate.

$\mathcal{L}_{I_{k,\uparrow}}(.)$ ..... Laplace transform of the cumulative UL interference from the kth tier.

$\mathcal{D}_{SC}$ ..... Expected distance to the nearest small cell's footage.

$\mathcal{P}_0$ ..... Reference UE's path.

$\mathcal{R}_{k,\uparrow}$ ..... UL average ergodic rate when associated to the kth tier.

$\mathcal{R}_{T,\uparrow}$ ..... Total UL average ergodic rate.

$\mathcal{ST}_{MC}$ ..... Macro cell sojourn time.

$\mathcal{ST}_{SCL}$ ..... Small cell sojourn time when λ_w is large.

$\mathcal{ST}_{SCS}$ ..... Small cell sojourn time when $S > 0$ and λ_w is small.

$\mathcal{ST}^0_{SCS}$ ..... Small cell sojourn time when $S = 0$ and λ_w is small.

$\mathcal{ST}^0_{SCS,m}$ ..... Small cell sojourn time of the mth tier when $S = 0$ and λ_w is small.

$\mathcal{ST}^s_{SCS,m}$ ..... Small cell sojourn time of the mth tier when $S > 0$ and λ_w is small.

$\mathcal{T}_{miss}$ ..... Total time $\mathcal{U}_0$ misses from the potential offloading time.

$\mathcal{T}_{t,l}$ ..... The lth transition time.

$\mathcal{T}_0$ ..... Total time $\mathcal{U}_0$ spends in small cells coverage.

$\mathcal{T}_T$ ..... Total time during one movement.

$\mathcal{U}_0$ ..... Reference UE.

$\mathfrak{C}_{mn}$ ..... One overlap coverage between small cells of mth and nth tiers on $\mathcal{P}_0$.

$\mathfrak{r}_{m,0}$ ..... Distance to the nearest small cell of the mth tier.

$\mathscr{A}_m$ ..... Area where the small cells of the mth tier located and crossed by $\mathcal{U}_0$.

$\mathscr{A}_{sys}$ ..... System area.

$\mathscr{L}_f$ ..... Path-loss at 1 metre of the fth frequency.

ω ..... Velocity of the wave.

$\| . \|$ ..... Euclidean distance.

Φ_k ..... PPP process of the kth tier.

Φ_u ..... PPP process of the UEs.

Φ_w ..... PPP process of the waypoints.

ψ ..... Total footage of any small cell served by other small cells.

$\Psi_{m,i}$ ..... Actual one side coverage of the ith small cell of the mth on $\mathcal{P}_0$.

$\rho_{m,0}$ ..... Received power from the nearest small cell of the mth tier.

$\rho_{m,j}$ ..... Received power from the jth small cell of the mth tier.

ρ_{min} ..... Minimum received power from any small cell.

σ^2 ..... Additive noise power.

$\tau_{m,i}$ ..... Closest distance between $\mathcal{P}_0$ and the ith small cell of the mth tier.

Υ_k ..... Time fraction $\mathcal{U}_0$ is associated to the kth tier.

$\varkappa$ ..... UL energy efficiency.

Ξ_1 ..... Group of small cells $\mathcal{U}_0$ travels at least $t_p + t_{min}$ in their coverages.

Ξ_2 ..... Group of small cells $\mathcal{U}_0$ travels between t_{pm} and t_{min} in their coverages.

Ξ_3 ..... Group of small cells $\mathcal{U}_0$ travels less than t_{min} in their coverages.

$B(.)$ ..... Beta function.

$C_{m,i}$ ..... Coverage of the ith small cell from the mth tier on $\mathcal{P}_0$.

C_{min} ..... Maximum coverage of each small cell of Ξ_3 on $\mathcal{P}_0$.

C_{mp} ..... Minimum coverage of each small cell of Ξ_1 on $\mathcal{P}_0$.

C_{OL} ..... Total overlap coverage on $\mathcal{P}_0$.

C_T ..... Summation of each small cell coverage on $\mathcal{P}_0$.

$D_{m,j}$ ..... Vertical distance between $\mathcal{P}_0$ and the jth small cell of the mth tier.

E_{DC} ..... Total SCD energy consumption in the DC.

$E_{DCU,i}$ ..... Total SCD energy consumption at the ith UE in the DC.

E_k ..... Energy consumption for UL transmission when associated to the kth tier.

E_T ..... Total energy consumption.

E_{TC} ..... Total SCD energy consumption in the TC.

$E_{TCSC,j}$ ..... Total SCD energy consumption at the jth small cell in the TC.

$E_{TCU,i}$ ..... Total SCD energy consumption at the ith UE in the TC.

E_{UL} ..... Energy consumption for UL transmission.

E_s ..... Energy required for one IRF scan.

$f_{(\|\bar{y}_i - W_0\|)}(\mathrm{d})$ .. PDF of the distance between W_0 and the ith path point.

$f_{\hat{q}}(\hat{q})$ ..... PDF of the distance between an interfering UE and its serving cell.

$f_C(c)$ ..... PDF of the small cell coverage on $\mathcal{P}_0$.

$f(\mathfrak{r}, \theta)$ ..... Spatial UE distribution between two waypoints when $S = 0$.

$f_{t_1}(t)$ ..... PDF of the time missed from each small cell of Ξ_1.

$f_{t_2}(t)$ ..... PDF of the time missed from each small cell of Ξ_2.

$f_{x_k}(x)$ ..... PDF of the distance between $\mathcal{U}_0$ and its serving cell of the kth tier.

g_0 ..... Channel gain of the desired link.

h_j ..... Channel gain of the jth interfering link.

$I_{k,\uparrow}$ ..... Total UL interference power when $\mathcal{U}_0$ is associated to the kth tier.

K ..... Number of tiers in the network.

N_{HF} ..... Total number of handoffs during one movement.

$N_{OL,max}$ ..... Maximum number of overlaps on $\mathcal{P}_0$.

N_{OL} ..... Number of overlaps on $\mathcal{P}_0$.

N_0 ..... Number of small cells crossed by $\mathcal{U}_0$.

N_m ..... Total number of small cells of the mth tier in the system.

$p_{f,k,rs}$ ..... RSs transmit power of the kth tier on the $f$the frequency.

$p_{k,\uparrow}$ ..... Transmit power of $\mathcal{U}_0$ when associated to the kth tier.

p_0 ..... Transmit power of the transmitter of interest.

p_c ..... Baseline UE transmit power.

p_j ..... Transmit power of the jth transmitter.

$P_s(.)$ ..... Distribution of the pause time.

$P_v(.)$ ..... Distribution of the UE's speed.

q_k ..... Distances between the desired receiver to the interferers of kth tier.

$r_{m,j}$ ..... Radius of the jth small cell from the mth tier.

$S_{\bar{K}}$ ..... Pause time $\mathcal{U}_0$ spends in the small cells.

s_{max} ..... Maximum pause time.

s_{min} ..... Minimum pause time.

S_l ..... Pause time during lth movement.

$SINR_{k,\uparrow}$ ..... UL SINR when $\mathcal{U}_0$ is associated to the kth tier.

T_{Ξ_1} ..... Time missed from each small cell of Ξ_1.

T_{Ξ_2} ..... Time missed from each small cell of Ξ_2.

t_{min} ..... Minimum time for successful or beneficial offloading.

t_{p_A} ..... IAF scan periodicity.

t_{pm} ..... Minimum time $\mathcal{U}_0$ travels in each small cell of Ξ_1.

t_1 ..... Time $\mathcal{U}_0$ spends in a small cell of Ξ_1.

t_2 ..... Time $\mathcal{U}_0$ spends in a small cell of Ξ_2.

t_p ..... IRF scan periodicity.

v_{max} ..... Maximum speed.

v_{min} ..... Minimum speed.

V_l ..... UE's speed during the lth movement.

W_l ..... lth waypoint.

x_k ..... Distance between $\mathcal{U}_0$ to the serving BS of the kth tier.

$y_{m,j}$ ..... Location of the jth small cell (or transmitter) from the mth tier.

P_{Ξ_1} ..... Probability of any small cell being from Ξ_1.

P_{Ξ_2} ..... Probability of any small cell being from Ξ_2.

Chapter 1

Introduction

Contents

1.1 Motivation

The continuing growth in data demand, better experience and, different applications and services has established a need for a number of performance targets for the future wireless communication systems. These performance targets include very high capacity where the number of terminals will be 10-100x more, 1000x more data rate than what the current cellular systems can offer, latency of down to 1 millisecond, and very high energy efficiency, Fig. 1.1 [7–10]. It is anticipated that in addition to overcoming all the current challenges and limitations, using all approaches and technologies to boost the spectral efficiency and energy efficiency is of vital importance to meet the future requirements [11–13].

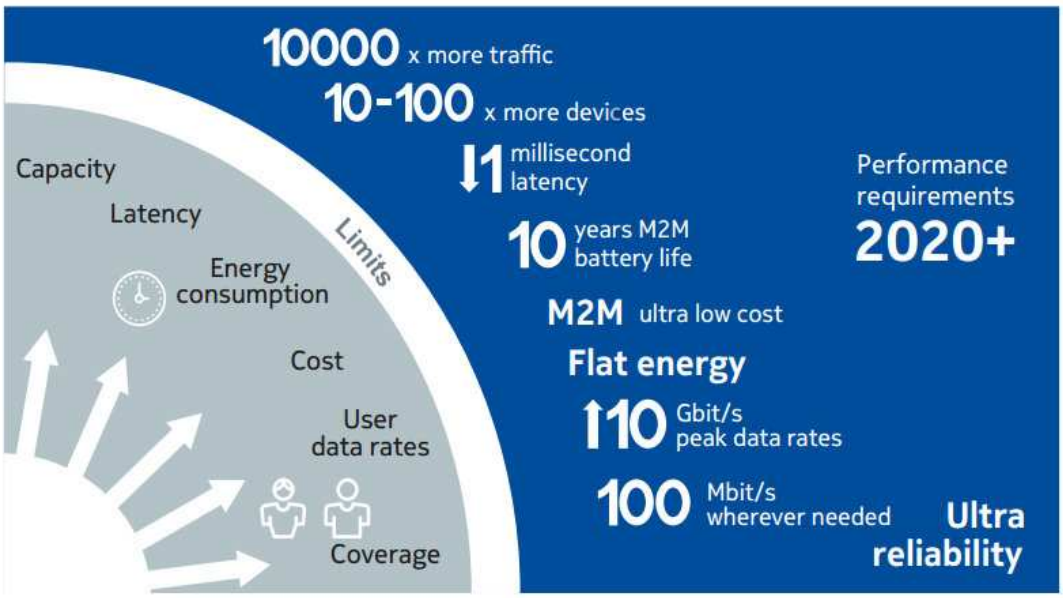

Figure 1.1: The main performance targets [10]

Adding new spectrum to the cellular systems to accompany boosting the spectral efficiency is considered to be the main approach to meet the future data rate [7, 8]. Here, regarding the first approach, adding new spectrum seems to be essential and high frequency bands, e.g. millimetre waves (mmWaves) from 3 - 30 GHz, have attracted significant attention as they are available with wide bandwidths, while the low frequency bands are either unlicensed or have been densely occupied. However, the high frequency can only be used for short range transmissions (small cells applications) as they suffer from high propagation loss and are more sensitive to the environment [14, 15]. Considering the second approach, boosting the spectral efficiency, it is very important to achieve the high spectral efficiency by using a number of techniques and strategies, which can be classified into solutions related to area spectral efficiency and solutions related to node spectral efficiency. The area spectral efficiency can be achieved by using device-to-device technology (D2D) and the heterogeneous networks (HetNets) [16], which can benefit from short transmission distance. The node spectral efficiency can be achieved by using antenna techniques, such as the multi-input multi-output (MIMO) and the distributed antenna system (DAS) [17, 18] and/or by using duplexing techniques such as the time division duplex (TDD) [5].

HetNet is a network which includes different types of nodes, and it has been introduced as one of the essential techniques to improve the spectral efficiency, coverage and capacity [7, 16, 19]. Different types of nodes in the HetNet have different characteristics such as transmit power, coverage, density and access policy (some of the nodes operate in close-mode where access to these nodes is restricted to a number of users equipment (UEs)). The nodes can also be classified according to the size of their coverage footprint such as femto cells, pico cells and macro cells, as shown in Fig. 1.2. The femto cells have coverage of tens of metres and they can be deployed indoors and outdoors in an unplanned manner by the end users. The pico cells and the macro cells have a coverage of tens to a few hundreds of metres and a few hundreds to a few thousands of metres respectively. All types of nodes are deployed in a planned manner by the operators. Generally speaking, femto cells and pico cells are categorized as small cells. The spectral efficiency can be enhanced by reusing the same frequency channel among same cells. Furthermore, the HetNets can also improve the energy efficiency as the transmission links are shortened when deploying more small cells within the local area range and the hot spots.

Utilizing both the potential benefits of HetNets and system resources efficiently depends significantly on the offloading process and mobility management [2, 20]. Offloading UEs and their traffic from overloaded cells to lightly-loaded cells is highly desired. For example, since large cells (e.g. macro cells) cover wide areas, a large number of UEs are served by these cells and share the limited resources, which degrades user-specific performance. Therefore, offloading UEs from the large overloaded macro cells to the small cells can shorten the transmission links and improve both the energy and spectral efficiencies as well as the data rate. On the other hand, mobility is considered as one of the important features in the cellular systems and has a significant impact on the system resources utilization and the offloading process in addition to the UE's quality of service (QoS) [1, 21]. Although offloading UEs to the small cells can benefit from abundant resources and the minimized transmit power, keeping high mobility UEs associated to the large cells minimizes the interruptions in service continuation and the signalling overhead due to frequent handovers. Therefore, mobility management and the offloading process will play an important role to meet the future requirements, which motivates us to carry

out this work.

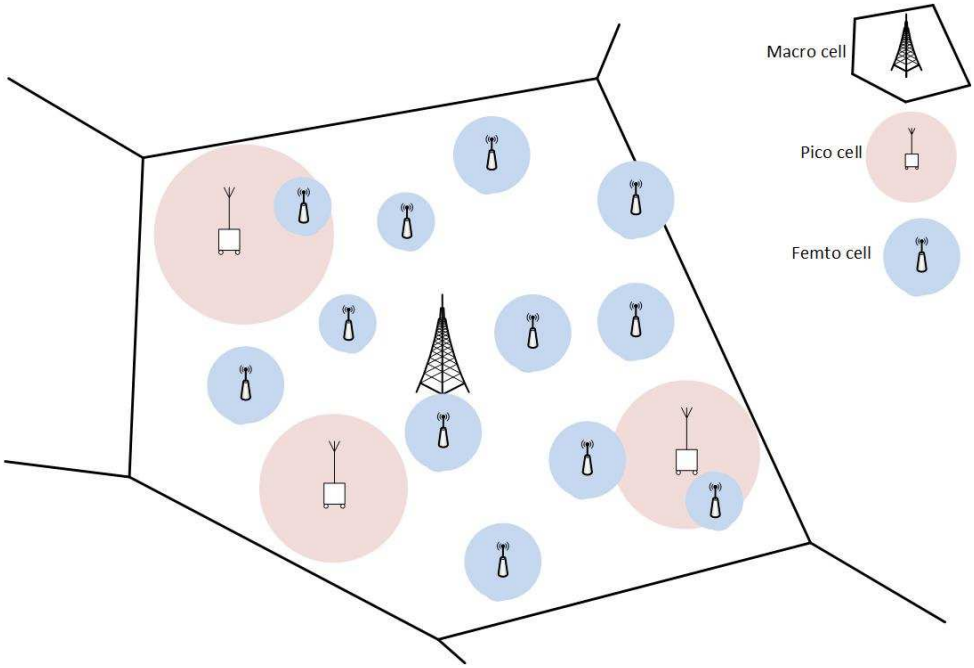

Figure 1.2: HetNet

The offloading process and load balance have been investigated in the conventional HetNets where the frequency channel is reused by all nodes in the network (co-channel HetNet) [22,23]. In these research works, each type of cell, e.g. femto cell or macro cell, is also considered as a tier. In [23], a multi-tier HetNet was studied where the basestations (BSs) of each tier form an independent Poisson point process (PPP). Then, a framework with a flexible cell association was provided to model and derive the signal to interference plus noise ratio (SINR) distribution of downlink (DL) and the average ergodic rate. It was shown in [23] that the cell association (bias) has a significant impact on the load balancing since the nodes with low transmit power (e.g. small cells) have a very small coverage when no bias is applied. Although increasing the bias to the pico cells increases the outage probability as some UEs are associated to the cells that do not offer the highest received power, it improves the data rate in the lightly-loaded HetNets. In [22], the coverage rate and the SINR distribution were studied in a multi-tier HetNet under a flexible cell association. The impact of the association on the offloading was captured and it was also shown that an optimum fraction of traffic, which depends on the ratio of the frequency resources at each cell and the UE's requirements, should be offloaded to

achieve the maximum coverage rate.

It is widely believed that the co-channel HetNets will not be able to meet the future requirements as the current system resources (e.g. frequency resources) are very limited and the interference management is one of the biggest challenges in the dense HetNets. Since adding the high frequency bands is essential to meet the future requirement, the future HetNets may adopt the inter-frequency (IRF) deployment in which the macro cells generally use low frequency (e.g. 2 GHz) to provide a wide coverage, and the small cells are densely deployed on a dedicated spectrum (in a high frequency range) for capacity and data rate enhancements.

User's mobility in the future HetNet will cause challenges to mobility management and offloading process which can affect the system performance and system resources utilization significantly. It is anticipated that offloading data from the macro cells with a limited bandwidth to the small cells with a wide bandwidth will save power and provide the UEs with high data rate [4, 20, 24]. As shown earlier [22, 23] that the offloading in the co-channel HetNet plays an important role to enhance the system performance, and a number of system parameters such as bias, transmit power and nodes densities need to be taken into consideration. Different from co-channel HetNet, the offloading process in the future HetNet has different challenges and requires a small cell discovery process (SCD) prior offloading due to user's mobility and small cells using a dedicated frequency channel. A periodic IRF scan has been introduced as small cell discovery, however, this mechanism suffers from a significant trade-off between the energy consumption for performing the periodic IRF scan and utilizing the system resources [4, 24]. The mobility management will be more complex and challenging in the future HetNet when high dense small cells with small coverage areas are deployed [1, 25]. There is a real need for developing an accurate model to evaluate the system performance and to design a new system which is more suitable for the requirements of the mobility management in the future. Both the handoff rate and the cell sojourn time are considered as the main parameters in the mobility management as they affect the system performance significantly. The handoff rate is defined as the expected number of handoffs per unit time and it directly affects the signalling load and the UE's QoS. The cell sojourn time is defined as the time that

a UE resides in the coverage of a typical cell. The cell sojourn time directly affects the efficiency of the system resources utilization. The handoff rate and the cell sojourn time can also be used to estimate the UE's speed [26, 27].

Stochastic geometry is a mathematical tool used to model and deal with the random spatial processes in one or higher dimensions [28, 29]. An increasing interest into this tool has been shown by different branches of science and engineering. In recent years, stochastic geometry has been used to model and evaluate the wireless communications as it can capture some of the characteristics and behaviour of fourth generation of cellular networks (4G) and beyond wireless networks [30]. Stochastic geometry has been widely used in different fields of cellular systems such as modelling and analysing uplink (UL) and DL cellular systems [23, 30–38], mobility model [21, 39], load balancing [40, 41], duplexing techniques [5, 42], D2D technology [43–45], MIMO systems [46–50], and beamforming [51, 52]. Although, the hexagonal grid was widely used to model the first generation, second generation and third generation of cellular networks, Fig. 1.3 shows that this model is not sufficient for the 4G and beyond and the PPP is more accurate to model the actual 4G networks [30]. Also, the PPP is more accurate, more suitable to model the HetNets and tractable. In addition, the nodes in the future HetNet will be more random and dense. Therefore stochastic geometry will have an important role in modelling, analysing and evaluating the future HetNets. For this reason, this tool is considered in this thesis.

1.2 Challenges

This section addresses some of the challenges imposed in the future HetNets, such as the trade-off between the offloading UEs and their traffic to the small cells, and the energy consumption in the SCD process as well as the mobility management in dense HetNets.

1.2.1 Offloading Process

It is anticipated that offloading data from the macro cells with a limited bandwidth to the small cells with a wide bandwidth will enhance the system resources utilization in addition to the system capacity. Since the small cells will be deployed densely on

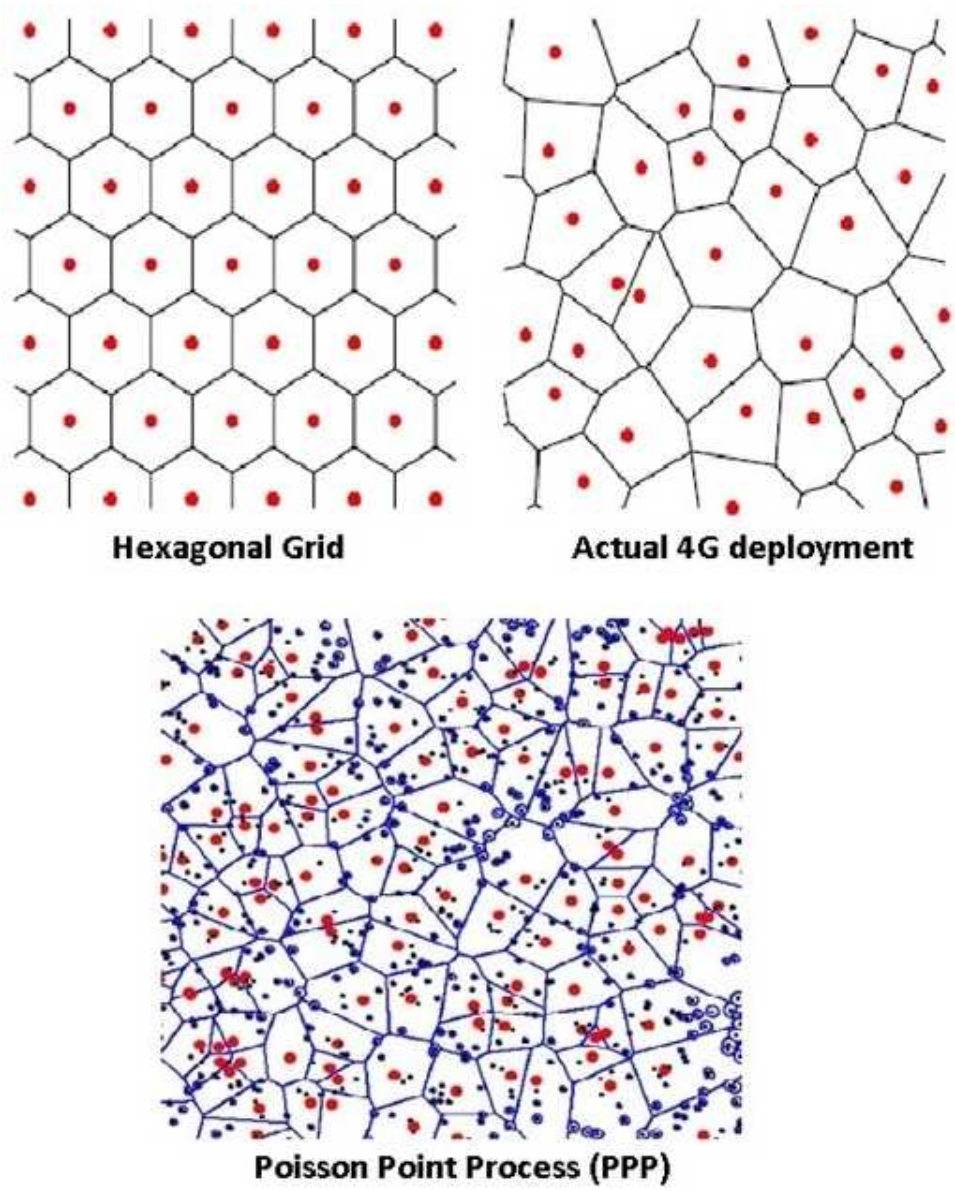

Figure 1.3: The PPP model is more accurate than the hexagonal grid model to model the actual 4G networks [30].

frequency channels different from the channels used by the macro cells and operate in different access modes, the offloading process is considered as one of the essential processes to utilize the system resources efficiently (e.g. frequency, signalling and power) [4, 20, 24]. The offloading process includes performing the IRF scan by the UEs prior to offloading them and their traffic from the macro cells to the small cells. However, there is a trade-off in the offloading process between the energy consumption in the SCD process and the

offloading loss. The offloading loss can be defined as the potential offloading opportunities to small cells that UEs miss partly or completely due to a long IRF scan periodicity. Although, the UEs will cross a number of small cells during their movement, they fail to discover some of these small cells on time because the UEs perform a small number of IRF scans per unit time. Increasing the number of IRF scans per unit time can invest more offloading opportunities, but significant power consumption takes place at the UEs' side. It is also expected that this issue will be more serious and a significant amount of power consumption and signalling load will take place when two or more high frequency channels are used in the system (UEs perform the IRF scan on multiple frequency channels, when the small cells are deployed on several frequency channels). Therefore, the role of the IRF scan will be essential in the offloading process in the future HetNets when the number of UEs increases significantly and these UEs have to perform the IRF scan on multiple frequency bands to exploit the potential offloading opportunities [2]. Since the UEs with limited power will have to handle the heavy traffic next to performing the IRF scan extensively, an effective offloading mechanism will be of vital importance to solve those issues and to utilize the system resources efficiently.

1.2.2 Mobility Model

The mobility management is considered to be one of the challenges that the future HetNet will face when the small cells with short footprints are deployed densely [1]. Due to high density of small cells in the future HetNet, the distance among the small cells will be minimized, which maximizes the overlap coverage among different small cells. As a results, the overlaps among the small cells can not be ignored in dense HetNets. Therefore, an accurate mobility framework with taking into consideration the overlaps among the small cells is essential for accurate speed estimation, estimating the energy consumption in the SCD process, and estimating the required resources at the different cells. For instance, estimating the time that UEs are associated to the first tier and, the number of handoffs that the first tier is involved in, will help in estimating the required overhead (e.g. signalling) and required resources (e.g. frequency) at the overloaded macro cells. Ignoring the overlaps among the small cells will result in misleading information. Furthermore,

finding the fraction of the time that the UEs spend in the small cells coverage can help to estimate the power consumption in the SCD process [4, 20, 24].

1.3 Thesis Contribution

The contributions of this thesis are summarized as follows:

- The locations of the small cell base stations (SCBSs), macro cell base stations (MCBSs) and waypoints of a reference UE during its movement in the system are randomly distributed on the plane and form independent PPPs. The distribution of the SCSBs around a reference UE's path is studied and the small cells crossed by the reference UE during one movement are mapped into a marked point process (MPP) on $\mathbb{R}^+$. This assumption is validated through simulations. Based on the mapping, a novel framework is proposed to model the coverage of the small cells in a multi-tier HetNet with consideration of the overlap coverage among the small cells from different tiers.

- Two types of handoff are introduced in this thesis. The inter-frequency handoff (IRH) is defined as the handoff taking place between cells that use different frequency channels, e.g. between the high frequency small cells and the macro cells, and the intra-frequency handoff (IAH) is defined as the handoff taking place between cells that use the same frequency, e.g. high frequency small cells. Both the IRH rate and the IAH rate can help to estimate the amount of signalling needed for handoffs at the overloaded macro cells (first tier). The cell sojourn time in a multi-tier HetNet is also addressed and derived by using the proposed framework. Results are presented to show the impact of different system parameters such as the density of the small cells, the transmit power of the small cells and the different mobility characteristics, on the availability of the small cells, the handoff rates and the cell sojourn time.

- By using the proposed mobility framework, the offloading loss of the reference UE that moves with a constant speed and performs the IRF scan every t_p, is derived by taking into account different parameters such as the small cell density, the small cell

transmit power, the overlaps among the small cells and the minimum time required for successful offloading.

- The uplink energy efficiency (ULEE) and the energy consumption in the SCD process are given as performance metrics to evaluate different system parameters and their impacts on the system performance. The optimum value of t_p to achieve the best system performance in the periodic scan mechanism is also derived.

- A novel trio-connectivity system (TC) is proposed to overcome the current issues in the offloading process. The proposed system which includes a control-plane (C-plane), a user-plane (U-plane) and an indication-plane (I-plane) takes into consideration the need to add more frequency channels from different frequency bands to the future cellular system. The I-plane is a function of broadcasting the system information of the small cells on the low frequency in parallel with the high frequency to enable UEs discovering the small cells without performing the IRF scan periodically. The TC can help to exploit the system resources (e.g. frequency, signalling load and power) efficiently by not only overcoming some of the mobility management challenges, but also by minimizing the energy consumption and signalling load in the offloading process.

- The energy consumption in the proposed SCD mechanism is addressed and a comparison with the conventional mechanism (e.g. periodic scan) is presented in terms of energy efficiency.

1.4 Thesis Structure

This thesis contains nine chapters and an appendix as follows:

In Chapter 1, the motivation, feasibility and challenges of HetNets in the future wireless communications systems are discussed. Both the main contributions and the structure of this thesis are also presented.

In Chapter 2, the principles of some aspects of the HetNet, such as mobility, offloading process and duplex techniques are presented as well as the state-of-the-art literature. The

system model, which includes the cell association, the SINR at the desired receiver and the mobility model, is also presented in this chapter.

In Chapter 3, the small cells distribution around a reference UE's path is studied. Also, the impact of the system parameters on the small cells coverage, the cell sojourn time and the handoff rate are investigated. Representative simulations and numerical results to show the impact of small cells overlapping and other system parameters such as the small cell density on the cell sojourn time and handoff rate, are also presented.

In Chapter 4, the offloading loss which is defined as the time that the reference UE misses from the second tier, is derived. The total energy consumption which includes the energy consumption for maintaining the UL transmission and the SCD energy consumption, is studied. Furthermore, the ULEE is defined as the ratio of the average ergodic rate in the UL to the total energy consumption, is derived as performance metric. The TC which includes three planes is introduced, and the system design and the functions of each plane are presented. Furthermore, a SCD mechanism based on the TC is introduced and the energy consumption in this mechanism is investigated. A comparison between the DC and the TC in terms of ULEE and energy consumption is also presented through results.

In Chapter 5, the conclusions of this thesis are drawn, and possible future work is discussed.

In Appendix A.1, the expectation of one overlap coverage on the reference UE's path in a two-tier HetNet is derived.

In Appendix A.2, the expectation of the overlaps number on the reference UE's path in a two-tier HetNet is derived.

In Appendix A.3, the expectation of one overlap coverage on the reference UE's path in a K-tier HetNet is derived.

In Appendix A.4, the expectation of a small cell's footprint served by another small cell on the reference UE's path in a K-tier HetNet is derived.

In Appendix A.5, the probability of the reference UE spending the pause time in the coverage of small cell of interest is derived.

In Appendix A.6, the UL average achievable rate of the reference UE is derived.

Chapter 2

Literature Review and System Model

Contents

2.1 Small Cell Discovery

The cell discovery is a procedure done by UEs to identify the nearby cells and measure their signal quality. There are two types of cell discovery: i) intra-frequency (IAF) and ii) IRF. In the current systems, UEs perform the IAF measurements on a predefined time-frequency basis on the pilots or the reference signals (RSs) of the cells that are using the same frequency of the serving cells. These measurements are sent to the serving cells. The IAF measurements are of vital importance not only for inter-cell mobility, but also for estimating the channel between the UEs and the serving cells. The IRF measurements take place when UEs are triggered by their serving cells to discover the

cells deployed on a different frequency from the serving cells. In the current mobile systems, a periodic scan has been introduced to allow UEs to detect the small cells. Each UE performs the IRF measurements and sends these measurements to their serving macro cells either periodically or on an event based manner to identify the nearby small cells [53, 54]. The offloading process is initiated when a number of offloading requirements are met. For example, a UE receives signal of enough quality and meets the access policy of the discovered small cells.

Some work has been done to tackle the SCD issue in the conventional HetNets by proposing schemes and strategies to achieve a good trade-off between the power consumption needed for performing the IRF scan and exploiting the offloading opportunities [3, 4, 20, 55–58]. [55] proposed an IRF scanning scheme based on the UE mobility status, by increasing the periodicity of the scan to avoid unnecessary power consumption and reduce handover failure for high mobility UEs. Although this scheme can be beneficial for high mobility UEs, it still forces UEs with low mobility to perform the IRF scan frequently. [57, 58] proposed to use received signal strength (RSS) based on radio fingerprint as an indicator to estimate UEs' locations. The macro cells motivate UEs to perform IAF scanning to check if RSS matches entries in a fingerprint database stored at the macro cells or at the UE. Estimating the UEs' physical locations as well as the large memory and the amount of signalling to store and update the fingerprint database are the main challenges in this scheme.

In [20], stochastic geometry was used to investigate the impact of the IRF scan periodicity (t_p) on the average energy efficiency. The offloading loss was approximated as a function of the IRF scan periodicity t_p via a polynomial curve fitting for a fixed small cell density and the UE's speed. This approximation may not be accurate for more diverse system parameters, and it does not show the impact of other system parameters such as the small cell transmit power, the minimum time for successful offloading, and the overlaps among the small cells on the path. In [20], it was assumed that the fraction of the reference UE's path covered by the small cells is a product of the second tier association and the total transition time. This assumption ignores the effects of the overlapping and the distribution of the small cells around the reference UE's path. The simulations and

the analysis in this thesis will show that this assumption does not hold. In [3, 4], the impact of the periodic IFR scan on the system performance was modelled by taking into consideration the effect of different system parameters including the transmit power of the small cells, the density of small cells and the speed of the terminals. In [4], a framework was also presented to obtain the optimum IFR scan periodicity to achieve the best system performance in a two-tier HetNet. Both [3, 4] did not take into account the small cells overlaps on the reference UE's path and the minimum time for successful offloading when modelling the offloading loss and the fraction of the reference UE's path covered by the small cells. All [3, 4, 20, 55–58] assumed that the small cells are deployed on one frequency channel. However, it is expected that the role of the IRF scan will be critical in the future HetNets when the number of UEs increases significantly and these UEs have to perform the IRF scan on multiple frequency bands (different frequency channels from different bands may be deployed in the future HetNets).

The DC has been proposed to overcome some of the current technical challenges such as signalling load in the mobility management [59, 60]. The DC includes the C-plane and the U-plane, where the C-plane is always provided by the macro cells and the U-plane is provided by either the macro cells or the small cells. [61] proposed a handover scheme in the DC for high speed railway. In [62], a DL traffic scheduling scheme was proposed to enhance the system throughput and also to manage the DL traffic for UEs in the DC network. In [63], an adaptive scheme was proposed in which the UEs in the system are allocated the transmit power based on backhaul load and channel link quality indicators by using minimized overhead. A survey regarding some of the technical aspects of the DC was presented in [60]. Since the DC is based on the IRF deployment, it is expected that the DC will inherit the offloading issue. The trend of offloading more UEs from the macro cells to the small cells in the future HetNets will not only make the energy consumption a serious issue but also cause significant signalling load. Therefore, an effective offloading process will be of vital importance to ease the aforementioned issues and to exploit the system resources efficiently.

2.2 Mobility Management

The mobility model is defined as a tool to study and investigate the movement pattern of UEs. The mobility model also describes the changes in the UEs' locations, behaviours and speed over time as they have a great impact on the protocol performance. The random waypoint (RWP) model is considered as one of the simple models to study and model a UE's movement and it was investigated by [64]. It is also adopted by some of the simulation software such as network simulator-2 (NS-2). In this model a UE moves in a finite domain and chooses its destination point on the domain according to uniform distribution and moves towards it with a constant speed. However, RWP has two issues as shown in [65, 66]. The first issue is that the stationary spatial node distribution tends to concentrate on the centre of the finite domain when UEs are uniformly distributed in the network. The second issue concerns the transition lengths in the RWP, which are of the same order as the size of the domain. [21] proposed improved random waypoint (IRWP) to mitigate some of the issues that the classical RWP suffers from. In the IRWP, the direction of movement is chosen uniformly in $[0, 2\pi]$, and each of the length of transition, the speed and the pause time are chosen from some distributions.

In [21], the handoff rate and the cell sojourn time in a one-tier network were investigated by using the IRWP. It is expected that the future cellular network will include multiple tiers with different frequency bands (e.g. high frequency small cells), and in the presence of a multi-tier HetNet, the mobility management is more complex and more system parameters need to be considered. When studying the mobility management in HetNets, modelling the cells has taken two main directions, Voronoi Tessellations cells (VTCs) assumption and regular shapes assumption (e.g. circle and hexagonal). Regarding the first direction, in the conventional HetNets (all tiers use the same frequency channel) different tiers in the network are assumed to form VTCs. [39] used stochastic geometry to propose a framework for vertical and horizontal handoff rates experienced by a UE with arbitrary movement trajectory in co-channel HetNets. Although the VTCs assumption is reasonable for this type of deployment, it is expected that the future HetNets will include dense small cells operating on different frequency channel. The VTCs assumption has also been considered in the IRF HetNet [26, 27]. In [26], the number of

handoffs made during a time window was used to estimate the UE's speed in dense small cell networks. Stochastic geometry was used to derive approximations to the Cramer-Rao lower bound (CRLB) for the speed estimate of a UE. In [27], the UE's speed was estimated by using the cell sojourn time, where CRLB for the sojourn time-based speed estimation was analysed. Both [26] and [27] assumed that the single-tier small cells in the network forms VTCs which means that the whole network is covered by the small cells. However, a huge infrastructure will be required for the high frequency small cells to cover the whole network as the high frequency suffers from a very large propagation loss [14]. Also this assumption restricts the analysis to one-tier cellular systems similar to [21].

Considering the second direction, [67, 68] assumed that the small cells in two-tier HetNets have regular shapes. [67] addressed the cell sojourn time in a two-tier HetNet where the small cells were assumed to have fixed hexagonal shapes in the network and the overlap coverage among the small cells was not taken into consideration. [68] investigated the mobility in a two-tier HetNet and also derived the cell sojourn time and the cross-tier handoff rate by using the proposed model in [21]. The overlaps among small cells of ellipse shape on a reference UE's path was also neglected in this work. Therefore, some of the intra-tier handoffs (handoffs among the small cells due to overlap) will be counted as cross-tier handoffs. Ignoring the overlaps will not only affect the accuracy of the handoff rate analysis but also affect the accuracy of the cell sojourn time as shown later in Chapter 3.

2.3 System Model

Consider a K-tier HetNet, where each tier is characterized by the tuple $\{\lambda_k, \alpha_k, p_{f,k,rs}\}$ as shown in Fig. 2.1, where λ_k is the BSs density, α_k is the path-loss exponent of the kth tier and $p_{f,k,rs}$ is the RS transmit power of the kth tier on the fth frequency . The first-tier (macro cells) uses low frequency for providing a wide coverage, and high frequency channels are used at the small cells in the rest of the network tiers $2, 3, \cdots, K$ for enhancing the capacity and data rate. For tractability and clarifying the system model, we make the following assumptions:

- **Assumption 1**: It is assumed that the BSs of different tiers and the UEs in the network are randomly distributed as independent PPPs Φ_k and Φ_u with density λ_k and λ_u respectively, where $k \in [1, 2, \cdots, K]$ [28]. Although the distribution of small cells in the system might be different in some areas, for instance, small cells form clusters in some areas such as a city centre, the PPP assumption has been widely accepted in literature due to its accuracy and tractability [5, 20, 22, 23].

- **Assumption 2**: Maximum received power association is reasonable in the co-channel HetNet due to co-channel interference as in [23]. However, it causes load imbalance and minimizes the small cells coverage significantly in the IRF HetNets due to big differences in transmit powers and propagation losses [5, 14]. Offloading UEs from the first tier to the small cells is highly desired and prioritized in order to increase the system capacity and exploit the abundant resources at the small cells efficiently. The resources at the small cells will not be exploited efficiently in the future HetNets if the cell association is based on the best received power. Since there is no interference between the first tier and the other tiers, it is assumed that the association to the small cells is based on the minimum received power from any small cell and the association among the tiers $2, 3, \cdots, K$ is based on the maximum average received power. When the small cell tiers use the same frequency F_2, any UE will be associated to a small cell of the mth tier, if the received power satisfies the condition below:

$$\rho_{min} \leq \rho_{m,j} \geq \max_{i \in \Phi_n} \rho_{n,i} \tag{2.1}$$

  where $m, n \in [2, 3, \cdots, K]$, ρ_{min} is the minimum received power to consider the UEs in the small cell coverage and, $\rho_{m,j}$ and $\rho_{n,i}$ are the received power from the jth small cell of the mth tier and from the ith small cell of the nth tier respectively.

- **Assumption 3**: It is also assumed that small cells operate in an open-access mode.

- **Assumption 4**: The network operates in full-buffer mode.

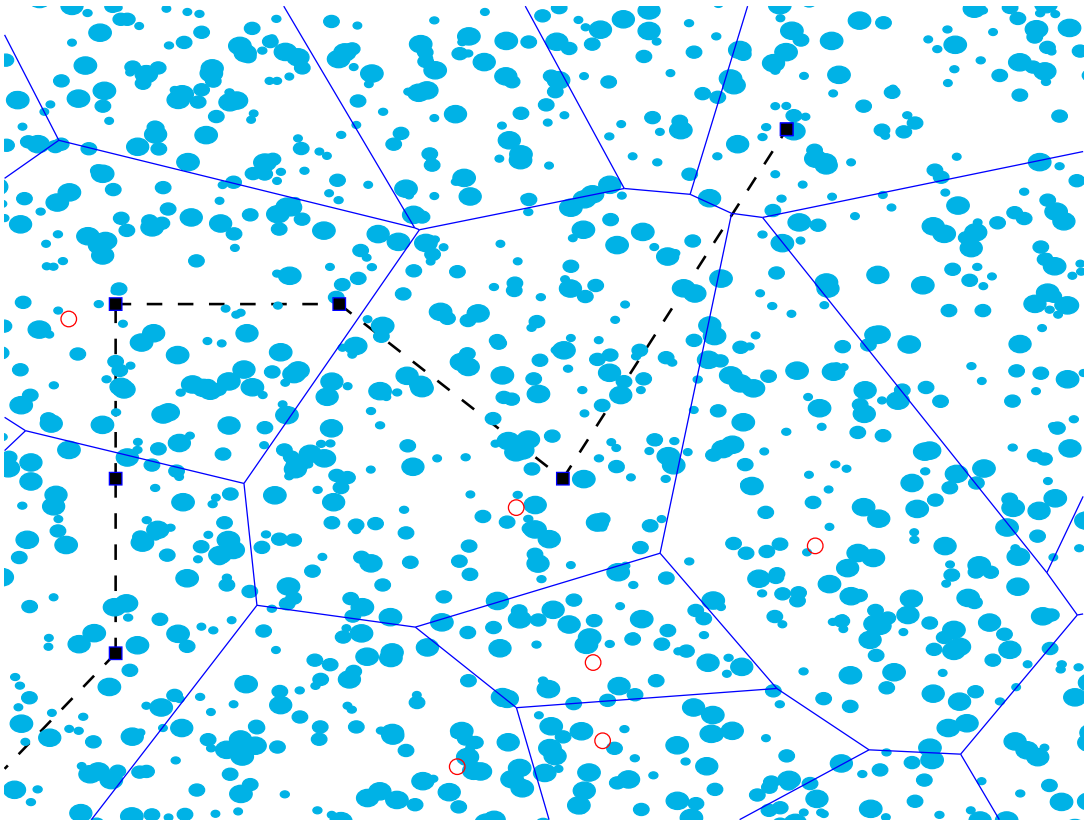

Figure 2.1: System Model. Red circles represent the locations of the MCBSs, blue dots represent the small cells coverage (different small cells tiers), black squares represent the waypoints, and the black dashed lines represent the reference UE's path between any two waypoints.

2.3.1 Association and SINR

Stochastic geometry is used to derive the cell association in multi-tier HetNets. In practice ping-pong takes place if the cell association is based on instantaneous received power. For this reason, it is assumed that the cell association is based on the average value of received power (fading is averaged out). However, we consider the instantaneous value of the received power to derive the average achievable rate later in this thesis. From Assumption 2 and Assumption 3, the probability that a reference UE ($\mathcal{U}_0$) is connected to any small cell in the system can be obtained as follows.

Lemma 1 The probability that $\mathcal{U}_0$ is associated to any small cell is expressed as:

$$\mathcal{A}_{\bar{K}} = 1 - \exp\left(-\pi \sum_{m=2}^{K} \lambda_m \left(\frac{\rho_{min}}{\mathscr{L}_2 p_{2,m,rs}} \right)^{\frac{-2}{\alpha_m}} \right) \tag{2.2}$$

where $\bar{K}$ represents the set of the small cell tiers (it also represents the number of the

small cell tiers in the network $\bar{K} = K - 1$), and $\mathscr{L}_2 = (\frac{\omega}{F_2 4\pi})^2$ is the path-loss at 1 metre of the high frequency F_2 and ω is the velocity of the wave.

Proof: Without loss of generality, assume that $\mathcal{U}_0$ is located at the origin and $\mathcal{A}_k$ is the probability that $\mathcal{U}_0$ is associated to the kth tier. It is also assumed that $\mathcal{U}_0$ must be associated to some tier and it is associated to the first tier when not associated to any small cell. Thus, the probability of $\mathcal{U}_0$ associated to the first tier can be found as:

$$\begin{aligned}\mathcal{A}_1 &= \prod_{m=2}^{K} \mathbb{P}\Big[\rho_{m,0} < \rho_{min}\Big] \\ &= \prod_{m=2}^{K} \mathbb{P}\Big[\mathfrak{r}_{m,0} > \Big(\frac{\rho_{min}}{\mathscr{L}_2 p_{2,m,rs}}\Big)^{\frac{-1}{\alpha_m}}\Big] \\ &= \prod_{m=2}^{K} \exp\Big(-\pi\lambda_m\Big(\frac{\rho_{min}}{\mathscr{L}_2 p_{2,m,rs}}\Big)^{\frac{-2}{\alpha_m}}\Big)\end{aligned} \tag{2.3}$$

where $\mathbb{P}[.]$ indicates the probability, $\rho_{m,0}$ is the received power from the nearest small cell of the mth tier, $\mathbb{P}\Big[\rho_{m,0} < \rho_{min}\Big]$ is the probability of the received power from the mth tier being less than ρ_{min}, $\mathfrak{r}_{m,0}$ is the distance from the origin to the nearest SCBS of the mth tier, and $\exp\Big(-\pi\lambda_m\big(\frac{\rho_{min}}{\mathscr{L}_2 p_{2,m,rs}}\big)^{\frac{-2}{\alpha_m}}\Big)$ is the probability of no SCBS of the mth tier within the area $\pi\big(\frac{\rho_{min}}{\mathscr{L}_2 p_{2,m,rs}}\big)^{\frac{-2}{\alpha_m}}$ and it is obtained from the null probability [28]. Eq. (2.2) is obtained from $\mathcal{A}_{\bar{K}} = \mathcal{A}_K - \mathcal{A}_1$ where $\mathcal{A}_K = \sum_{k=1}^{K} \mathcal{A}_k = 1$. ■

The received SINR from a transmitter at its receiver is expressed as:

$$SINR = \frac{p_0 g_0 \mathscr{L} x^{-\alpha}}{\sigma^2 + \sum_{j,j\neq 0} p_j h_j \mathscr{L} q_j^{-\alpha}} \tag{2.4}$$

where p_0 and p_j are the transmit powers of the transmitter of interest and the jth interferer respectively, x and q_j represent the distances from the desired receiver to the transmitter of interest and to the jth interferer respectively, g_0 and h_j are the channel gains of the desired link and the interfering link respectively, and σ^2 is the additive noise power.

The power control is considered to be a very important technique in the cellular wireless networks, not only for reducing the interference and improving the performance at the cell edge but also for saving power at the terminal side. The power control in the DL transmission is not complicated, as the inter-cell interference mitigation can be achieved by link adaptation and scheduling techniques rather than adjusting the transmit power of the BSs. In contrast, the UL power control, which is used to fully or partially compensate

for the path-loss and shadowing and to guarantee minimum SINR received at the serving BSs, is a crucial issue. Using fast power control is of vital importance in some cellular systems, such as code division multiple access (CDMA), due to the near-far problem in these systems as multiple UEs in the same cell share the same spectrum resources [69]. In the current systems (e.g. orthogonal frequency-division multiple access (OFDMA)) [70, 71], there is no intra-cell interference as spectrum resources are not assigned to more than one UE in the same cell. Nevertheless slow power control is still important to reduce the inter-cell interference and the power consumption at the terminal side. In this thesis, the distance-proportional fractional power control (FPC) is considered in the UL transmissions while no power control is considered in the DL transmissions. When a UE is at distance x from its serving BS, the UL transmit power can be expressed as:

$$p_0 = p_c x^{\alpha\epsilon} \tag{2.5}$$

where p_c represents the baseline UE transmit power and ϵ is the UL power control factor (PCF) and takes a value between 0 and 1.

2.3.2 Mobility Model

The IRWP proposed in [21] is considered in this thesis. The movement trace of any UE is modelled by the quadruples $\{W_{l-1}, W_l, V_l, S_l\}_{l\in\mathbb{L}}$ where l denotes the lth movement. During the lth movement, W_{l-1} and W_l denote the starting waypoint and the destination waypoint respectively, and V_l and S_l denote the velocity of the UE and the pause time respectively. The velocities V_l are independent and identically distributed (i.i.d) with distribution $P_V(.)$ and pause times S_l are i.i.d with distribution $P_S(.)$. The waypoints $\{W_0, W_1, \cdots W_{l-1}, W_l, \cdots W_L\}$ are a homogeneous PPP $\Phi_w(l)$ with density λ_w, and the nearest point in $\Phi_w(l)$ is selected as the destination waypoint:

$$W_l = \underset{w\in\Phi_w(l)}{\arg\min} \parallel w - W_{l-1} \parallel \tag{2.6}$$

where $\parallel . \parallel$ indicates the Euclidean distance. The transition lengths $\{\parallel W_1 - W_0 \parallel, \parallel W_2 - W_1 \parallel^{\cdots} \parallel W_l - W_{l-1} \parallel^{\cdots}\}$ are i.i.d. The cumulative distribution function (CDF) of the

transition length during the lth period can be obtained as:

$$\mathbb{P}(W_l - W_{l-1} \leq \mathfrak{l}) = 1 - \exp(-\lambda_w \pi \mathfrak{l}^2) \tag{2.7}$$

The expected value of the transition length during the lth period can be obtained as:

$$\begin{aligned} \mathbb{E}[\| W_l - W_{l-1} \|] &= \int_0^\infty \mathfrak{l} \frac{d}{d\mathfrak{l}}\big(1 - \exp(-\lambda_w \pi \mathfrak{l}^2)\big) d\mathfrak{l} \\ &= 2\pi\lambda_w \int_0^\infty \mathfrak{l}^2 \exp(-\lambda_w \pi \mathfrak{l}^2) d\mathfrak{l} \\ &= \frac{1}{2\sqrt{\lambda_w}} \end{aligned} \tag{2.8}$$

The mean transition time when the speed is a constant $V = v$ becomes:

$$\mathbb{E}[\mathcal{T}_{t,l}] = \frac{1}{2v\sqrt{\lambda_w}} \tag{2.9}$$

When V is uniformly distributed on $[v_{min}, v_{max}]$, the mean transition time becomes [21]:

$$\begin{aligned} \mathbb{E}[\mathcal{T}_{t,l}] = \mathbb{E}[\| W_l - W_{l-1} \|]\mathbb{E}[\frac{1}{V}] \\ \frac{\ln v_{max} - \ln v_{min}}{2\sqrt{\lambda_w}(v_{max} - v_{min})} \end{aligned} \tag{2.10}$$

It is expected that users have different mobility characteristics in different areas, for instance, the user's transition length is short and direction switch rate is high when walking and shopping in a city. The user's transition length is long and the direction switch rate is low when driving. Showing the different mobility behaviours requires different values of waypoint density. High values of λ_w is suitable to model the movement of user walking and low values of λ_w are more suitable to model movement of driving user. The impact of λ_w on the mobility parameters will be shown later in the next chapter.

Chapter 3

Mobility Model

Contents

In this chapter, we study the handoff rate, the small cell sojourn time and the macro cell sojourn time in a multi-tier HetNet.

3.1 Small Cells Coverage

In this section, the coverage of small cells on the $\mathcal{U}_0$'s path is investigated by taking into consideration that some overlaps may take place on the path. Since all transition lengths are i.i.d., for brevity we consider the $\mathcal{U}_0$'s path from W_0 to W_1 ($\mathcal{P}_0$). When λ_w is small ($\mathcal{P}_0$ is long as shown in Eq. (2.8) and $\mathcal{U}_0$ crosses a number of small cells during it is movement in a dense HetNet as shown in Fig. 2.1) and $D_{m,j}$ represents the vertical distance between

$\mathcal{P}_0$ and the jth SCBS with radius $r_{m,j}$ from the mth tier, the number of small cells crossed by $\mathcal{U}_0$ is given by:

$$N_0 = \sum_{m=2}^{K} \sum_{j \in \Phi_m} \mathbf{1}(D_{m,j} \leq r_{m,j}) \tag{3.1}$$

where $\mathbf{1}(.)$ is the indicator function. It is assumed that $\mathscr{A}_{sys}$ is the total system area and $\mathscr{A}_m$ is the area surrounding $\mathcal{P}_0$, and any small cell from the mth tier will be crossed by $\mathcal{U}_0$ if its SCBS is located in this area. The conditional distribution of the number of small cells crossed by $\mathcal{U}_0$ (ν) for $\mathscr{A}_m \subseteq \mathscr{A}_{sys}$ is binomial since $\mathscr{A}_{sys} \subset \mathbb{R}^2$, [28]:

$$\mathbb{P}(N(\mathscr{A}_m) = \nu \mid N(\mathscr{A}_{sys}) = N_m) = \binom{N_m}{\nu} \mathbb{P}_m^{\nu} (1 - \mathbb{P}_m)^{N_m - \nu} \tag{3.2}$$

where $\mathbb{P}_m = \frac{\mathscr{A}_m}{\mathscr{A}_{sys}}$ is the probability of any small cell located in $\mathscr{A}_m$ and N_m is the total number of small cells of the mth tier in the system.

The expected number of small cells from all tiers crossed by $\mathcal{U}_0$ is obtained as follows.

Proposition 1 The expected number of small cells crossed by $\mathcal{U}_0$ along $\mathcal{P}_0$ can be expressed as:

$$\mathbb{E}[N_0] = \sum_{m=2}^{K} \lambda_m \mathscr{A}_m \tag{3.3}$$

Proof: Since SCBSs are distributed as PPP, the number of SCBSs from the mth tier in $\mathscr{A}_m$ has a Poisson distribution with a mean value of $\lambda_m \mathscr{A}_m$. ■

$\mathcal{U}_0$ spends the pause time associated either to one of the small cells or to the first tier. The expected value of the pause time that $\mathcal{U}_0$ spends in the small cells coverage is obtained in the next Lemma.

Lemma 2 The expected value of the time $\mathcal{U}_0$ resides in any small cell during the pause time is obtained as:

$$\mathbb{E}[S_{\bar{K}}] = \frac{\mathcal{A}_{\bar{K}}(s_{max} + s_{min})}{2} \tag{3.4}$$

where s_{min} and s_{max} are the minimum and the maximum pause time respectively.

Proof: $\mathcal{U}_0$ spends the pause time associated to a small cell if the destination point (W_1) is located at a distance equal to or less than the radius of the small cell from its

SCBS:

$$S_{\bar{K}} = S\ \mathbf{1}(\parallel W_1 - y_{m,j} \parallel \leq r_{m,j}) \tag{3.5}$$

where S is the pause time, $y_{m,j}$ is the location of the jth SCBS of the mth tier. Without loss of generality, we assume that W_1 is located at the origin. The probability that this point is located in the small cells coverage is $\mathcal{A}_{\bar{K}}$ as shown in Lemma 1 in Chapter 2, then the expected pause time that $\mathcal{U}_0$ spends in the small cells coverage can be expressed as:

$$\mathbb{E}[S_{\bar{K}}] = S\mathcal{A}_{\bar{K}} \tag{3.6}$$

The result in Eq. (3.4) is reached when S is uniformly distributed on $[s_{min}, s_{max}]$. ■

Next, the distribution of the one-tier small cells around $\mathcal{P}_0$ is investigated in order to propose a framework to estimate the coverage of the small cells on $\mathcal{P}_0$. The one-tier small cell framework will be expanded to a multi-tier small cell framework later in this chapter.

3.1.1 One-Tier Small Cell Network

The analysis in the subsection is based on the following assumption.

Definition 1 When $\mathbb{R}^\delta$ is a δ-dimensional Euclidean space, a uniform PPP on $\mathbb{R}^\delta \times [0, \eta]$ of intensity λ can be interpreted as an MPP on $\mathbb{R}^\delta$ with marks from $[0, \eta]$ and intensity $\eta\lambda$ [29].

Assumption 5: Without loss of generality, if $r_j = r \ \ \forall j$ and the point W_0 is at the origin, the SCBSs at distance of r or less from the line that starts from the origin and passes through W_1, can be interpreted as a MPP on $\mathbb{R}^+ \times [0, r]$, $\bar{\Phi} = \{(\bar{y}_i, \tau_i)\}$ of intensity $\bar{\lambda}$. $\bar{y}$ are the path points that represent the nearest points on the line to the SCBSs of the crossed small cells as shown in Fig. 3.1. The path points are assumed to be distributed on the line as PPP. The accuracy of this assumption is validated through simulations in Fig. 3.2. τ_i represents the shortest distance between the location of the ith SCBS and the path point $\bar{y}_i$. Since the locations of the SCBSs are uniformly distributed and can be at any distance from $\mathcal{P}_0$, it is also assumed that τ is uniformly distributed in the range $[0, r]$. The density of the new process $\bar{\Phi} = \{(\bar{y}_i, \tau_i)\}$ is obtained as follows.

Lemma 3 The density of the MPP on the straight line from W_0 and passes through W_1 can be expressed as:

$$\bar{\lambda} = 2r\lambda \tag{3.7}$$

Proof: Assuming that the number of the path points on $\mathcal{P}_0$ is denoted as $\bar{N}_0$. According to Assumption 5, $\bar{N}_0 = N_0$ and the expected value of $\mathbb{E}[\bar{N}_0]$ can be expressed as:

$$\begin{aligned} \mathbb{E}[\bar{N}_0] &= \mathbb{E}[N_0] \\ \bar{\lambda} \parallel W_1 - W_0 \parallel &= \mathscr{A}_2\lambda \\ \bar{\lambda} &= \frac{\mathscr{A}_2\lambda}{\parallel W_1 - W_0 \parallel} \end{aligned} \tag{3.8}$$

where $\mathbb{E}[N_0]$ is obtained in Prop. 1, $\mathscr{A}_2 = 2r \parallel W_1 - W_0 \parallel$ is the area surrounding $\mathcal{P}_0$ and $K = 2$ in the one-tier small cell network. The result in Eq. (3.7) is reached. ■

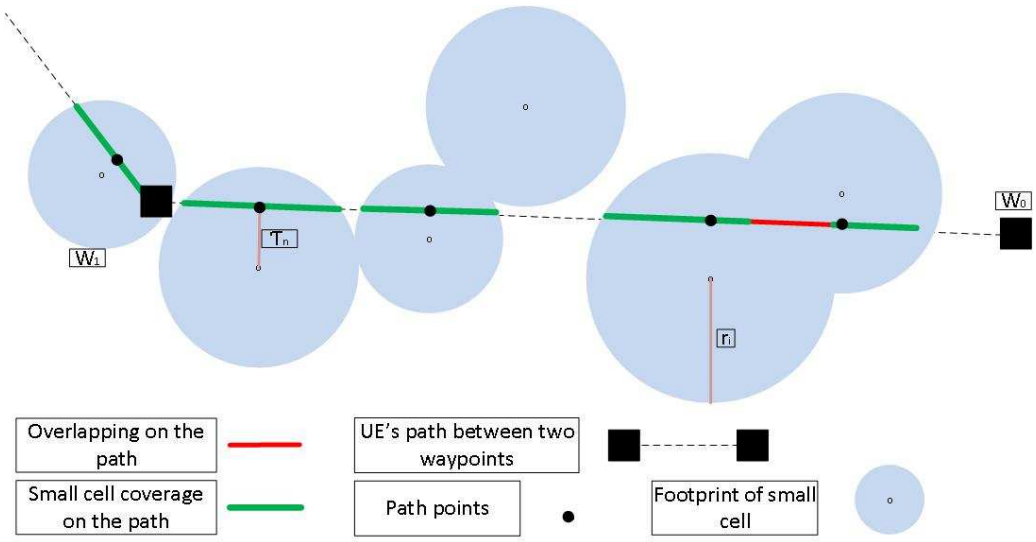

Figure 3.1: The coverage of small cells from different tiers on $\mathcal{P}_0$

Assume that the path points are set in order according to the distance from W_0 as $(\bar{y}_1, \bar{y}_2, \cdots, \bar{y}_i, \cdots, \bar{y}_{\bar{N}_0})$. The path point inter-distance (e.g. the first path point inter-distance represents the distance between the points W_0 and $\bar{y}_1$) has an exponential distribution with $\bar{\lambda}$:

$$\mathbb{P}(\parallel \bar{y}_{i+1} - \bar{y}_i \parallel \leq \mathrm{d}) = 1 - \exp(-\bar{\lambda}\mathrm{d}) \qquad \mathrm{d} > 0 \tag{3.9}$$

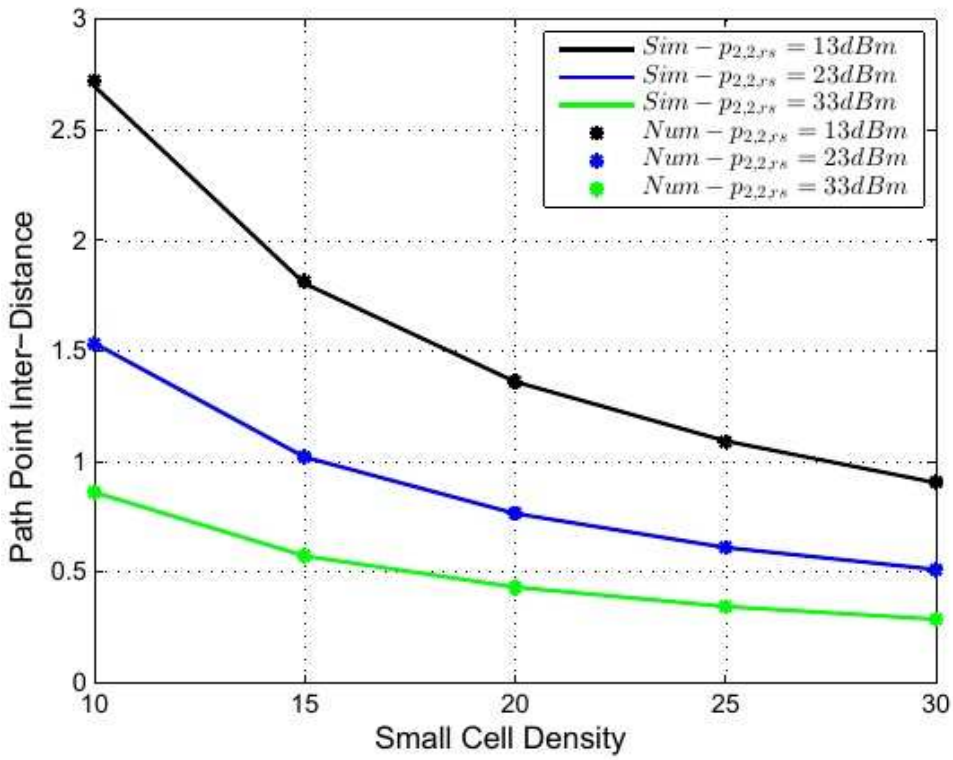

Figure 3.2: Assumption 5 is validated in this figure, where Num. is the numerical result obtained by using Eq. (3.10) and Sim. is the results obtained from simulations. The small cell density in SCBSs per km^2 and the path point inter-distance in km.

Lemma 4 The expected value of the distance from W_0 to $\bar{y}_i$ can be expressed as:

$$\mathbb{E}(\| \bar{y}_i - W_0 \|) = \frac{i}{\bar{\lambda}} \tag{3.10}$$

where $i \in (1, 2, \cdots, N_0)$.

Proof: Since the path points $(\bar{y})$ follow PPP on $\mathbb{R}^+$, the distance $\| \bar{y}_i - W_0 \|$ for $i > 0$ has an Erlang or Gamma distribution with i and $\bar{\lambda}$ [28]. The probability density function (PDF) of the distance $\| \bar{y}_i - W_0 \|$ is expressed as:

$$f_{(\|\bar{y}_i - W_0\|)}(\mathrm{d}) = \begin{cases} \frac{\bar{\lambda}^i}{\Gamma(i)} \mathrm{d}^{i-1} e^{-\bar{\lambda}\mathrm{d}}, & \mathrm{d} > 0 \\ 0, & \text{otherwise} \end{cases} \tag{3.11}$$

where $\Gamma(.)$ represents the gamma function. The expected value of distance $\| \bar{y}_i - W_0 \|$ is:

$$\begin{aligned}\mathbb{E}[\| \bar{y}_i - W_0 \|] &= \int_{-\infty}^{\infty} \mathrm{d}\, f_{(\|\bar{y}_i - W_0\|)}(\mathrm{d}) d\mathrm{d} \\ &= \int_{0}^{\infty} \mathrm{d} \frac{\bar{\lambda}^i}{\Gamma(i)} \mathrm{d}^{i-1} e^{-\bar{\lambda}\mathrm{d}} d\mathrm{d} \\ &= \frac{\bar{\lambda}^i \Gamma(i+1)}{\Gamma(i)\bar{\lambda}^{i+1}}\end{aligned} \tag{3.12}$$

where $\frac{\Gamma(i+1)}{\Gamma(i)} = i$ and the desired result in Eq. (3.10) is reached. ■

To enhance the tractability, the total coverage of cells has been assumed to have a regular shape (e.g. circle) for estimating the handoff rate and the cell sojourn time in the cellular systems [21, 67, 72, 73]. This assumption holds in estimating the small cells coverage in the IRF deployment (the small cells are deployed on a different frequency from the macro cells), if the overlap coverage among the small cells are taken into consideration. Since the association between the first tier and the small cell tier is based on the minimum received power (Assumption 2 in Chapter 2), the coverage of small cells is independent of the distance to the MCBSs. It is assumed that the coverage of any small cell forms a circle (including some overlaps). Therefore the covered segment of $\mathcal{P}_0$ by the ith small cell with radius r_i and at distance τ_i from $\mathcal{P}_0$ can be obtained as:

$$C_i = \sqrt{4r_i^2 - 4\tau_i^2}, \qquad \tau_i \leq r_i \tag{3.13}$$

The coverage of each small cell is a random variable depending on the small cell's radius and the distance from its SCBS to the path. The PDF of any small cell coverage on $\mathcal{P}_0$ is derived in the following Lemma.

Definition 2 If $\mathcal{Y} = g(\mathcal{X})$ where $\mathcal{X}$ is a random variable with $f_{\mathcal{X}}(x)$ as a PDF. The PDF of the random variable $\mathcal{Y}$ can be obtained by using the transforming density function as $f_{\mathcal{Y}}(y) = f_{\mathcal{X}}(x(y))|\frac{dx}{dy}|$ if $f_{\mathcal{X}}(x) \geq 0$ for all x and $\int_{-\infty}^{\infty} f_{\mathcal{X}}(x)dx = 1$.

Lemma 5 The PDF of the ith small cell coverage on $\mathcal{P}_0$ can be expressed as:

$$f_{C_i}(c) = \frac{c}{4r_i^2\sqrt{1 - \frac{c^2}{4r_i^2}}} \tag{3.14}$$

where $0 \leq c \leq 2r_i$

Proof: Since the total coverage of the ith small cell on $\mathcal{P}_0$ is obtained in Eq. (3.13), and τ_i is uniformly distributed in $[0, r_i]$, the PDF of the coverage can be found similar to

Definition 2 as:

$$\begin{aligned} f_{C_i}(c) &= f_{\tau_i}(\tau(c_i))\,|\frac{d\tau}{dc}| \\ &\overset{(a)}{=} \frac{1}{r_i}\frac{d}{dc}\left(\sqrt{r_i^2 - \frac{c_i^2}{4}}\right) \end{aligned} \tag{3.15}$$

where $f_{\tau_i}(\tau) = 1/r_i$ is the PDF of the distance between the ith SCBS and $\mathcal{P}_0$, (a) follows from Eq. (3.13). The result in Eq. (3.14) is reached after solving Eq. (3.15). ■

The total coverage of small cells on $\mathcal{P}_0$ can be obtained as:

$$C_T = \sum_{i \in \bar{\Phi}} C_i \tag{3.16}$$

when $r_i = r$, the expected value of any small cell coverage crossed by $\mathcal{U}_0$ is obtained as:

$$\begin{aligned} \mathbb{E}[C] &= \int_0^\infty c f_c(c) dc \\ &= \int_0^{2r} \frac{c^2}{4r^2\sqrt{1 - \frac{c^2}{4r^2}}} dc \end{aligned} \tag{3.17}$$

The integral limits follow from that the maximum and the minimum coverage of any small cell with radius r on $\mathcal{P}_0$ are $2r$ and 0 respectively. Since all the small cells are randomly distributed and have the same distribution around $\mathcal{P}_0$ and the locations of the SCSBs are uncorrelated, the expected value of the total small cells coverage on the path can be obtained by summing up all the small cells crossed by $\mathcal{P}_0$ (linearity of expectation) as:

$$\mathbb{E}[C_T] = \frac{\bar{\lambda}\mathbb{E}[C]}{2\sqrt{\lambda_w}} \tag{3.18}$$

where $\frac{\bar{\lambda}}{2\sqrt{\lambda_w}}$ represents the expected number of path points on $\mathcal{P}_0$. The result in Eq. (3.18) includes some overlap coverage on $\mathcal{P}_0$. The overlaps can be ignored when the density of small cells is very low. However, it is anticipated that the small cells density in the future cellular networks is very high and the overlap coverage needs to be taken into consideration. Some overlaps will occur on $\mathcal{P}_0$ and the number of these overlaps depends on various parameters such as the density of small cells and the footprint of each small cell. Finding the overlap areas will not only help to estimate the cell sojourn time and the handoff rate precisely, but also help to find the fraction of time that any UE spends in the small cells coverage in order to estimate the energy consumption needed for the SCD process in the HetNets [4, 24]. Next, the overlap coverage on $\mathcal{P}_0$ is investigated.

Lemma 6 The expected value of one overlap coverage on $\mathcal{P}_0$ can be obtained as:

$$\mathbb{E}[\mathfrak{C}_i] = \frac{\mathbb{E}[\bar{C}_i]}{2} \tag{3.19}$$

where $\bar{C}_i = \frac{C_i}{2} + \frac{C_{i+1}}{2}$ is the maximum distance between $\bar{y}_i$ and $\bar{y}_{i+1}$ for the ith overlap to take place and, $\frac{C_i}{2}$ and $\frac{C_{i+1}}{2}$ are the half coverage of the ith small cell and the half coverage of the $(i+1)$th small cell on $\mathcal{P}_0$ respectively, as shown in Fig. 3.3.

Proof: See Appendix A.1. ■

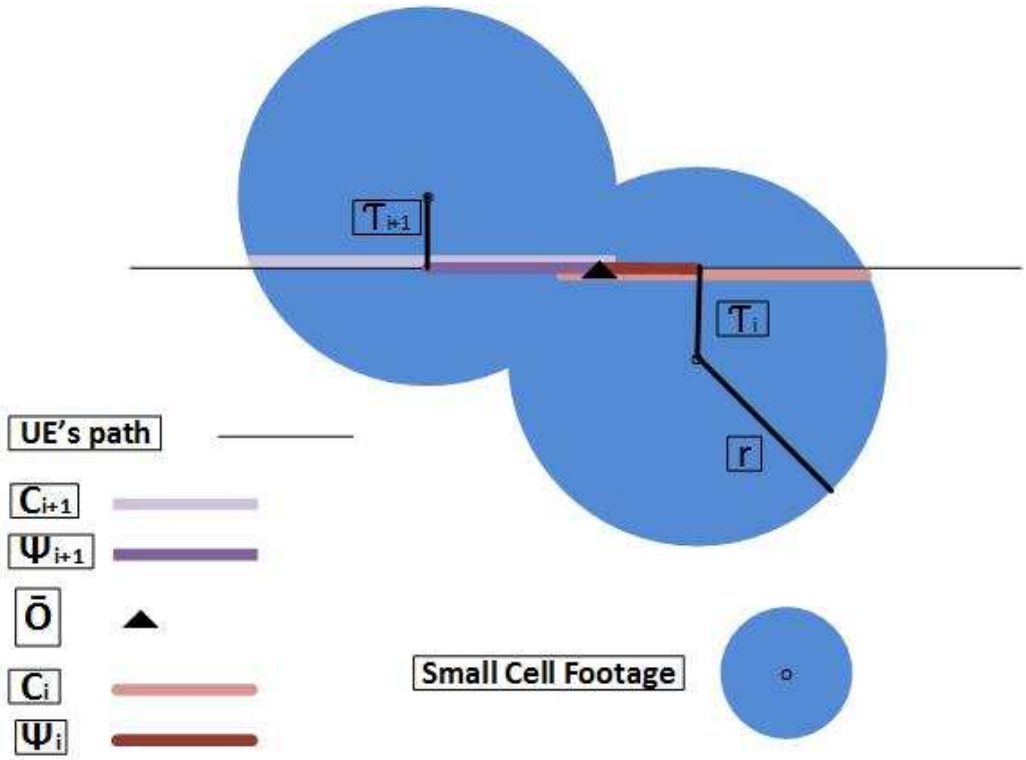

Figure 3.3: Overlap coverage on $\mathcal{P}_0$

After finding the expected value of any overlap coverage on $\mathcal{P}_0$ in Lemma 6, the expected number of overlaps taking place on $\mathcal{P}_0$ is obtained as follows.

Lemma 7 The expected number of overlaps on $\mathcal{P}_0$ can be expressed as:

$$\mathbb{E}[N_{OL}] = \mathbb{E}[N_{OL,max}]\left(1 - e^{-\bar{\lambda}\int_0^{4r} \bar{c}\, f_{\bar{C}_i}(\bar{c})\, d\bar{c}}\right) \tag{3.20}$$

where $\mathbb{E}[N_{OL,max}] = \mathcal{A}_1\left(\frac{\bar{\lambda}}{2\sqrt{\lambda_w}} - 1\right) + \frac{\mathcal{A}_{\bar{K}}}{2}\left(\frac{\bar{\lambda}}{\sqrt{\lambda_w}} - 1\right)$ and $f_{\bar{C}_i}(\bar{c})$ is the PDF of $\bar{C}_i$ and given in Eq. (A.1.2).

Proof: See Appendix A.2. ■

The expectation of the total transition time that $\mathcal{U}_0$ stays in the coverage of small cells during its movement on $\mathcal{P}_0$ with a constant speed $V = v$, can be obtained as:

$$\mathbb{E}[\mathcal{T}_0] = \frac{\mathbb{E}[C_T] - \mathbb{E}[C_{OL}]}{v} \tag{3.21}$$

where $\mathbb{E}[C_{OL}] = \mathbb{E}[N_{OL}]\mathbb{E}[\mathfrak{C}_i]$ is the expectation of the total overlap coverage on $\mathcal{P}_0$.

3.1.2 Multi-Tier Small Cell Network

In this subsection, we expand the one-tier small cell framework proposed in the previous subsection to a multi-tier small cell framework. Now we need to consider different densities and coverages of small cells. The analysis in this subsection will be based on the following definition.

Definition 3 Superposition of two independent PPPs is a PPP with intensity of the sum of both densities [28].

From Definition 3, the small cells from different tiers in the system form one PPP $\Phi_{\bar{K}}$ with density of $\lambda_{\bar{K}} = \sum_{m=2}^{K} \lambda_m$. Therefore, the small cells crossed by $\mathcal{U}_0$ from different tiers can also be interpreted as one MPP on $\mathbb{R}^+ \times [0, r_m]$, $\bar{\Phi}_{\bar{K}} = \{(\bar{z}_i, \tau_i)\}$ of intensity $\bar{\lambda}_{\bar{K}}$ where r_m takes a value in the range $[r_2, r_3, \cdots, r_m, \cdots, r_K]$. The density of path points on the straight line from the origin and passes through W_1 can be found similar to Lemma 3 as:

$$\begin{aligned} \bar{\lambda}_{\bar{K}} &= \sum_{m=1}^{\bar{K}} \bar{\lambda}_m \\ &= \sum_{m=1}^{\bar{K}} 2r_m \lambda_m \end{aligned} \tag{3.22}$$

If the path points on $\mathcal{P}_0$ are set in order $(\bar{z}_1, \bar{z}_2, \cdots, \bar{z}_i, \cdots, \bar{z}_{\bar{N}_0})$. The path points inter-distance has an exponential distribution with density $\bar{\lambda}_{\bar{K}}$:

$$\mathbb{P}(\| \bar{z}_i - \bar{z}_{i+1} \| \leq d) = 1 - \exp(-\bar{\lambda}_{\bar{K}} d) \qquad d > 0 \tag{3.23}$$

Given a small cell of the mth tier overlaps with another small cell on $\mathcal{P}_0$, the expected value of the overlap coverage can be obtained similar to Lemma 6 as follows.

Lemma 8 The expected value of one overlap occurring between the ith small cell of the mth tier and the $(i+1)$th small cell of the nth tier, can be found as:

$$\mathbb{E}[\mathfrak{C}_{mn}] = \frac{\sum_{n=2}^{K} \bar{\lambda}_n \mathbb{E}[\bar{C}_{mn}]}{2\bar{\lambda}_{\bar{K}}} \tag{3.24}$$

where $\bar{C}_{mn} = \frac{C_{m,i}}{2} + \frac{C_{n,i+1}}{2}$ is the maximum distance between $\bar{z}_i$ of the mth tier and $\bar{z}_{i+1}$ of the nth tier for the ith overlap to occur, $\frac{C_{m,i}}{2}$ and $\frac{c_{n,i+1}}{2}$ are the half coverage of the ith small cell of the mth tier and the half coverage of the $(i+1)$th small cell of the nth tier on $\mathcal{P}_0$ respectively, and $\frac{\bar{\lambda}_n}{\bar{\lambda}_{\bar{K}}}$ is the probability of the $(i+1)$th small cell being from the nth tier.

Proof: See Appendix A.3. ■

In the multi-tier small cell network, there are different small cells with different footprints and different densities crossed by $\mathcal{U}_0$ during its movement. The probability of a small cell of the mth tier overlapping with another small cell on $\mathcal{P}_0$ can be also found from the null probability and similar to Lemma 7 as:

$$\begin{aligned}
\mathbb{P}_{OL,mn} &= 1 - \prod_{n=2}^{K} \mathbb{P}\Big[\parallel \bar{z}_{n,i+1} - \bar{z}_{m,i} \parallel > \int_0^{2r_m+2r_n} \bar{c}\, f_{\bar{C}_{mn}}(\bar{c})\, d\bar{c}\Big] \\
&= 1 - \exp\Big(- \bar{\lambda}_{\bar{K}} \sum_{n=2}^{K} \frac{\bar{\lambda}_n}{\bar{\lambda}_{\bar{K}}} \int_0^{2r_m+2r_n} \bar{c}\, f_{\bar{C}_{mn}}(\bar{c})\, d\bar{c}\Big] \Big) \\
&= 1 - \exp\Big(- \sum_{n=2}^{K} \bar{\lambda}_n \int_0^{2r_m+2r_n} \bar{c}\, f_{\bar{C}_{mn}}(\bar{c})\, d\bar{c}\Big] \Big)
\end{aligned} \tag{3.25}$$

where $\exp\Big(-\sum_{n=2}^{K} \bar{\lambda}_n \int_0^{2r_m+2r_n} \bar{c}\, f_{\bar{C}_{mn}}(\bar{c})\, d\bar{c}\Big)$ represents the probability that the small cell of the mth tier does not overlap with the next small cell on $\mathcal{P}_0$. The expected number of overlaps can be expressed as:

$$\mathbb{E}[N_{OL}] = \mathbb{E}[N_{OL,max}] \frac{\sum_{m=2}^{K} \bar{\lambda}_m \mathbb{P}_{OL,mn}}{\bar{\lambda}_{\bar{K}}} \tag{3.26}$$

where $\frac{\bar{\lambda}_m}{\bar{\lambda}_{\bar{K}}}$ is the probability of the ith small cell being from the mth tier. Since the locations of the small cells crossed by $\mathcal{U}_0$ and their coverage are independent, the expectation of the total transition time that $\mathcal{U}_0$ spends in the small cells coverage when the speed is constant

$V = v$ becomes:

$$\begin{aligned}\mathbb{E}[\mathcal{T}_0] &= \frac{\mathbb{E}[C_T] - \mathbb{E}[C_{OL}]}{v} \\ &= \frac{1}{v}\sum_{m=2}^{K}\left(\frac{\bar{\lambda}_m \mathbb{E}[C_m]}{2\sqrt{\lambda_w}} - \mathbb{E}[N_{OL,max}]\sum_{n=2}^{K}\frac{\bar{\lambda}_m}{\bar{\lambda}_{\bar{K}}}\mathbb{P}^2_{OL,mn}\mathbb{E}[\mathfrak{C}_{mn}]\right)\end{aligned} \tag{3.27}$$

The result in Eq. (3.27) shows that the fraction of time that $\mathcal{U}_0$ spends in the small cells coverage does not only depend on the cell association and the total transition time as it was assumed in [20], but also depends on other system parameters such as transmit power and the density of each tier as well as the probability of an overlap occurring on $\mathcal{P}_0$.

3.2 Sojourn Time

The cell sojourn time is defined as the expected time that $\mathcal{U}_0$ stays in the coverage of a cell of interest and it directly affects the efficiency of system resources utilization. Since all transition lengths are i.i.d., the expected sojourn time will be derived during one transition time (e.g. $\| W_1 - W_0 \|$). The small cells crossed by $\mathcal{U}_0$ have different coverages on $\mathcal{P}_0$ as they have different transmit powers and they are located at different distances from $\mathcal{P}_0$. Since the cell association among the small cell tiers is based on the maximum received power, the overlap coverage will be served by different small cells depending on the transmit power and the locations of the SCBSs around the path. The expected value of the ith small cell's footprint of the mth tier, served by the $(i+1)$th small cell of the nth tier is obtained in the following Lemma.

Lemma 9 Given that an overlap occurs on the path between the ith small cell of the mth tier and the $(i+1)$th small cell of the nth tier, the expected value of the footprint of the ith small cell served by the $(i+1)$th small cell due to overlapping is expressed as:

$$\mathbb{E}[\chi_{n\mapsto m}] = \frac{\mathbb{E}[\mathfrak{C}_{mn}]\left(\frac{p_{2,m,rs}}{p_{2,n,rs}}\right)^{\frac{-1}{\alpha_m}}}{1 + \left(\frac{p_{2,m,rs}}{p_{2,n,rs}}\right)^{\frac{-1}{\alpha_m}}} \tag{3.28}$$

Proof: See Appendix A.4. ■

3.2.1 Small Cell Sojourn Time

The expectation of the small cell sojourn time when the pause time is zero can be expressed in the next Theorem.

Theorem 1 When λ_w is small, $V = v$ and $S = 0$, the average small cell sojourn time during one movement can be expressed as:

$$\mathbb{E}[\mathcal{ST}^0_{SCS}] = \sum_{m=1}^{\bar{K}} \frac{\bar{\lambda}_m}{\bar{\lambda}_{\bar{K}}} \left(\mathbb{E}[C_m] - \mathbb{P}_{OL,mn} \sum_{n=1}^{\bar{K}} \frac{\bar{\lambda}_n}{\bar{\lambda}_{\bar{K}}} \mathbb{E}[\chi_{n \mapsto m}] - \mathbb{P}_{OL,ma} \sum_{a=1}^{\bar{K}} \frac{\bar{\lambda}_a}{\bar{\lambda}_{\bar{K}}} \mathbb{E}[\chi_{a \mapsto m}] \right) \tag{3.29}$$

where $\mathbb{P}_{OL,mn}$ and $\mathbb{P}_{OL,ma}$ are the probability that the reference small cell of an mth tier overlaps with the $(i+1)$th small cell of the nth tier and the $(i-1)$th small cells of the ath tier on $\mathcal{P}_0$ respectively. C_m is the coverage of the reference small cell of the mth tier and its PDF is obtained in Lemma 5.

Proof: Given that the reference small cell is crossed by $\mathcal{U}_0$, the small cell sojourn time when $V = v$ and $\bar{K} = 1$ can be expressed as:

$$\mathcal{ST}^0_{SCS} = \frac{C_i - \psi}{v} \tag{3.30}$$

where ψ represents the footprint of the reference small cell on the path and served by other small cells due to overlapping. ψ can take a value between 0 when no overlap occurs, and C_i when one overlap or more occur with other small cells on the path. Given that the ith small cell has C_i coverage on the path and overlaps with other small cells, the expectation of ψ can be expressed as:

$$\mathbb{E}[\psi] = 2\mathbb{P}_{OL}\mathbb{E}[\chi] \tag{3.31}$$

where $\mathbb{P}_{OL}$ is obtained in Eq. (A.2.4), and $\mathbb{E}[\chi]$ is the expected value of the ith small cell's footprint served by the $(i+1)$th small cell or the $(i-1)$th small cell on the path and is obtained in Eq. (3.28). When $\bar{K} > 1$, the ith small cell can overlap with small cells of the nth tier and the expectation of the ith small cell's footprint of the mth tier served by a small cell of the nth tier becomes $\mathbb{P}_{OL,mn} \sum_{n=1}^{\bar{K}} \frac{\bar{\lambda}_n}{\bar{\lambda}_{\bar{K}}} \mathbb{E}[\chi_{n \mapsto m}]$. Therefore, the expectation $\mathbb{E}[\psi]$ can be obtained as:

$$\mathbb{E}[\psi] = \sum_{n=1}^{\bar{K}} \frac{\bar{\lambda}_n \mathbb{P}_{OL,mn}}{\bar{\lambda}_{\bar{K}}} \mathbb{E}[\chi_{n \mapsto m}] + \sum_{a=1}^{\bar{K}} \frac{\bar{\lambda}_a \mathbb{P}_{OL,ma}}{\bar{\lambda}_{\bar{K}}} \mathbb{E}[\chi_{a \mapsto m}] \tag{3.32}$$

Since the locations of the SCBSs are uncorrelated and the expected value of the small cell sojourn time in any small cell of the mth tier can be expressed as:

$$\mathbb{E}[\mathcal{ST}^0_{SCS,m}] = \frac{1}{v}\Big(\mathbb{E}[C_m] - \mathbb{E}[\psi]\Big) \tag{3.33}$$

Since there are $\bar{K}$ small cell tiers, the expected value of the small cell sojourn time in any small cell during one transition when $V = v$, can be expressed as:

$$\mathbb{E}[\mathcal{ST}^0_{SCS}] = \sum_{m=1}^{\bar{K}} \frac{\mathbb{E}[\mathcal{S}^0_{SCS,m}]\bar{\lambda}_m}{\bar{\lambda}_{\bar{K}}} \tag{3.34}$$

The result in Eq. (3.29) is reached. ■

Before we derive the small cell sojourn time in a multi-tier small cell network when $S \neq 0$, the probability of $\mathcal{U}_0$ spending the pause time in the coverage of the reference small cell is given. When $S > 0$, some of the pause time will be spent in the small cells coverage as shown in Lemma 2. Since the waypoints are distributed randomly as a PPP on the plane with density λ_w, and the locations of the SCBSs are also distributed as PPP with density $\lambda_{\bar{K}}$, the probability that $\mathcal{U}_0$ spends the pause time in the small cell of interest can be found as follows.

Lemma 10 The probability that $\mathcal{U}_0$ spends the pause time in the reference small cell is the probability of the destination point (W_1) served by the reference small cell:

$$\mathbb{P}_{\mathcal{S},m} = \frac{2\pi\left(\frac{\rho_{min}}{\mathscr{L}_2 p_{2,m,rs}}\right)^{-\frac{2}{\alpha_m}}}{\mathscr{A}_m\left(\sum_{n=2}^{K}\left(\frac{p_{2,n,rs}}{p_{2,m,rs}}\right)^{\frac{2}{\alpha_m}} + 1\right)} \tag{3.35}$$

Proof: See Appendix A.5. ■

Next, we find the average small cell sojourn time during one movement as follows.

Theorem 2 The expected sojourn time that $\mathcal{U}_0$ spends in any small cell when $S \neq 0$ and $V = v$ can be expressed as:

$$\mathbb{E}[\mathcal{ST}_{SCS}] = \sum_{m=1}^{\bar{K}} \frac{\bar{\lambda}_m}{\bar{\lambda}_{\bar{K}}}\Big(\mathcal{A}_{\bar{K}}\mathbb{E}[\mathcal{ST}^s_{SCS,m}] + \mathcal{A}_1\mathbb{E}[\mathcal{ST}^0_{SCS,m}]\Big) \tag{3.36}$$

where $\mathbb{E}[\mathcal{ST}^s_{SCS,m}] = \mathbb{P}_{\mathcal{S},m}\Big(\mathbb{E}[S]+\mathbb{E}[\mathcal{ST}^0_{SCS,m}]\Big)+\Big(1-\mathbb{P}_{\mathcal{S},m}\Big)\mathbb{E}[\mathcal{ST}^0_{SCS,m}]$ is the expectation of the mth cell sojourn time when $S \neq 0$ and $\mathbb{E}[\mathcal{ST}^0_{SCS,m}]$ is obtained in Eq. (3.33).

Proof: When W_1 is located in the small cells coverage with a probability of $\mathcal{A}_{\bar{K}}$, $\mathcal{U}_0$ spends the pause time in the coverage of the small cell of the mth tier with a probability of $\mathbb{P}_{\mathcal{S},m}$. The expectation of the total sojourn time that $\mathcal{U}_0$ resides in any small cell can be obtained in Eq. (3.36). ■

The above results are more suitable for small values of λ_w as $\mathcal{U}_0$ is expected to cross a number of small cells during one movement as shown in Fig. 3.4. The larger values of λ_w are suitable for users walking [21]. The small cell sojourn time when the actual coverage of each small cell is assumed to have a hexagonal shape (this assumption does not affect the accuracy of the analysis [67]) can be obtained as:

$$\mathbb{E}[\mathcal{ST}_{SCL}] = \frac{4\sqrt{\lambda_w}\mathbb{E}[\mathcal{T}_T]}{\pi}\Big(\int_0^{\frac{\mathcal{Q}}{2}}\int_0^{\frac{\sqrt{3}\mathcal{Q}}{2}} \bar{f}(\mathfrak{x},\mathfrak{y})d\mathfrak{x}d\mathfrak{y} + \int_{\frac{\mathcal{Q}}{2}}^{\mathcal{Q}}\int_0^{-\sqrt{3}\mathfrak{x}+\sqrt{3}\mathcal{Q}} \bar{f}(\mathfrak{x},\mathfrak{y})d\mathfrak{x}d\mathfrak{y}\Big) \quad (3.37)$$

where $\bar{f}(\mathfrak{x},\mathfrak{y}) = e^{-\lambda_w\pi(\mathfrak{x}^2+\mathfrak{y}^2)}/\sqrt{\mathfrak{x}^2+\mathfrak{y}^2}$ is the spatial UE distribution between W_0 and W_1 and is derived in [21,74], $\mathbb{E}[\mathcal{T}_T] = \mathbb{E}[\mathcal{T}_{t,l}]+\mathbb{E}[S]$, $\mathcal{Q} = \sum_{m=1}^{\bar{K}} \frac{\bar{\lambda}_m}{\bar{\lambda}_{\bar{K}}}\big(r_m - \sum_{n=1}^{\bar{K}} \frac{\mathbb{P}_{OL,mn}\bar{\lambda}_n}{\bar{\lambda}_{\bar{K}}}\mathbb{E}[\chi_{n\mapsto m}]\big)$ is found similar to Lemma 9.

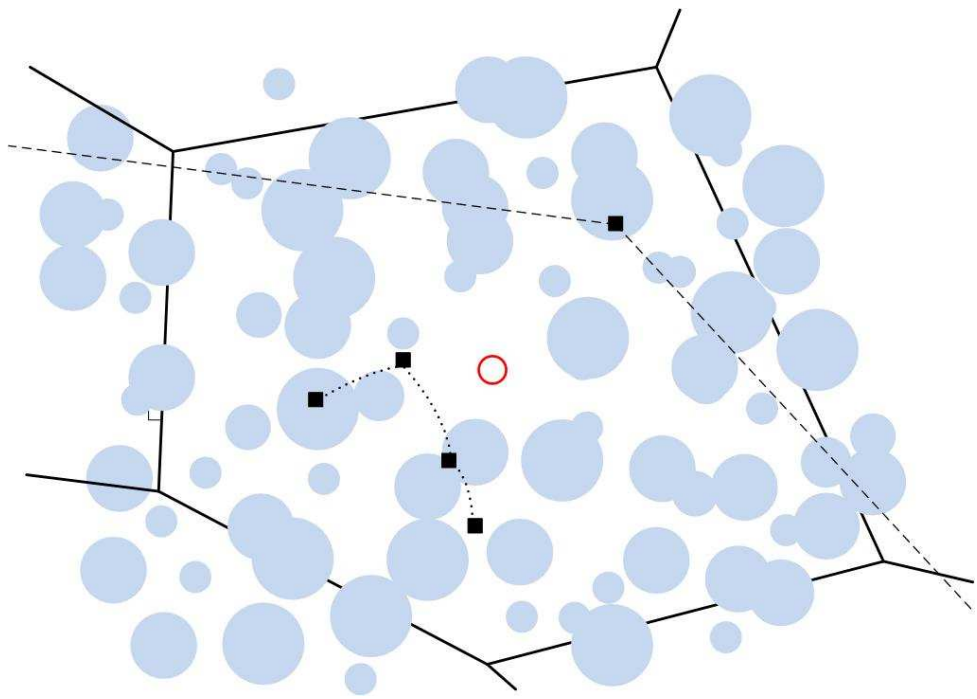

Figure 3.4: The cell sojourn time. Red circles represent the locations of the MCBSs, blue dots represent the small cells coverage (different small cell tiers), black squares represent the waypoints, and the black dashed and the black dotted lines represent the reference UE's path between any two waypoints for a small value of λ_w and a large value of λ_w respectively.

3.2.2 Macro Cell Sojourn Time

Deploying dense small cells in the network will not only affect the small cell sojourn time but also affect the macro cell sojourn time. Since the macro cells form VTCs, the expectation of the macro cell sojourn time can be obtained as:

$$\mathbb{E}[\mathcal{ST}_{MC}] = \frac{\mathbb{E}[\mathcal{T}_T]}{\bar{\lambda}_{\bar{K}} + \lambda_{MCB}} \Big(\lambda_{MCB} \int_0^{2\pi} \int_0^{R_{MC}} f(\mathfrak{r}, \theta) d\mathfrak{r} d\theta + \bar{\lambda}_{\bar{K}} \int_0^{2\pi} \int_0^{\mathcal{D}_{SC}} f(\mathfrak{r}, \theta) d\mathfrak{r} d\theta \Big) \tag{3.38}$$

where R_{MC} is the average macro cell radius, $\lambda_{MCB} = \frac{2}{\sqrt{\pi} R_{MC}}$ is the length intensity of the macro-macro boundaries [39], $f(\mathfrak{r}, \theta) = \frac{\sqrt{\lambda_w}}{\pi \mathfrak{r}} e^{-\lambda_w \pi \mathfrak{r}^2}$ is the spatial UE distribution when $S = 0$ [21], $\frac{\lambda_{MCB}}{\lambda_{\bar{K}} + \lambda_{MCB}}$ ($\frac{\lambda_{\bar{K}}}{\lambda_{\bar{K}} + \lambda_{MCB}}$) represents the probability that $\mathcal{U}_0$ reaches the macro-macro (macro-small) boundaries before the macro-small (macro-macro) boundaries, and $\mathcal{D}_{SC}$ is the expectation of the distance to the nearest small cell coverage on the path and obtained as:

$$\begin{aligned} \mathcal{D}_{SC} &= \int_0^{\infty} l \frac{d}{dl} \Big(1 - \exp\Big(- \bar{\lambda}_{\bar{K}} \big(l - \sum_{m=2}^{K} \frac{\bar{\lambda}_m \mathbb{E}[C_m]}{2 \bar{\lambda}_{\bar{K}}} \big) \Big) dl \\ &= \int_0^{\infty} l \bar{\lambda}_{\bar{K}} \exp\Big(- \bar{\lambda}_{\bar{K}} l + \sum_{m=2}^{K} \frac{\bar{\lambda}_m \mathbb{E}[C_m]}{2} \Big) dl \\ &= \frac{\exp\Big(\sum_{m=2}^{K} \frac{\bar{\lambda}_m \mathbb{E}[C_m]}{2} \Big)}{\bar{\lambda}_{\bar{K}}} \end{aligned} \tag{3.39}$$

where $\Big(1 - \exp\Big(- \bar{\lambda}_{\bar{K}} \big(l - \sum_{m=2}^{K} \frac{\bar{\lambda}_m \mathbb{E}[C_m]}{2 \bar{\lambda}_{\bar{K}}} \big) \Big)$ is the probability of that the first path point of the small cell with an expected coverage of $\sum_{m=2}^{K} \frac{\bar{\lambda}_m \mathbb{E}[C_m]}{\bar{\lambda}_{\bar{K}}}$ is at distance greater than l.

3.3 Handoff Rate

The handoff rate is defined as the expected number of handoffs taking place per unit time. It is considered to be one of the important parameters in the cellular systems as it affects the amount of signalling. Increasing the number of UEs and the number of small cells in the system will affect the amount of signalling significantly and also affect the QoS. It is also anticipated that the first tier will have to deal with a large number of UEs, therefore an accurate framework will help in network dimensioning and also to

estimate the required resources at the first tier. We introduce the IRH rate and the IAH rate to reflect the required resources at the first tier. The IRH is defined as the number of handoffs taking place between cells using different frequencies (e.g. small cell to macro cell and/or macro cell to small cell). The IAH is defined as the number of handoffs taking place between cells of the same frequency (e.g. macro cell to macro cell or/and small cell to small cell). In this chapter, we consider the IAH rate among the small cells since the handoff rate in the first tier was already studied in [21]. The total expected handoff rate in a multi-tier HetNet is defined as the expected number of handoffs during one movement.

$$\mathbb{E}[\mathcal{H}_T] = \mathbb{E}[\mathcal{H}_{IR}] + \mathbb{E}[\mathcal{H}_{IA}] = \frac{\mathbb{E}[N_{HF}]}{\mathbb{E}[\mathcal{T}_{t,l}]} \tag{3.40}$$

where $\mathcal{T}_{t,l}$ represents the total time that $\mathcal{U}_0$ needs to travel along $\mathcal{P}_0$ and its expectation is obtained in Eq. (2.9) and in Eq. (2.10), N_{HF} represents the number of handoffs that $\mathcal{U}_0$ experiences during its movement along $\mathcal{P}_0$, and $\mathcal{H}_{IR}$ and $\mathcal{H}_{IA}$ represent the IRH rate and the IAH rate respectively. $\mathcal{U}_0$ can experience up to $2N_0$ handoffs during its movement (maximum of $2N_0$ handoffs take place when there is no overlap on $\mathcal{P}_0$). The expectations of both the IRH rate and the IAH rate are obtained as follows.

Theorem 3 The expected IRH rate can be expressed as:

$$\mathbb{E}[\mathcal{H}_{IR}] = \frac{2\mathcal{A}_1 + \mathcal{A}_{\bar{K}}}{2\mathbb{E}[\mathcal{T}_{t,l}]}\Big(2\mathbb{E}[N_0] - \mathbb{E}[N_{OL}]\Big) - \frac{\mathcal{A}_{\bar{K}}}{2\mathbb{E}[\mathcal{T}_{t,l}]}\Big(2\mathbb{E}[N_0] - \mathbb{E}[N_{OL}] - 1\Big) - \mathbb{E}[N_{OL}] \tag{3.41}$$

where $\mathcal{A}_{\bar{K}}$ and $\mathcal{A}_1$ are the probabilities that the destination point W_1 is located in the coverage of the small cells and the coverage of the first tier respectively as shown in Lemma1.

Proof: The IAH rate is defined as the number of handoffs between cells operating on the same frequency during one movement divided by the total time of movement. Since the IAH takes place on the high frequency F_2 when $\mathcal{U}_0$ moves between small cells overlapped on $\mathcal{P}_0$, the number of IAH can also be interpreted as the total number of overlaps on $\mathcal{P}_0$. Therefore, the expectation of the number of IAHs in a multi-tier small cells network can be obtained in Eq. (3.26). Since some of the handoffs will be between two small cells due to overlaps, the total number of handoffs can be expressed as $2N_0 - N_{OL}$. On the other hand, $\mathcal{U}_0$ will either leave the last small cell on the path and experience the last handoff

with a probability of $\mathcal{A}_1$, stay in the coverage of the last small cell with a probability of $\frac{\mathcal{A}_{\bar{K}}}{2}$, or it will enter another small cell coverage with a probability of $\frac{\mathcal{A}_{\bar{K}}}{2}$. Therefore the expectation of the total handoff rate becomes:

$$\mathbb{E}[\mathcal{H}_T] = \frac{2\mathcal{A}_1 + \mathcal{A}_{\bar{K}}}{2\mathbb{E}[\mathcal{T}_{t,l}]}\Big(2\mathbb{E}[N_0] - \mathbb{E}[N_{OL}]\Big) - \frac{\mathcal{A}_{\bar{K}}}{2\mathbb{E}[\mathcal{T}_{t,l}]}\Big(2\mathbb{E}[N_0] - \mathbb{E}[N_{OL}] - 1\Big) \tag{3.42}$$

The desired result in Eq. (3.41) is reached after substituting Eq. (3.42) in Eq. (3.40). ■

3.4 Results

In this section, simulation and numerical results are presented to show the impact of different parameters such as the waypoint density λ_w, the transmit power of small cells, the number of small cell tiers and the density of the small cells in the system on the handoff rate and the cell sojourn time. Some figures in this section include two scenarios. The first scenario (A) represents the analysis in this paper which considers the overlaps among the small cells. The second scenario (B) represents the analysis when the overlaps are ignored. The different system parameters can be found in Table 3.1, unless given otherwise.

Fig. 3.5 shows the accuracy of the analytical results. The expectation of the path points inter-distance is shown when a different number of small cell tiers and different values of the small cells density are deployed in the system. Fig. 3.5 shows that the assumption of the path points forming a PPP with density of $\sum_{m=1}^{\bar{K}} 2r_m\lambda_m$ is very accurate. It is also shown that the path points inter-distance decreases when the density of small cells increases for a different number of tiers. This is because the distances among the small cells in the system are minimized and the reference UE crosses more small cells during its movement when the small cell density increases.

Table 3.1: System Parameters

Parameter	Symbol	Value
Minimum received power	ρ_{min}	-90 dBm
MCBS density	λ_1	0.5 MCBS/km^2
SCBS density	λ_2	40 SCBS/km^2
RSs transmit power from F_2	$p_{2,2,rs}$	33 dBm
RSs transmit power from F_1	$p_{1,2,rs}$	19 dBm Eq. (4.15)
UE baseline transmit power	p_c	20 dBm
Number of small cell tiers	$\bar{K}$	1
Waypoint density	λ_w	0.001 waypoints/km^2
Path-loss exponent	α_k	4
UE's speed	v	5 km/h
Number of high frequency channels	$\mathcal{F}$	1
Minimum time for beneficial offloading	t_{min}	0
Low frequency	F_1	2 GHz
High frequency	F_2	10 GHz
Power control factor	ϵ	0.5
IAF scan periodicity	t_{p_A}	0.2 Sec
Energy cost for one IRF scan	E_s	2.25 mJ [54, 75]
UE density	λ_u	200 UEs/km^2
Pause time	S	0

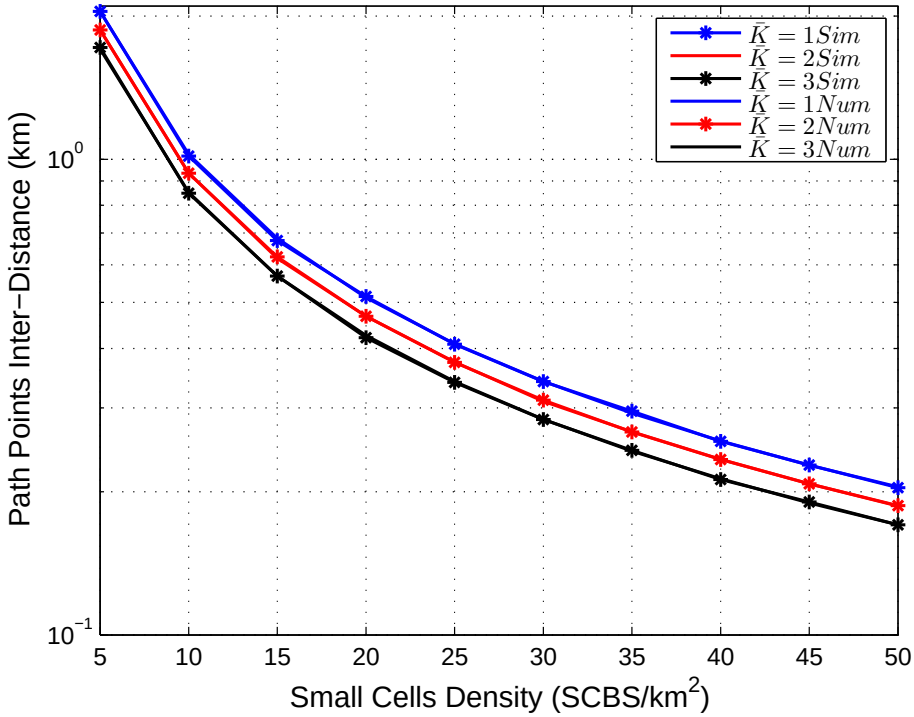

Figure 3.5: The path points inter-distance assumption in a single- and multi-tier HetNet.

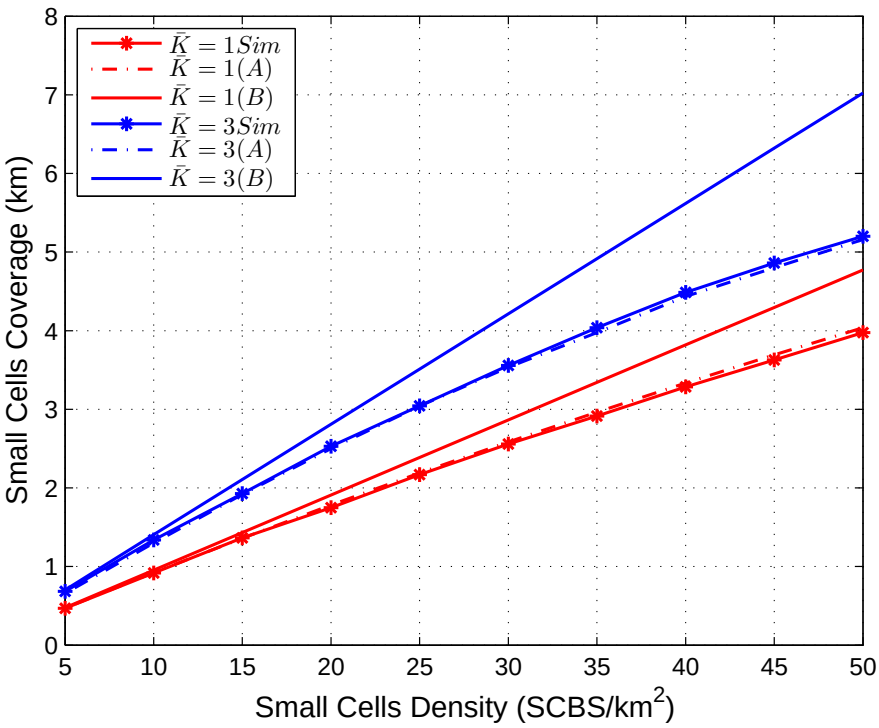

Figure 3.6: The small cells coverage, where (A) considering cell overlap, (B) not considering cell overlap.

Fig. 3.6 shows the total coverage of the small cells in the both scenarios (A) and (B) for a different number of tiers and different values of the small cell density. The coverage of the small cells on the reference UE's path increases when the density of small cells increases in (A) and (B). However, the coverage of small cells in (B) is doubled when the density of small cells is doubled, while the pace of increment slows down in (A) when the density increases due to overlaps. As a result, the gap between the result in (A) and result in (B) increases when the density of small cells increases for a different number of tiers. On the other hand, it is shown that the gap between (A) and (B) is greater when $K = 4$ for the same small cell density. It is likely to have larger overlap coverage when considering small cells with larger footprints (higher transmit power). Fig. 3.6 also shows that the overlap coverage can be neglected when the density of the small cells is very low, however, the overlap coverage increases in the dense small cell networks and ignoring the overlap coverage will affect the accuracy of the small cells coverage in these networks.

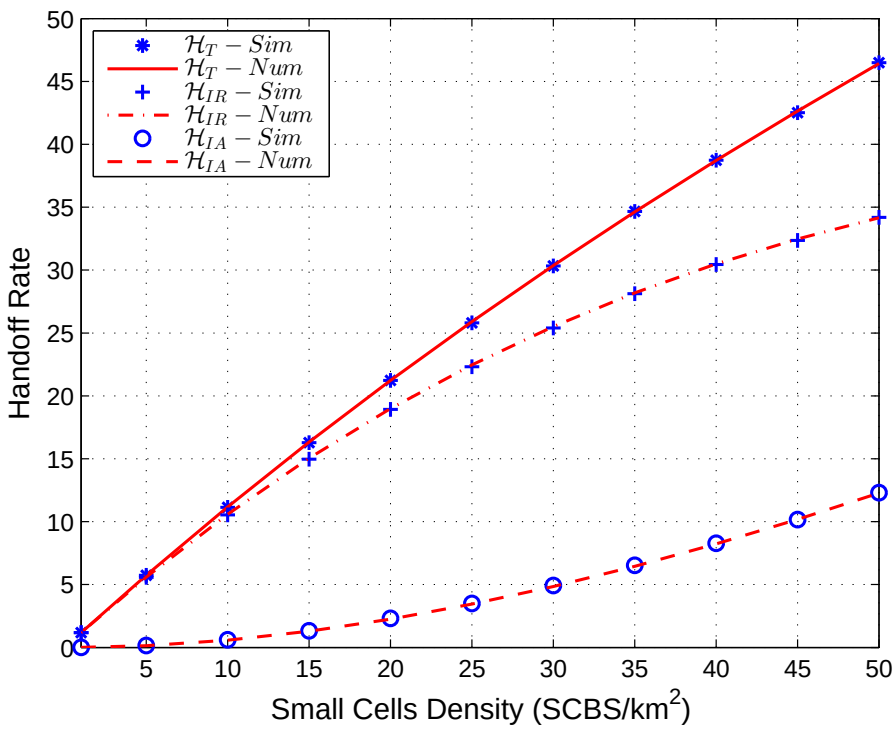

Figure 3.7: IRH rate, IAH rate and total handoff rate, where $\bar{K} = 3$.

Fig. 3.7 shows the total handoff rate, the IRH rate and the IAH rate for different values of the small cell density when $\bar{K} = 3$. As expected, it is shown that the total

handoff rate increases when the density of the small cells increases as the UEs will cross more small cells in the denser small cell network. Fig. 3.7 also shows the impact of the small cell density on the IAH rate and the IRH rate. For low small cell density, most of the handoffs are IRHs, from or to the first tier (macro cells). Although increasing the small cell density will maximize the total handoff rate, it turns some of these handoffs to IAHs due to some overlaps. Increasing IAH means a greater fraction of the handoffs and their cost (e.g. signalling) will be handled by the other tiers.

When ignoring the overlaps on the path, all the IAHs will be counted as IRHs and the accuracy of the total handoff rate will be affected significantly in the dense small cell network. Fig. 3.8 shows a comparison between the scenario (A) and the scenario (B) in terms of total handoff rate. The total handoff rate in (B) is always greater, as the overlaps are ignored and two IRHs are assumed to take place for each small cell (one IRH for entering the small cell and another one for leaving it). In fact, one IRH or no IRH is required when the reference UE moves among two or three overlapped small cells on the path.

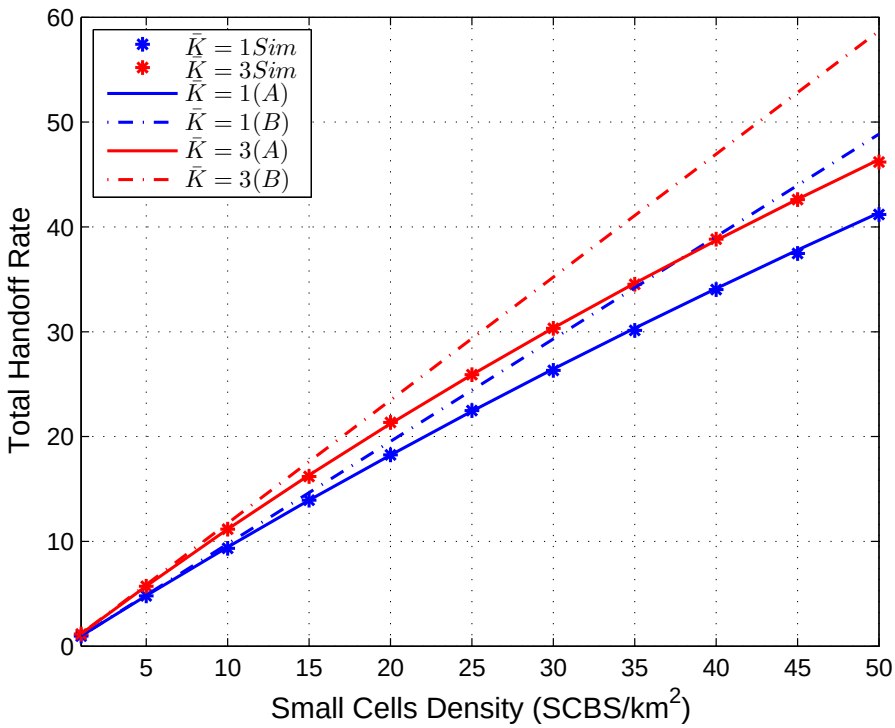

Figure 3.8: Total handoff rate, where (A) considering cell overlap and (B) not considering cell overlap.

Fig. 3.9 illustrates the fraction of the handoffs that the first tier is involved in, which is expressed as a ratio of the IRH rate to the total handoff rate for different small cell transmit powers. The fraction of handoffs that the first tier needs to handle decreases when the density of small cells increases, for instance, when $p_{2,2,rs} = 37$ dBm, less than 65% of the handoffs will be managed by the first tier when $\lambda_2 = 50$ while over 80% and 95% of the handoffs will be managed by the first tier when $\lambda_2 = 25$ and $\lambda_2 = 5$ respectively. Fig. 3.9 also shows that when the footprint of the small cell increases (higher transmit power), the fraction of the handoffs managed by the first tier decreases. This is because more overlaps are more likely to occur when the footprint of the small cell is larger for the same small cell density.

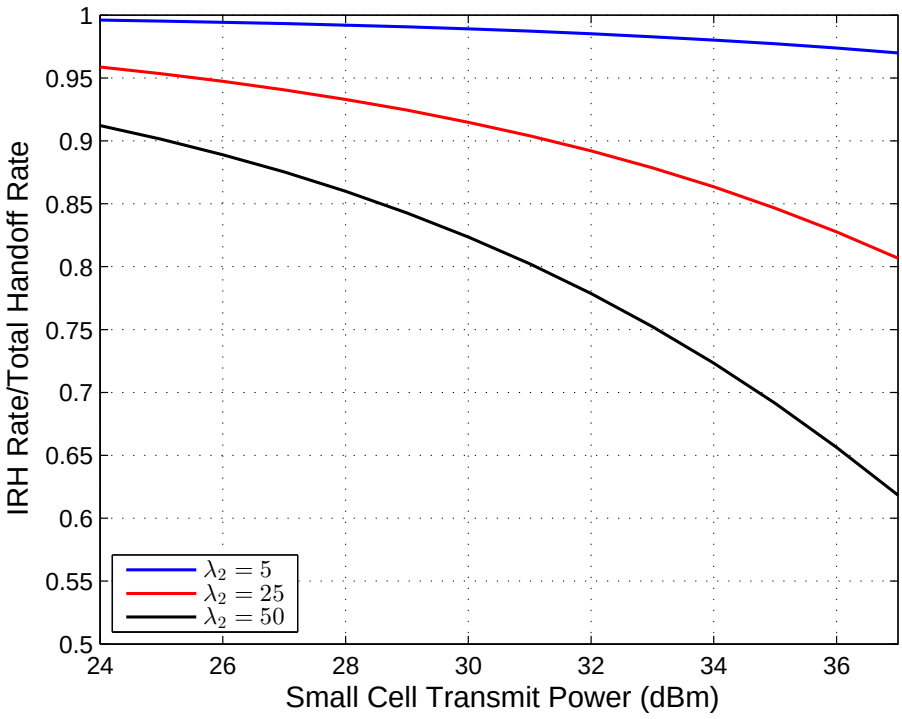

Figure 3.9: The ratio of IRH rate to total handoff rate where $\bar{K} = 1$.

The number of handoffs for different values of the small cell density and different values of the mobility parameter λ_w is shown in Fig. 3.10. It is shown that the total number of handoffs during one movement increases when the mobility parameter decreases. This is because the expected distance that the reference UE needs to travel from the starting point to the destination point decreases when λ_w increases as shown in Eq. (2.10). It can be also

seen from Fig. 3.10 that the number of IRHs for different values of λ_w starts increasing dramatically with low and medium small cell density while the number of IAHs increases slightly with low and medium density of small cells. However, the number of IRHs starts dropping with high density of small cells around the density of 65 for all values of λ_w. It can furthermore be observed that higher the value of λ_w, the more gradually the number of IRHs decreases. The number of IAHs keeps increasing until it exceeds the number of IRHs. Note that IAHs exceeds IRHs at different small cell densities when different values of λ_w are considered. For instance, the number of IAHs exceeds the number of IRHs at a small cell density of 75 when $\lambda_w = 0.01$, while the number of IAHs exceeds the number of IRHs at a small cell density of 90 when $\lambda_w = 1$. This is because the effect of the tier association on the number of IAHs and IRHs is greater when the number of the crossed small cells is smaller (greater value of λ_w) since the number of overlaps on the path is a function of the cell association as shown in Eq. (3.20).

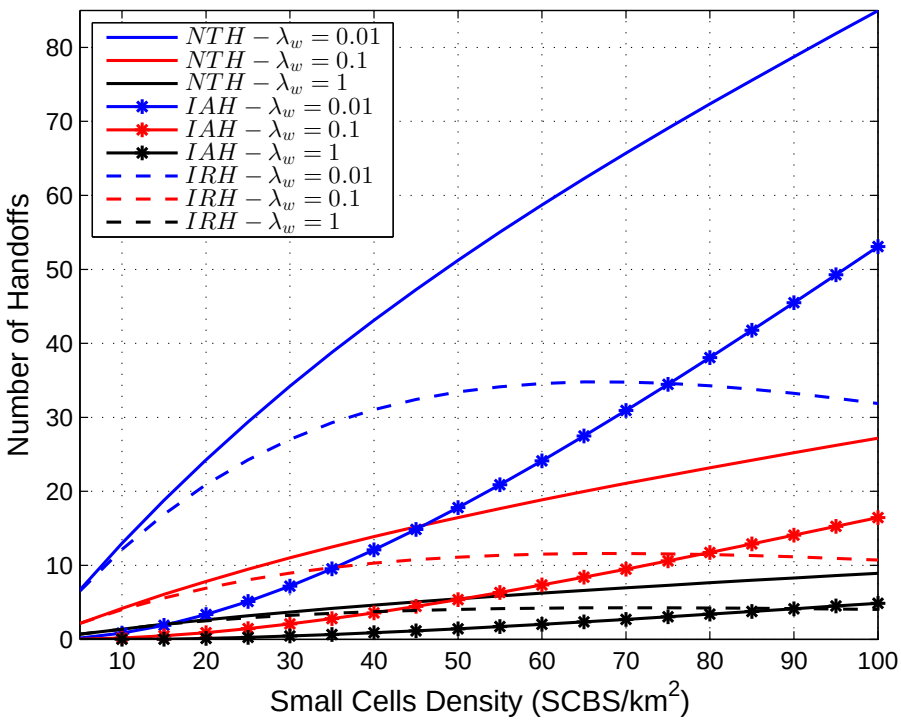

Figure 3.10: Number of IAHs, IRHs and total handoffs (NTH), where $\bar{K} = 3$.

The expectation of the small cell sojourn time when $\lambda_w = 0.01$ and $\lambda_w = 100$ are shown in Fig. 3.11 and Fig. 3.12. It is seen that the scenario (A) is very accurate in different

densities of HetNets and the small cell sojourn time is minimized in the dense HetNet due to the small cells overlapping. Furthermore, it is also seen that when the overlaps are ignored, e.g. scenario (B) [67], the small cell sojourn time becomes independent of the small cell density. However, our analysis (A) and the simulations show that the small cell sojourn time is not only affected by the number of tiers and the small cells' footprints, but also affected by the small cell density in the network. The gap between the two scenarios (A) and (B) increases when the small cell density increases and/or the transmit power of the small cells increases. This implies that the analysis becomes very inaccurate when ignoring the overlaps.

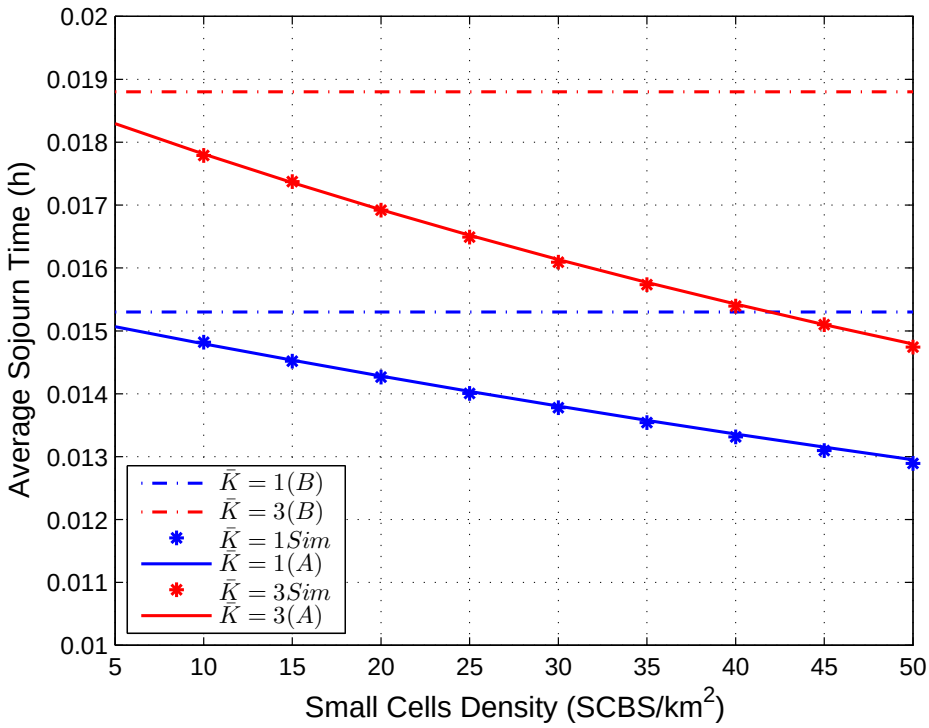

Figure 3.11: The small cell sojourn time, where (A) considering cell overlap, (B) not considering cell overlap.

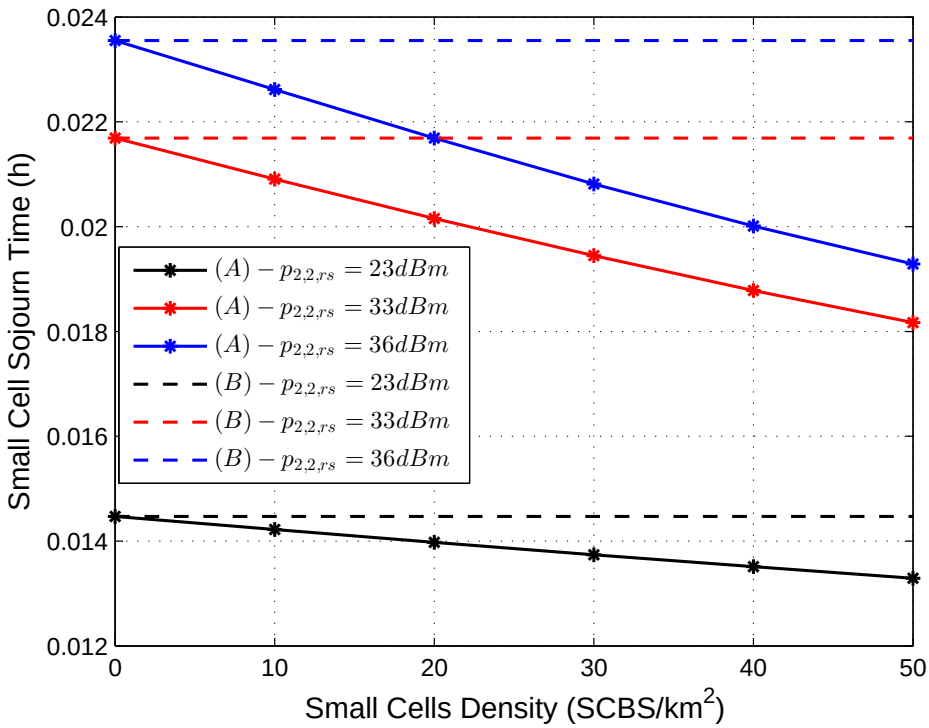

Figure 3.12: The small cell sojourn time, where (A) our analysis, (B) from [67], $\lambda_w = 100$ and $S = 60$ sec.

Fig. 3.13 shows the macro cell sojourn time for different values of the mobility parameter λ_w. In this figure, two scenarios are considered, the first scenario shows the impact of the small cells with different densities on the macro cell sojourn time. The second scenario $(No - SCs)$ represents the macro cell sojourn time when no small cells are deployed in the network [21]. It can be seen that when the small cell density increases the macro cell sojourn time decreases. In the single-tier network (e.g. $No - SCs$ scenario), the macro cell sojourn time depends on the macro cell density and the total transition time, while the macro cell sojourn time in the HetNets is affected by the density and the footprints of the small cells in addition to the macro cell density and the total transition time. Deploying more small cells will minimize the macro cell sojourn time as the probability of the UEs encountering the macro-small boundaries is greater than the probability of they encountering the macro-macro boundaries in a dense small cell network.

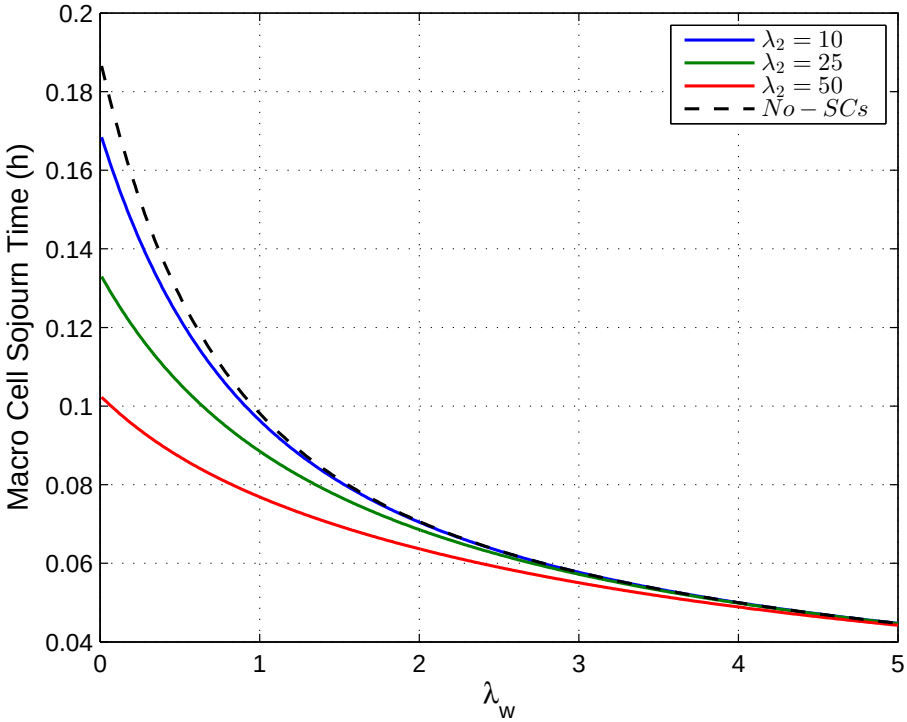

Figure 3.13: The macro cell sojourn time, where $No - SCs$ represents the result from [21], $R_{MC} = 1$ km and $\bar{K} = 1$.

Chapter 4

Uplink Energy Efficiency

Contents

In this chapter, the total energy consumption, the offloading loss and the achievable data rate are derived in a two-tier HetNet by taking into consideration the impact of the IRF scan periodicity (t_p).

4.1 Offloading Loss

In this section, the offloading loss is investigated as it is considered to be one of the important issues that the SCD faces. It is shown in Chapter 3 that $\mathcal{U}_0$ travels $\mathcal{T}_0$ in the second tier coverage ($\mathcal{T}_0$ can also be defined as the potential offloading time along $\mathcal{P}_0$). It is expected that $\mathcal{U}_0$ is associated to the second tier shorter time than the potential offloading time $\mathcal{T}_0$. This is because $\mathcal{U}_0$ needs to perform the IRF scan to discover every small cell on the path before the offloading to the second tier is initiated. The offloading loss can also be defined as $\mathcal{U}_0$ fails to detect small cells when entering their coverage, as a result it misses offloading to these small cells completely or partly. This is because of the long periodicity of the IRF scan (high value of t_p) and/or the high mobility of $\mathcal{U}_0$. Although UEs sometimes need to repeat the scan for more accurate measurements, it is assumed that $\mathcal{U}_0$ discovers the small cells from the first IRF measurements in their coverage. Assume that t_{min} is the minimum time needed to consider the offloading beneficial (the offloading procedure costs a significant amount of signalling at both the UE's side and network's side), or it can also be defined as the minimum time needed to complete the offloading procedure successfully. During its movement, $\mathcal{U}_0$ moves with speed v and performs scanning every t_p. The offloading is considered useful if $\mathcal{U}_0$ stays associated to the small cell for t_{min}. Since the small cells are randomly distributed around $\mathcal{P}_0$, the small cells can be grouped into three groups according to the time that $\mathcal{U}_0$ with speed v travels in their coverages. $\mathcal{U}_0$ travels at least $t_p + t_{min}$ in each small cell of the first group (Ξ_1), $\mathcal{U}_0$ travels between $t_p + t_{min}$ and t_{min} in each small cell of the second group (Ξ_2), and $\mathcal{U}_0$ travels less than t_{min} in each small cell of the third group (Ξ_3).

Therefore $\mathcal{U}_0$ misses each small cell of Ξ_1 partly from 0 to t_p as it enters the coverage of each small cell at a random time between two IRF scans. The expected value of the time missed by $\mathcal{U}_0$ from each small cell of Ξ_1 can be obtained as:

$$\begin{aligned}\mathbb{E}[T_{\Xi_1}] &= P_{\Xi_1} \int_0^{t_p} t_1 f_{t_1}(t) dt \\ &= \Big(1 - \int_0^{C_{mp}} f_C(c) dc\Big) \int_0^{t_p} t_1 f_{t_1}(t) dt\end{aligned} \tag{4.1}$$

where $f_{t_1}(t)$ is the PDF of the missed time from any small cell coverage which is assumed to be uniformly distributed in the range $[0, t_p]$, P_{Ξ_1} is the probability that any small

cell crossed by $\mathcal{U}_0$ belongs to Ξ_1, which can also be interpreted as the probability that $\mathcal{U}_0$ travels at least $C_{mp} = vt_{mp}$ in any small cell coverage, $t_{mp} = t_p + t_{min}$ and $f_C(c)$ is obtained in Eq (3.14). $\mathcal{U}_0$ travels t_2 in any small cell coverage of Ξ_2, where $t_{min} \leq t_2 < t_{mp}$. Therefore, it misses the coverage of these small cells partly or completely. The expected value of the time missed from a small cell of Ξ_2 can be expressed as:

$$\begin{aligned}\mathbb{E}[T_{\Xi_2}] &\overset{(a)}{=} P_{\Xi_2}\mathbb{E}_{t_2}\Big(\Big(1-\frac{t_2}{t_{pm}}\Big)t_2 + \frac{t_2}{t_{pm}}\int_0^{t_2} t f_t(t)dt\Big) \\ &\overset{(b)}{=} \frac{\Big(P_{\Xi_1} - \int_0^{C_{min}} f_C(c)dc\Big)}{v}\int_{C_{min}}^{C_{mp}} c\Big(c - \frac{c^2}{2vt_{pm}}\Big)f_C(c)dc\end{aligned} \tag{4.2}$$

where P_{Ξ_2} is the probability that any small cell belongs to Ξ_2, $C_{min} = vt_{min}$, the first term and the second term in (a) represents that $\mathcal{U}_0$ misses any small cell of Ξ_2 completely with probability $1 - \frac{t_2}{t_{pm}}$ and partly from 0 to t_2 with probability $\frac{t_2}{t_{pm}}$ respectively, and (b) follows from $t_2 = \frac{C_2}{v}$. The expected value of the time that $\mathcal{U}_0$ misses from small cells coverage during its movement is obtained in the following Theorem.

Theorem 4 The total average time missed by $\mathcal{U}_0$ during its movement is expressed as:

$$\mathbb{E}[\mathcal{T}_{miss}] = \Big(\mathbb{E}[N_0] - \mathbb{E}[N_{OL}]\Big)\Big(\mathbb{E}[T_{\Xi_1}] + \mathbb{E}[T_{\Xi_2}]\Big) \tag{4.3}$$

Proof: Since there are some overlaps on $\mathcal{P}_0$, no offloading loss will take place when $\mathcal{U}_0$ moves between two overlapped small cells. The total expected time that $\mathcal{U}_0$ misses from the second tier coverage during its movement in Eq. (4.3) is reached. ■

Our analysis shows that the offloading loss depends on a number of the system parameters such as t_p, the small cell density, ρ_{min}, the small cell transmit power, t_{min} and the UE's speed.

4.2 Energy Consumption

In this section, both the energy consumption of the SCD process and the UL transmission are investigated.

4.2.1 Uplink Energy Consumption

Assuming that $\mathcal{U}_0$ has traffic to send during its movement, the expected value of the total energy consumption of $\mathcal{U}_0$ for sending UL traffic can be found as follows.

Lemma 11 The total energy consumption is the summation of the energy consumption when associated to the first tier and the second tier as:

$$\begin{aligned}\mathbb{E}[E_{UL}] &= \mathbb{E}[E_1] + \mathbb{E}[E_2] \\ &= p_c \sum_{k=1}^{2} \left(\frac{\Upsilon_k \Gamma\left(\frac{\alpha_k \epsilon + 2}{2}\right)}{(\pi \lambda_k)^{\frac{\alpha_k \epsilon}{2}}} \right)\end{aligned} \tag{4.4}$$

where $\mathbb{E}[E_1]$ and $\mathbb{E}[E_2]$ represent the UL energy consumptions when associated to the first tier and the second tier respectively, Υ_k is the expected time that $\mathcal{U}_0$ is associated to the kth tier, $\Upsilon_1 = \mathbb{E}[\mathcal{T}_{t,l}] - \mathbb{E}[\mathcal{T}_0] + \mathbb{E}[\mathcal{T}_{miss}]$ and $\Upsilon_2 = \mathbb{E}[\mathcal{T}_{t,l}] - \Upsilon_1$ represent the expected time that $\mathcal{U}_0$ is associated to the first tier and the second tier respectively, $\mathbb{E}[\mathcal{T}_{t,l}]$ is the expected time that $\mathcal{U}_0$ spends on $\mathcal{P}_0$ and obtained in Eq. (2.9), $\mathbb{E}[\mathcal{T}_0]$ is the expected time that $\mathcal{U}_0$ spends in the second tier (or the potential offloading opportunities to the second tier) and obtained in Eq. (3.21), and $\mathbb{E}[\mathcal{T}_{miss}]$ is obtained in Eq. (4.3).

Proof: When the distance-proportional FPC is used as in Eq. (2.5), the energy consumption of $\mathcal{U}_0$ when associated to the kth tier is expressed as:

$$\mathbb{E}[E_k] = \Upsilon_k \int_0^\infty p_c x_k^{\alpha_k \epsilon} f_{x_k}(x) dx \tag{4.5}$$

where $f_{x_k}(x)$ is the PDF of x_k. Since the tier association is based on ρ_{min} from the second tier, the association to the second tier is independent of the distances to the MCBSs. The distance from $\mathcal{U}_0$ to the serving BS is assumed to have a Rayleigh distribution and $f_{x_k}(x) = 2\pi\lambda_k e^{-2\pi\lambda_k x_k^2}$. The results in Eq. (4.4) is reached by using [76, 3.326.2]. ■

4.2.2 Energy Consumption in the DC

As explained earlier, the energy consumption for the discovery mechanism is one of the biggest challenges in the HetNets. In the periodic scan based systems (e.g. DC), most of the energy consumption takes place at the UEs' side. The UEs perform the IRF scan frequently, stop scanning when offloaded to the second tier and resume scanning

when leaving the second tier coverage. The total energy consumption at the UEs' side depends on the time the UEs spend off the second tier coverage and t_p. The total energy consumption for the SCD can be expressed:

$$E_{DC} = \sum_{i \in \Phi_u} E_{DCU,i} \tag{4.6}$$

where $E_{DCU,i}$ is the total energy that the ith UE consumes for performing the IRF scan per unit time. When there are $\mathcal{F}$ high frequency channels deployed in the system, each small cell of different frequency channels has the same footprint and each UE performs the IRF scan every t_p on each frequency channel, the expectation of E_{DCU} becomes:

$$\mathbb{E}\big[E_{DCU}\big] = E_s \mathcal{F} \frac{\Upsilon_1}{t_p} \tag{4.7}$$

where E_s the energy cost for one IFR scan, $\frac{\Upsilon_1}{t_p}$ represents the expected number of scans that $\mathcal{U}_0$ performs on each frequency channel during its movement. The expectation of E_{DC} can be obtained as:

$$\mathbb{E}\big[E_{DC}\big] = \mathscr{A}_{sys} \lambda_u \frac{E_s \mathcal{F} \Upsilon_1}{t_p} \tag{4.8}$$

where $\mathscr{A}_{sys}\lambda_u$ represents the mean number of UEs in the system. Although, minimizing t_p helps to exploit more potential offloading opportunities, it may maximize the energy consumption at the UEs' side and in the whole system significantly. The result in Eq. (4.8) also shows that the energy consumption in the SCD is linearly proportional to the number of frequency channels and the UE density in the system for the same small cell density. Since the number of UEs in the system will increase and there is a need to deploy more frequency channels in the system, the energy consumption for the SCD process will degrade the energy efficiency in the whole system.

4.3 Energy Efficiency

Consider ULEE as performance metric to demonstrate the impact of the SCD on the system performance. The ULEE is defined as the total UL average achievable data rate during $\mathcal{U}_0$'s movement divided by the expected total energy consumed for both the UL

transmission and the SCD process during the same movement. It is assumed that the handover process between any cells from different tiers is seamless and the short periods of zero rate are negligible. Therefore, the ULEE can be mathematically expressed as:

$$\begin{aligned}\varkappa &= \frac{\mathcal{R}_{T,\uparrow}}{E_T} \\ &= \frac{\Upsilon_1\mathcal{R}_{1,\uparrow} + \Upsilon_2\mathcal{R}_{2,\uparrow}}{\mathbb{E}[\mathcal{T}_{t,l}]\big(\mathbb{E}[E_{UL}] + \mathbb{E}[E_{DC}]\big)}\end{aligned} \tag{4.9}$$

where $\uparrow$ represents the UL direction, $\mathcal{R}_{T,\uparrow}$ is the total average ergodic rate, E_T is the total energy consumption, and $\mathcal{R}_{1,\uparrow}$ and $\mathcal{R}_{2,\uparrow}$ represent the average ergodic rates of $\mathcal{U}_0$ associated to the first tier and the second tier respectively. The average achievable rate of $\mathcal{U}_0$ associated to the kth tier $\mathcal{R}_{k,\uparrow}$ is obtained as follows.

Lemma 12 The average achievable rate when $\mathcal{U}_0$ is associated to the kth tier, can be expressed as:

$$\mathcal{R}_{k,\uparrow} = \int_0^\infty \int_0^\infty \mathcal{L}_{I_{k,\uparrow}}(.) f_{x_k}(x) d\iota dx \tag{4.10}$$

where $\mathcal{L}_{I_{k,\uparrow}}(.) = \exp\Big(-\frac{2(\pi\lambda_k)^{1-\epsilon}x_k^{\alpha_k(1-\epsilon)}(e^\iota-1)^{\frac{2}{\alpha_k}}}{\alpha_k}B\big(\frac{2}{\alpha_k}, 1-\frac{2}{\alpha_k}\big)\Gamma\big(\epsilon+1\big)\Big)$ is the Laplace transform of the cumulative interference from the UEs associated to the kth tier, ι is the threshold of the achievable data rate and $B(.)$ is the beta function.

Proof: See Appendix A.6. ■

4.3.1 Optimum Inter-Frequency Scan Periodicity

The optimum value of t_p to achieve the best energy efficiency is derived. It is assumed that $\mathcal{U}_0$ travels at least t_p in every small cell. The energy efficiency in Eq. (4.9) can be rewritten as shown:

$$\varkappa = \frac{\mathcal{C}_1 + \mathcal{C}_2 t_p}{\mathcal{C}_3 + \mathcal{C}_4 t_p + \mathcal{C}_5 t_p^{-1}} \tag{4.11}$$

where $\mathcal{C}_1 = \mathcal{R}_{1,\uparrow}(1 - \frac{\mathbb{E}[\mathcal{T}_0]}{\mathbb{E}[\mathcal{T}_{t,l}]}) + \mathcal{R}_{2,\uparrow}\frac{\mathbb{E}[\mathcal{T}_0]}{\mathbb{E}[\mathcal{T}_{t,l}]}$, $\mathcal{C}_2 = \frac{\mathbb{E}[N_0]-\mathbb{E}[N_{OL}]}{2\mathbb{E}[\mathcal{T}_{t,l}]}(\mathcal{R}_{1,\uparrow} - \mathcal{R}_{2,\uparrow})$, $\mathcal{C}_3 = (\mathbb{E}[\mathcal{T}_{t,l}] - \mathbb{E}[\mathcal{T}_0])\mathbb{E}[p_{1,\uparrow}] + \mathbb{E}[\mathcal{T}_0]\mathbb{E}[p_{2,\uparrow}] + 0.5E_s\mathcal{F}$, $\mathcal{C}_4 = 0.5(\mathbb{E}[N_0] - \mathbb{E}[N_{OL}])(\mathbb{E}[p_{1,\uparrow}] - \mathbb{E}[p_{2,\uparrow}])$, and $\mathcal{C}_5 = E_s\mathcal{F}(\mathbb{E}[\mathcal{T}_{t,l}] - \mathbb{E}[\mathcal{T}_0])$. $\mathbb{E}[p_{1,\uparrow}] = \frac{\mathbb{E}[E_1]}{\Upsilon_1\mathbb{E}[\mathcal{T}_{t,l}]}$ and $\mathbb{E}[p_{2,\uparrow}] = \frac{\mathbb{E}[E_2]}{\Upsilon_2\mathbb{E}[\mathcal{T}_{t,l}]}$ are the expected value of the UL transmit power when $\mathcal{U}_0$ is associated to the first tier and the second tier

respectively. The optimum value of t_p to maximize the energy efficiency can be found by setting the derivative $\frac{d\varkappa}{dt_p} = 0$. By considering some simplifications, it becomes:

$$(\mathcal{C}_2\mathcal{C}_3 - \mathcal{C}_1\mathcal{C}_4)t_p^2 + 2\mathcal{C}_2\mathcal{C}_5 t_p + \mathcal{C}_1\mathcal{C}_5 = 0 \tag{4.12}$$

The critical points are obtained by using the quadratic formula as shown below:

$$\frac{-2\mathcal{C}_2\mathcal{C}_5 \pm \sqrt{(2\mathcal{C}_2\mathcal{C}_5)^2 - 4(\mathcal{C}_2\mathcal{C}_3 - \mathcal{C}_1\mathcal{C}_4)\mathcal{C}_1\mathcal{C}_5}}{2(\mathcal{C}_2\mathcal{C}_3 - \mathcal{C}_1\mathcal{C}_4)} \tag{4.13}$$

Finding the optimum value of t_p for different values of small cells needs to be clarified by considering a few cases. From the facts that the density of small cells is very high in comparison to the density of macro cells ($\lambda_2 \gg \lambda_1$) and the IRF scan periodicity is equal or greater than zero ($t_p \geq 0$), two main cases are considered to find the optimum value of t_P:

Case 1: $(\mathcal{C}_2\mathcal{C}_3 - \mathcal{C}_1\mathcal{C}_4) = 0$.

When the density of small cells is equal to the density of macro cells ($\lambda_2 = \lambda_1$), both $\mathcal{C}_2$ and $\mathcal{C}_4$ will be zero. In this case, there is no optimal solution.

Case 2: $(\mathcal{C}_2\mathcal{C}_3 - \mathcal{C}_1\mathcal{C}_4) < 0$.

When the density of small cells is greater than the density of macro cells (it is expected that $\lambda_2 > \lambda_1$ in the future HetNet), $\mathcal{C}_2 < 0$ and $\mathcal{C}_4 > 0$. Since t_p can not be less than zero, the optimum value of t_p can be obtained as:

$$\hat{t}_p = \frac{-2\mathcal{C}_2\mathcal{C}_5 + \sqrt{(2\mathcal{C}_2\mathcal{C}_5)^2 - 4(\mathcal{C}_2\mathcal{C}_3 - \mathcal{C}_1\mathcal{C}_4)\mathcal{C}_1\mathcal{C}_5}}{2(\mathcal{C}_2\mathcal{C}_3 - \mathcal{C}_1\mathcal{C}_4)} \tag{4.14}$$

4.4 Trio-Connectivity (TC)

The current cellular system suffers from some of the technical challenges that affect exploiting the system resources efficiently and the QoS, and hamper meeting the future performance targets [2, 59, 61]. It is expected that the future cellular systems (e.g. DC) will inherit the offloading process issue from the conventional IRF HetNet.

To meet the future requirements and overcome the technical challenges, a new approach needs to be proposed by taking into consideration all the limitations and issues that the current systems suffer from. It is anticipated that the SCD will have a great

impact on the performance of the future cellular systems due to limited power at the UEs' side, multiple high frequency channels deployed in the system and limited resources at the macro cells. Therefore we propose a novel TC to solve the issues regarding the mobility management, and the offloading process [2]. The proposed TC includes three planes, the C-plane, the U-plane and the I-plane. The C-plane is maintained by the first tier to provide the required control information for maintaining wireless links with the UEs. The U-plane is maintained by either the first tier or the second tier to deliver the UEs' traffic. Splitting the C-pane and the U-plane can provide smoother mobility management [60, 61, 77]. The I-plane is provided by the second tier by reusing the low frequency at every small cell to advertise the small cells' information (e.g. cell identification (ID)). The purpose is to keep the offloading process (discovering and identifying the small cells) on one frequency (the low frequency) regardless of the number of frequency channels in the network. In other words, the whole SCD process will be based on the IAF scan instead of the IRF scan. The I-plane will act as an indicator for UEs to detect and discover the nearby high frequency small cells in order to offload the UEs' traffic to the discovered small cells as shown in Fig. 4.1. This can save power at the UEs' side as well as signalling load at the UEs' and the network' sides. However, this mechanism will result in power consumption within the network for maintaining the I-plane. Although there are substantial differences between the current cellular systems and future cellular systems, the technical specifications and the details of the offloading procedure and mobility management have not been characterized yet. Therefore, the proposed TC is modelled and designed by considering current cellular systems.

4.4.1 C-plane

The C-plane, which is provided by the first tier, includes the control information and some of the services that do not require large frequency resources. For instance, the voice service is one of the services that needs limited frequency resources, but it requires high reliability. Providing this service by the first tier will minimize the interruption in service continuation and also minimize the signalling load, in addition to guaranteeing more reliable communication. The control information includes all information needed

for setting up and maintaining communication links between the UEs and their serving cells. Therefore, the C-plane will not only control the U-plane when provided by the first tier, but also control the U-plane when provided by the second tier [60]. This implies that in the TC, the protocol stack at the macro cells will match the conventional protocol stack in the current cellular systems and include radio resources control (RRC), packet data convergence protocol (PDCP), radio link control (RLC), medium access control (MAC) and physical (PHY - F1) as shown in Fig. 4.1a. The RRC includes a number of functions such as the broadcast of system information, RRC connection control, measurements configuration and reporting, support of self-configuration and optimization and others [53]. Therefore, the first tier in the TC system will also be responsible for configuring, and managing measurements and reports regarding the cell search procedure for both IAF and IRF cells.

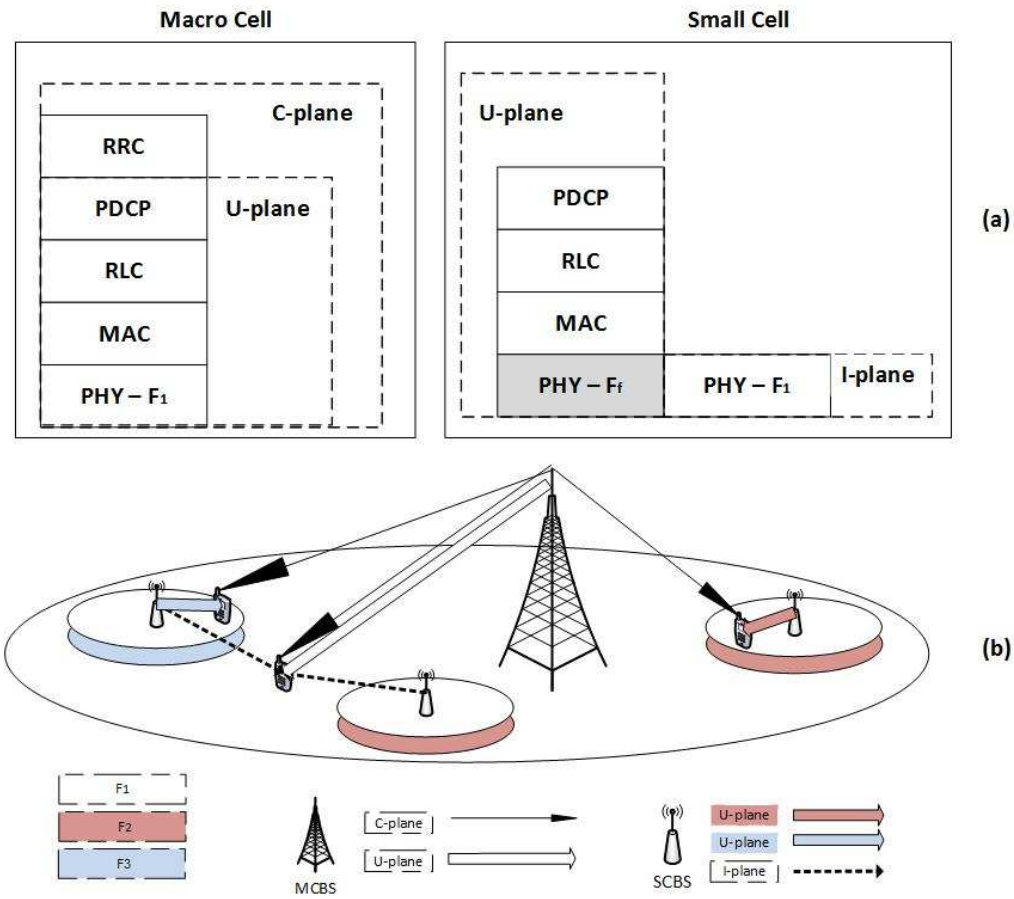

Figure 4.1: (a) The proposed protocol stack (b) The proposed TC.

4.4.2 U-plane

In the TC, the U-plane will be provided by the high frequency at the second tier or by the first tier according to the service requested by UEs and availability of the second tier. The U-plane will be provided by the first tier if the UEs are off the second tier coverage and/or the UEs request a low data rate service (e.g. voice service). Since the control information is provided by the C-plane, the second tier's role will be restricted to deliver UEs traffic supported by the C-plane. The protocol stack at the second tier will include all the protocols except the RRC. However, the U-plane at the second tier still needs some functions of the RRC (e.g. broadcast of system information). The second tier will need to include the RSs and the synchronization signals for the channel estimation between UEs and the serving small cells, and also for the cell search.

4.4.3 I-plane

The low frequency will be reused at each small cell, which will be functioning as an indicator to enable UEs to discover the surrounding small cells and also to estimate the proximity to the SCBSs. The system information of each small cell will be broadcasted not only on the high frequency (U-plane), but also on the low frequency (I-plane). Moreover, I-plane will not be used to serve UEs in the system to protect the UEs served by the first tier and also to minimize the interference with the C-plane. However, although very limited frequency resources are required for the I-plane, allocating limited low frequency resources for this purpose or some of the interference mitigation techniques may be applied, e.g. enhanced inter-cell interference coordination (eICIC) [78–80]. The I-plane only broadcasts the cell information (e.g. CID), the RSs and the synchronization signals. Decoding the synchronization signals allows UEs to obtain the CID [81]. The RSs exist at the physical layer to deliver a reference point for the DL power. Since the locations of RSs in the channel are based on the CID, the synchronization signals enable UEs to discover the small cells in the system and provide the serving cells with the required measurements of the surroundings [81–83]. Furthermore, the protocol stack at the I-plane will be limited to the physical layer (PHY - F1) and broadcast the system information as shown in Fig. 4.1a.

4.4.4 Proposed Small Cell Discovery Mechanism

The low frequency is used at each small cell next to one of the high frequencies as shown in Fig. 4.1b. It is assumed that both frequencies at each small cell are overlaid and cover the same area. Covering the same area by both spectrums requires compensation for the path-loss difference between the low frequency and the high frequency. The long-term average value of the received power from any small cell with the fth frequency at a reference point (e.g. cell edge) is expressed as $\bar{\rho}_f = p_{f,2,rs}\bar{r}_f^{-\alpha_2}\mathscr{L}_f$, where $p_{f,2,rs}$ is the transmit power of RSs from F_f, $\bar{r}_f$ is the distance between the reference point and the SCBS and $f \in [1, 2, \cdots, \mathcal{F}+1]$. The RSs transmit power of F_1 to receive the same received power from $F_f, f > 1$ at the same reference point, can be expressed as:

$$p_{1,2,rs} = p_{f,2,rs}\left(\frac{F_1}{F_f}\right)^2 \tag{4.15}$$

where $\bar{r}_1 = \bar{r}_f$ since both frequencies are transmitted from the same SCBS. The proposed SCD mechanism in the TC can be summarized as:

- The serving macro cells manage both the IAF and the IRF measurements. When a reference UE is provided with the C-plane and the U-plane by the same serving macro cell, the reference UE is triggered to perform the IAF measurements only. The reference UE performs the IAF measurements and send them back to the serving macro cell. These measurements will not only be used to estimate the channel between the reference UE and its serving macro cell, but also to discover the nearby small cells since all small cells broadcast their information on both low and high frequencies.

- Offloading requirements are the criterion to trigger the IRF scan at the reference UE as a final step before offloading the reference UE from the first tier to the second tier. These requirements could include signal level and quality, the current load at the discovered small cells (full or not) and the access restriction. The serving macro cell can use the IAF measurements provided by the reference UE to identify the discovered small cells, and check their current load status and whether the access to these small cells restricted or not.

- When the requirements are not met, the U-plane will remain maintained by the serving macro cell without performing the IRF scan. It is expected that keeping the cell search in the system on one frequency will help to save the power at the UE's side and also minimize the signalling overhead.

- When the offloading requirements are met, the reference UE is instructed by the serving macro cell to perform the IRF scan. Then the serving macro cell decides whether this UE is offloaded to the discovered small cell or not.

According to the IRF measurements sent to the serving macro cells from the UEs, the offloading decision to the small cell will be made. Fig. 4.2 shows the signalling diagram of the proposed cell discovery mechanism.

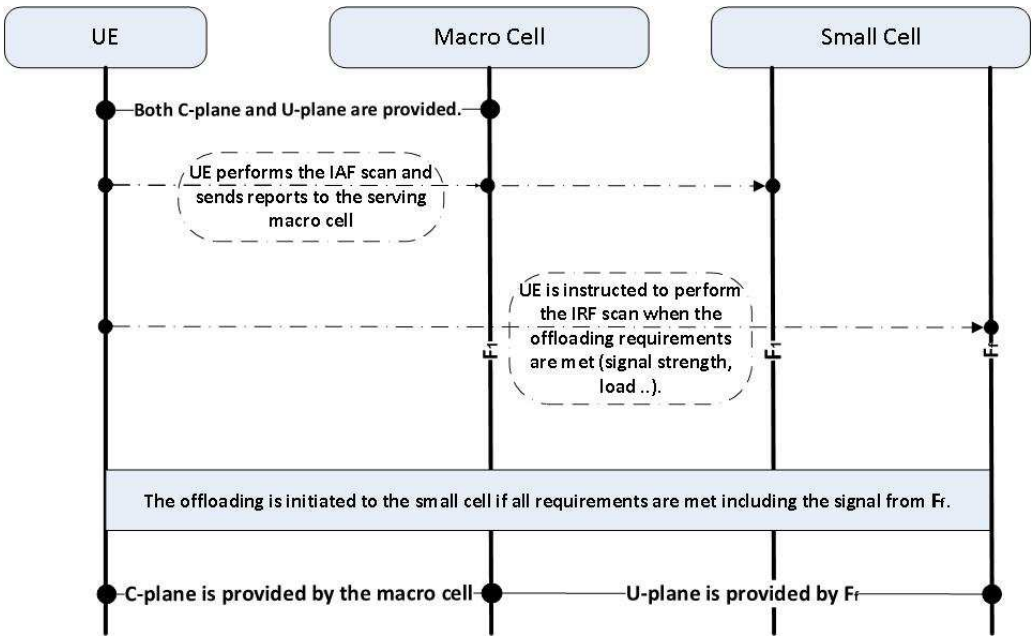

Figure 4.2: The signalling diagram of the proposed mechanism

4.4.5 Energy Consumption in the TC

Unlike the periodic mechanism where most of the energy consumption takes place at the UEs' side, most of the energy consumption in the proposed mechanism will take place at the network's side. Transferring the energy consumption from the terminals with limited power to the network with an unlimited power supply is considered highly desirable.

However, for a fair comparison, the total energy consumption in the system (at both UEs' and network' sides) for both mechanisms will also be considered. In the TC, the UEs will only perform the IRF scan after they have detected and discovered the surrounding small cells on the low frequency and when the offloading requirements are met. Therefore the total number of the IRF scans will be minimized and also the energy consumption at the UEs' side will be reduced significantly. The proposed mechanism is based on the IAF scan which saves a significant amount of energy at the UEs' side, but the small cells in the TC will have to consume more energy to broadcast their information on two frequency channels. Therefore the total energy consumption in the proposed mechanism becomes:

$$E_{TC} = \sum_{i \in \Phi_u} E_{TCU,i} + \sum_{j \in \Phi_2} E_{TCSC,j} \tag{4.16}$$

where $E_{TCU,i}$ is the energy consumption at the ith UE in the TC, and $E_{TCSC,j}$ is the total energy that the jth small cell consumes to maintain the I-plane in the TC. Under the same assumption made previously that each UE discovers the small cells from the first IRF scan in their coverage, the expected value of E_{TCU} can be expressed as:

$$\mathbb{E}\big[E_{TCU}\big] = \big(\mathbb{E}[N_0] - \mathbb{E}[N_{OL}]\big)E_s \tag{4.17}$$

While the expectation of E_{TCSC} during the time $\mathbb{E}[\mathcal{T}_{t,l}]$ can be expressed as:

$$\mathbb{E}\big[E_{TCSC}\big] = p_{1,2,rs}\mathbb{E}[\mathcal{T}_{t,l}] \tag{4.18}$$

where $p_{1,2,rs}$ is obtained in Eq. (4.15). Therefore the expectation of E_{TC} is obtained as:

$$\mathbb{E}\big[E_{TC}\big] = \mathscr{A}_{sys}\Big(\lambda_u\big(\mathbb{E}[N_0] - \mathbb{E}[N_{OL}]\big)E_s + \lambda_2 p_{1,2,rs}\mathbb{E}[\mathcal{T}_{t,l}]\Big) \tag{4.19}$$

where $\mathscr{A}_{sys}\lambda_2$ represents the mean number of small cells in the system. The first term on the right hand side of Eq. (4.19) represents the energy consumption at the UEs' side while the second term represents the energy consumption at the network side. It can be observed that unlike in the DC, the energy consumption in the proposed mechanism is independent of the IRF scan periodicity (t_p), since it is based on the IAF scan and the UEs do not need to perform the IRF scan periodically. It is also observed that increasing the density of small cells will reduce the energy consumption in the periodic scan mechanism

and increase the energy consumption in the proposed mechanism (at the network's side). However, the density of UEs will have a great impact on the energy consumption in the periodic scan mechanism as the number of UEs will be very large in the future.

4.5 Results

Some representative results are presented to show the impact of some parameters such as t_p and the small cell density on the cellular system performance, and also to show a comparison between the conventional SCD and the proposed mechanism in terms of ULEE and energy consumption in a two-tier HetNet. In the current mobile systems, the IAF scan (t_{p_A}) is performed every 200 ms for channel estimation and inter-cell handover [54, 75]. Since the SCD in the TC is based on the IAF scan, the measurements will also be used to discover the small cells by detecting the I-plane at each small cell. In the DC, the UEs have to perform the IRF scan in addition to the IAF scan to discover the surrounding small cells. Therefore, different values of t_p will be considered in the DC. The different system parameters can be found in Table 3.1 in the previous Chapter, unless given otherwise.

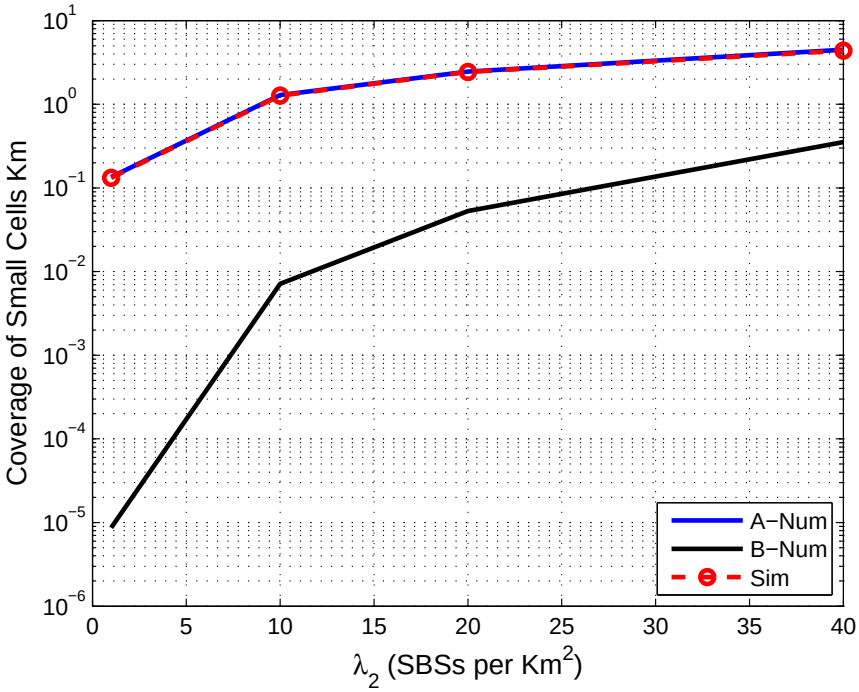

Figure 4.3: The small cells coverage on the $\mathcal{U}_0$'s path.

The analysis of the small cells coverage is validated in Fig. 4.3 through simulations. It can be seen from Fig. 4.3 that the second tier coverage on the $\mathcal{U}_0$'s path in our analysis (A) is very accurate in comparison to the assumption made in [20] (B), where the fraction of the $\mathcal{U}_0$'s path covered by the small cells coverage was obtained by multiplying the second tier association by the total length of the $\mathcal{U}_0$'s path $\frac{\mathcal{A}_2}{2\sqrt{\lambda_w}}$.

Fig. 4.4, Fig. 4.5 and Fig. 4.6 show the system performance of the conventional two-tier HetNet (or the DC) by using three different performance measures. Fig. 4.4 shows the total average ergodic rates $\mathcal{R}_T$ for different values of the small cell density and t_p. Although the system performance improves when the small cell density increases, it can be seen that $\mathcal{R}_T$ increases when t_p decreases for the same small cell density. This is because the UEs exploit more offloading opportunities when smaller values of t_p are adopted in the system. Fig. 4.5 shows the system performance in the energy efficiency measure of $\frac{\mathcal{R}_T}{E_{UL}}$ where only the UL energy consumption is considered. Fig. 4.5 shows that the energy efficiency for different small cell densities decreases when t_p increases as the UEs will miss more offloading opportunities to the small cells and keep associated to the macro cells for longer periods. Since the macro cell density is very low in comparison to the small cell density, being associated to the macro cells longer periods will cost the UEs higher power consumption for maintaining the UL transmission. Fig. 4.6 illustrates the energy efficiency when the total energy consumption (UL energy consumption and SCD energy consumption) is taken into account $\frac{\mathcal{R}_T}{E_{UL}+E_{DC}}$, for different small cell densities, t_p values and number of high frequency channels $\mathcal{F}$. It is seen from the figure that adopting different values of t_p for different values of the small cell densities and $\mathcal{F}$ is essential to achieve the best trade-off between the total energy consumption and the offloading loss. It can also be seen that the optimum value of t_p ($\hat{t}_p$ achieves the best energy efficiency) decreases when the small cell density increases and/or $\mathcal{F}$ decreases. For instance, when $\lambda_2 = 40$ and $\mathcal{F} = 1$, $\hat{t}_p$ is around 60 seconds, while $\hat{t}_p$ is over 65 seconds when $\lambda_2 = 40$ and $\mathcal{F} = 2$, and $\hat{t}_p$ is around 70 seconds when $\lambda_2 = 20$ and $\mathcal{F} = 1$.

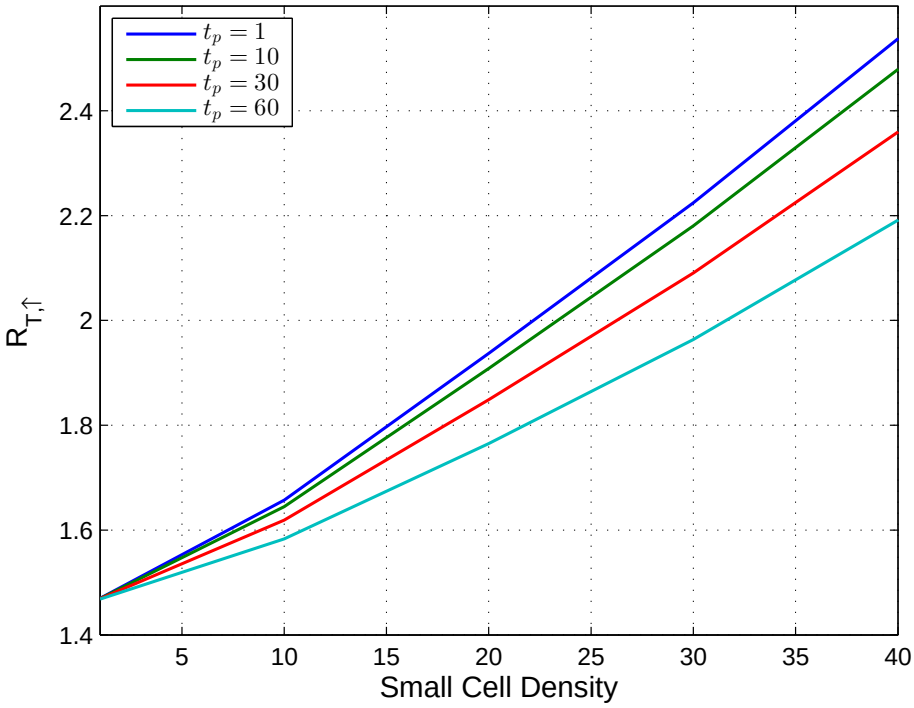

Figure 4.4: $\mathcal{R}_{T,\uparrow}$ in the DC.

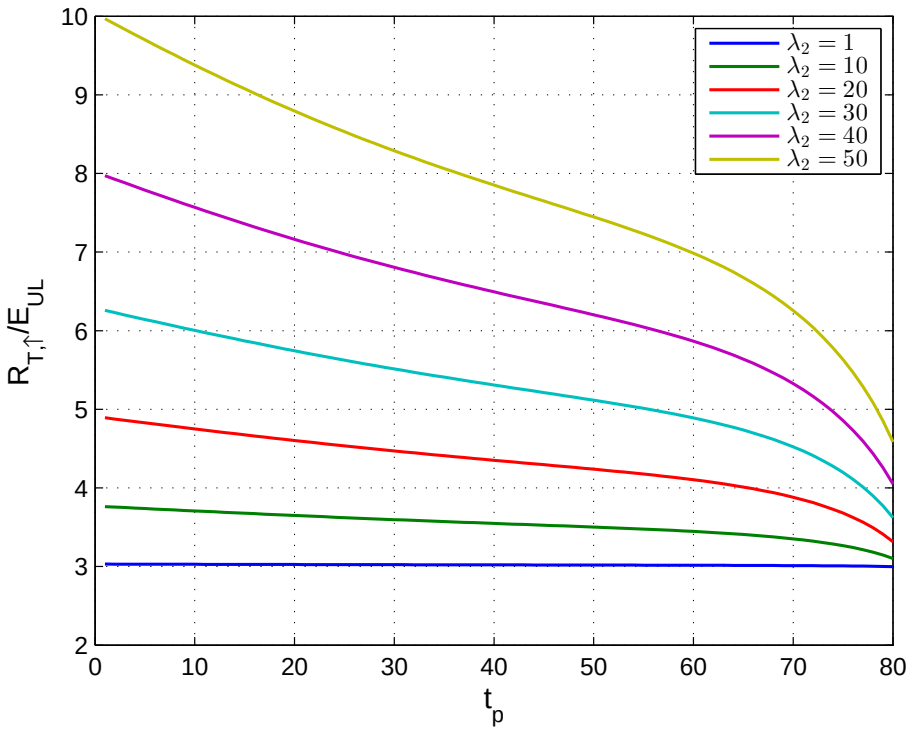

Figure 4.5: $\frac{\mathcal{R}_{T,\uparrow}}{E_{UL}}$ in the DC.

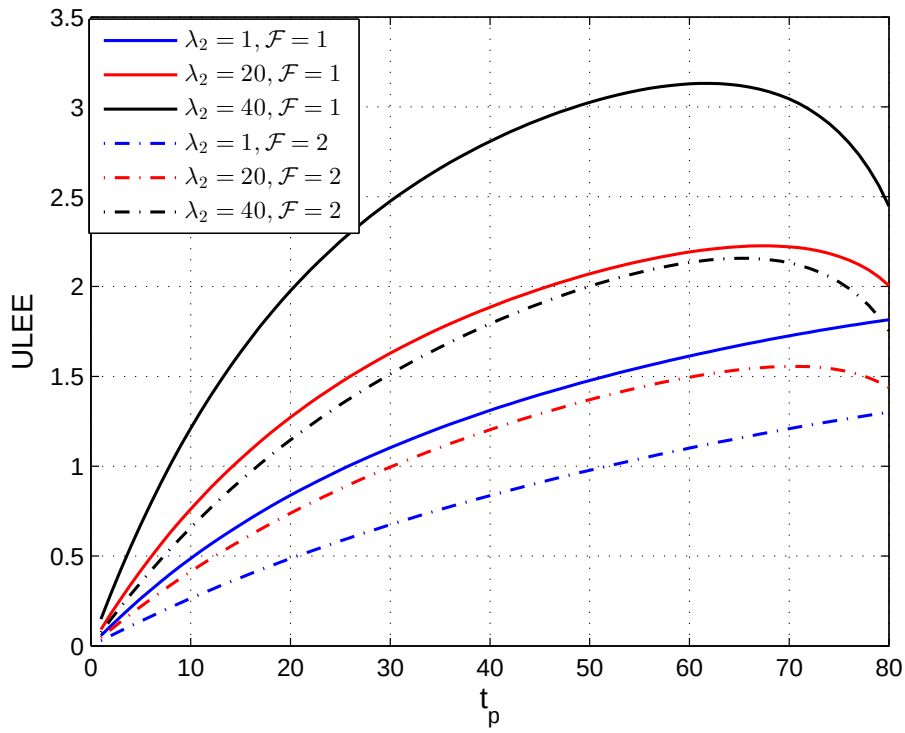

Figure 4.6: $\frac{\mathcal{R}_{T,\uparrow}}{E_{UL}+E_{DC}}$ in the DC.

Fig. 4.7 and Fig. 4.8 show the energy efficiency in both the DC and the TC where one high frequency channel is considered in the system (the best energy efficiency is achieved in the conventional HetNet or the DC when $\mathcal{F} = 1$ as shown in Fig. 4.6). In Fig. 4.7, the system performance of TC, and the system performance of DC when adopting different values of t_p as well as the optimum value $\hat{t}_p$, are shown for different values of the small cell density. Although increasing the small cell density will maximize the energy consumption in the proposed SCD as shown in Eq. (4.19), exploiting both more offloading opportunities that the TC can offer, and the minimized transmit power needed for the UL when the UEs are associated to the small cells for longer periods can minimize the impact of the energy consumed by the small cells and maximise the ULEE in the whole system. It is seen from Fig. 4.7 that the proposed mechanism in the TC can provide better performance than the DC for all different small cell densities. Furthermore, Fig. 4.7 shows that $\hat{t}_p$ achieves the best performance for different values of the small cell density in the DC. Once again, it is shown that some values of t_p can achieve better performance than other values for a specific range of small cell densities, for instance, $t_p = 80$ achieves better performance

than $t_p = 30$ when $\lambda_2 < 35$, while $t_p = 30$ achieves better performance than $t_p = 80$ when $\lambda_2 > 35$.

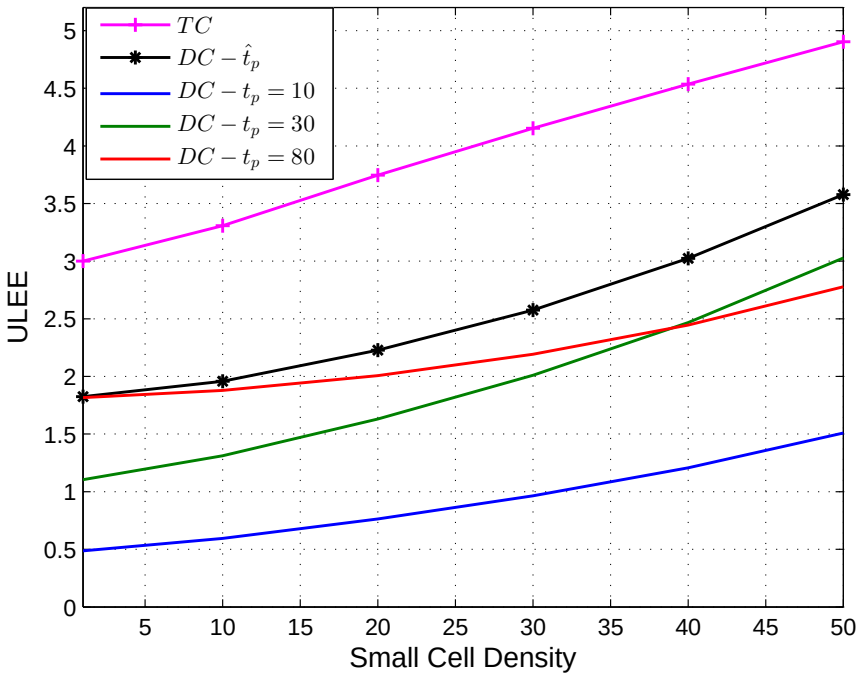

Figure 4.7: ULEE of both TC and DC vs. λ_2.

Fig. 4.8 shows the impact of the UE density on the system performance in the TC and the system performance in the DC for different values of t_p. It is shown that the DC performance is better than the TC performance when the density of UEs is very low, however it is anticipated that the density of UEs will be very high in the future cellular systems. The performance of the TC can provide a significant improvement in the energy efficiency in comparison to the optimum system performance in the DC for different UE densities. It can be seen from Fig. 4.8 that the energy efficiency in the DC is independent of the UE density when the density of small cells is fixed. However, the energy efficiency in the TC increases significantly when the ratio of UE density to small cell density increases. This is because a big fraction of the SCD energy consumption in the TC is brought to the network side and increasing the density of UEs with a fixed value of λ_2 will save more energy in the system in comparison to the DC.

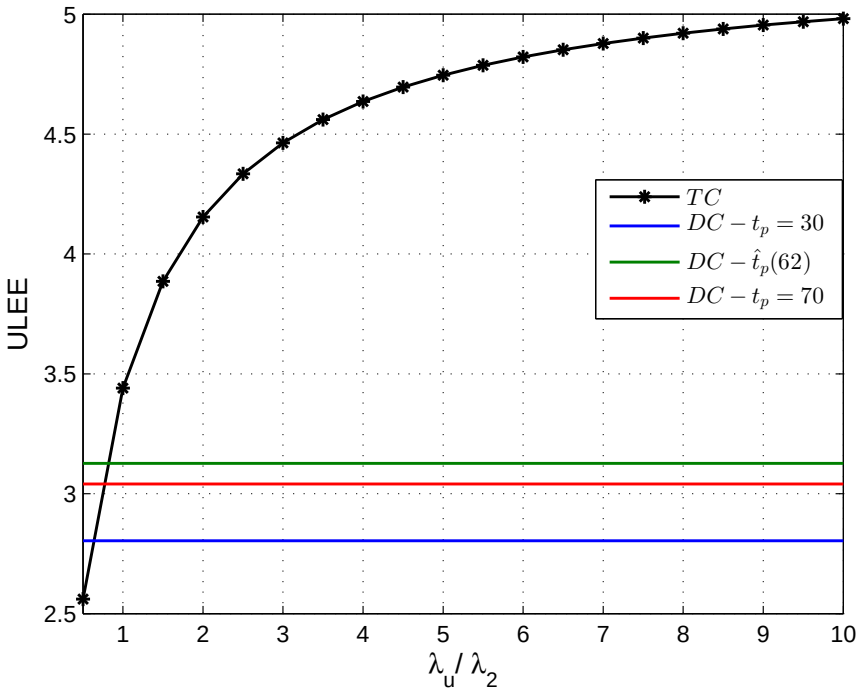

Figure 4.8: ULEE of both TC and DC vs. $\frac{\lambda_u}{\lambda_2}$.

Fig. 4.9 and Fig. 4.10 show the SCD energy consumption required at the UE and in the whole system in both the proposed mechanism in the TC and the periodic scan mechanism in the DC. A ratio of the small cell energy consumption in the whole system of the TC to the small cell energy consumption in the whole system of the DC is shown in Fig. 4.9 for two values of t_p. Adopting very low value, e.g. $t_p = 1$, maximizes the SCD energy consumption significantly for any number of high frequency channels. Fig. 4.9 also shows that adopting higher values of t_p can save significant energy in the system. However, the TC outperforms the DC for any number of high frequency channels and different values of t_p. Fig. 4.10 presents a ratio of energy consumption at the UE in the TC to energy consumption at the UE in the DC. It can be seen that the energy consumption needed for the SCD at the UEs in the TC is much less than at the UE in the DC for all values of t_p, $\mathcal{F}$ and λ_2. Note that saving power at the UEs is highly desirable in the cellular system due to limited battery capacities.

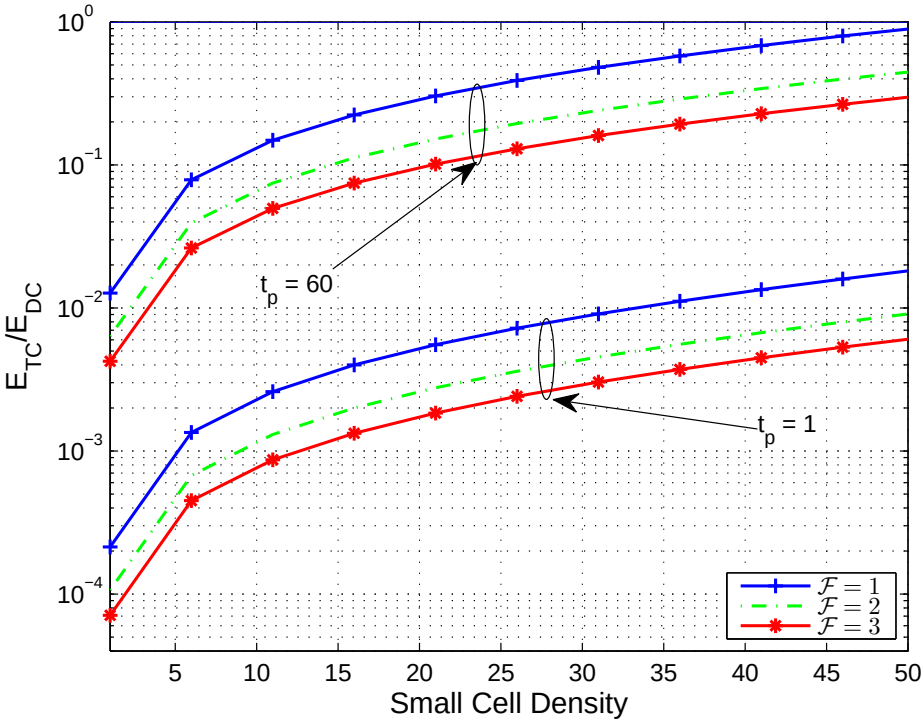

Figure 4.9: E_{TC} to E_{DC} ratio.

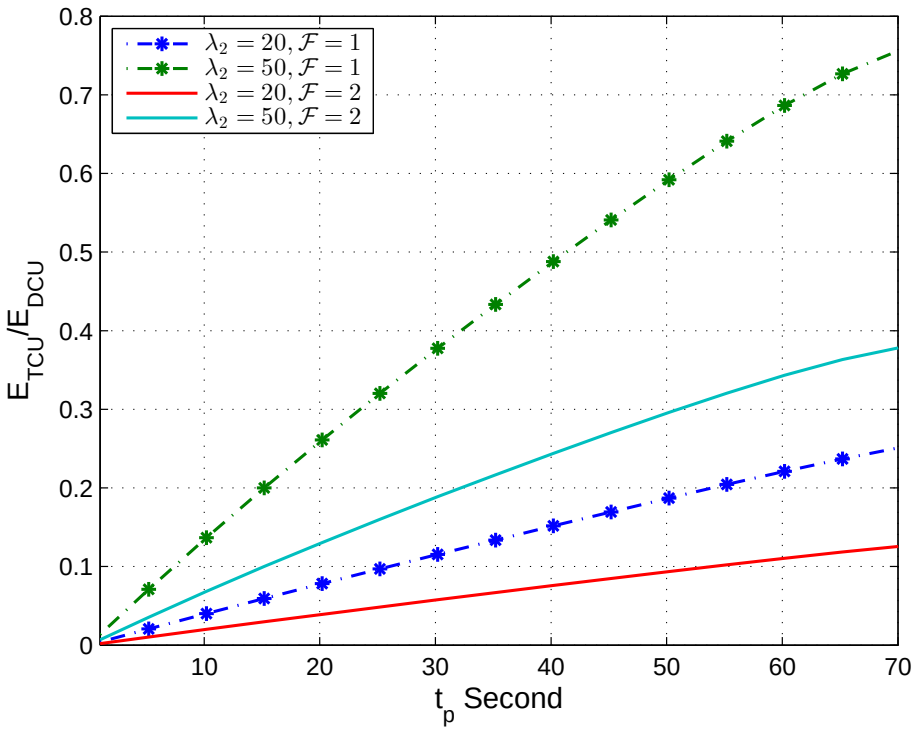

Figure 4.10: E_{TCU} to E_{DCU} ratio

Chapter 5

Conclusions and Future Work

Contents

5.1 Conclusion

In this thesis, we studied different aspects of the HetNet and tackled a number of challenges that affect the QoS and hinder to exploit the system resources efficiently. The conclusions can be summarized as following:

- The stochastic geometry tool was used to propose a mobility framework to model and analyse the main mobility parameters, the handoff rate and the cell sojourn time as well as the expected time that the UEs spend in the coverage areas of the small cells. In the proposed framework, the overlaps among the small cells from different tiers on a reference UE's path was taken into consideration. The simulation results showed that ignoring the overlaps will affect the accuracy of the cell sojourn time and the handoff rate significantly. Furthermore, the IAH rate and the IRH rate were introduced to illustrate the load and the resources required at the different network tiers, especially at the overloaded macro cells. The simulation results also demonstrated that increasing the small cells density can reduce the load for the

macro cells because the UEs will spend more time associated to the high frequency small cells. Furthermore, the fraction of handoffs managed by the macro cells will be minimized when more overlaps take place among the small cells. It was also shown that the small cell sojourn time becomes independent of the small cells density when the overlaps are not considered.

- The TC, including the C-plane, the U-plane and the I-plane, has been proposed to enhance both the mobility management and offloading process in the future HetNet. A system design (each plane's role and functions, and signalling diagram of the proposed offloading mechanism) was presented. The stochastic geometry tool was used to model the offloading loss, the average achievable rate and the energy consumption for the SCD process in a two-tier HetNet. The TC and the DC were compared in terms of offloading loss, ULEE and energy consumption. The comparison results showed that the TC saves power not only at the UEs' side but also in the offloading process as a whole in the high dense HetNet with no trade-off in exploiting the offloading opportunities in the system. Deploying more frequency channels in the system will increase the energy consumption in the DC. Meanwhile, the energy consumption in the proposed mechanism is not affected when more frequency channels are deployed, as the offloading process in the TC (discovering and identifying the small cells) is kept on one frequency regardless of the number of frequency channels.

5.2 Future Work

- **Further investigations on the TC performance**: It has been shown in this thesis that the TC is a promising system to solve some of the technical challenges that the HetNets suffer from. It is expected that the TC can improve not only the UL performance but also the DL performance as the DL energy efficiency will be improved significantly when exploiting more offloading opportunities and the UEs are associated to the small cells for longer periods. Since minimizing the number of IRF scans can also decrease the signalling load in the offloading process [2, 24],

the proposed SCD can provide further enhancement in terms of signalling load. Although the I-plane in the TC requires limited frequency resources to be reused at the small cells, as future work, considering the I-plane frequency resources next to the DL energy performance and the amount of signalling load will illustrate all the trade-offs and the benefits in the TC. On the other hand, some sleep-mode techniques have been investigated to minimize the energy consumption at the network's side by switching off a set of cells [84–86]. Proposing a sleep-mode technique in the TC by switching off one or both frequencies at a set of small cells can also help to save more power in the system and improve the energy efficiency in the future mobile systems.

- **Studying the DTDD system in the mm-Wave systems**: It has been shown that the DTDD system provides a significant improvement in the DL of HetNet for different traffic trends and different small cell densities [5]. It is expected that the performance in the UL is different from the performance in the DL. The UL performance is degraded when more small cells are in the DL mode due to a big difference between the UE's transmit power and SCBS's transmit power.

  It is anticipated that the mm-Waves and the beamforming technique will be part of the future cellular system [14] as shown in Fig. 5.1. Unlike the microwave systems, the mm-Wave systems are sensitive to the environment where the line of sight links (LOSs) and non-line of sight links (NLOSs) are very different in terms of received signal strength [14, 87]. The measurements in [14] showed that LOSs are not essential to maintain wireless links, while the measurements in [87] claimed that the LOSs are required. Therefore, it is anticipated that the impact of the SCBSs (the small cells in the DL mode) on the UL performance in the DTDD system will be minimized in the mm-Wave systems. Investigating the DTDD system by taking into consideration all the features and challenges in the mm-Wave systems as well as the different traffic trends and the structure of transmission-configuration (e.g. the frame-configuration) is essential to validate the feasibility of the DTDD in the future cellular systems. Although modelling the DTDD in the mm-Wave systems will be more challenging, studying the DTDD system as future work will be very

interesting.

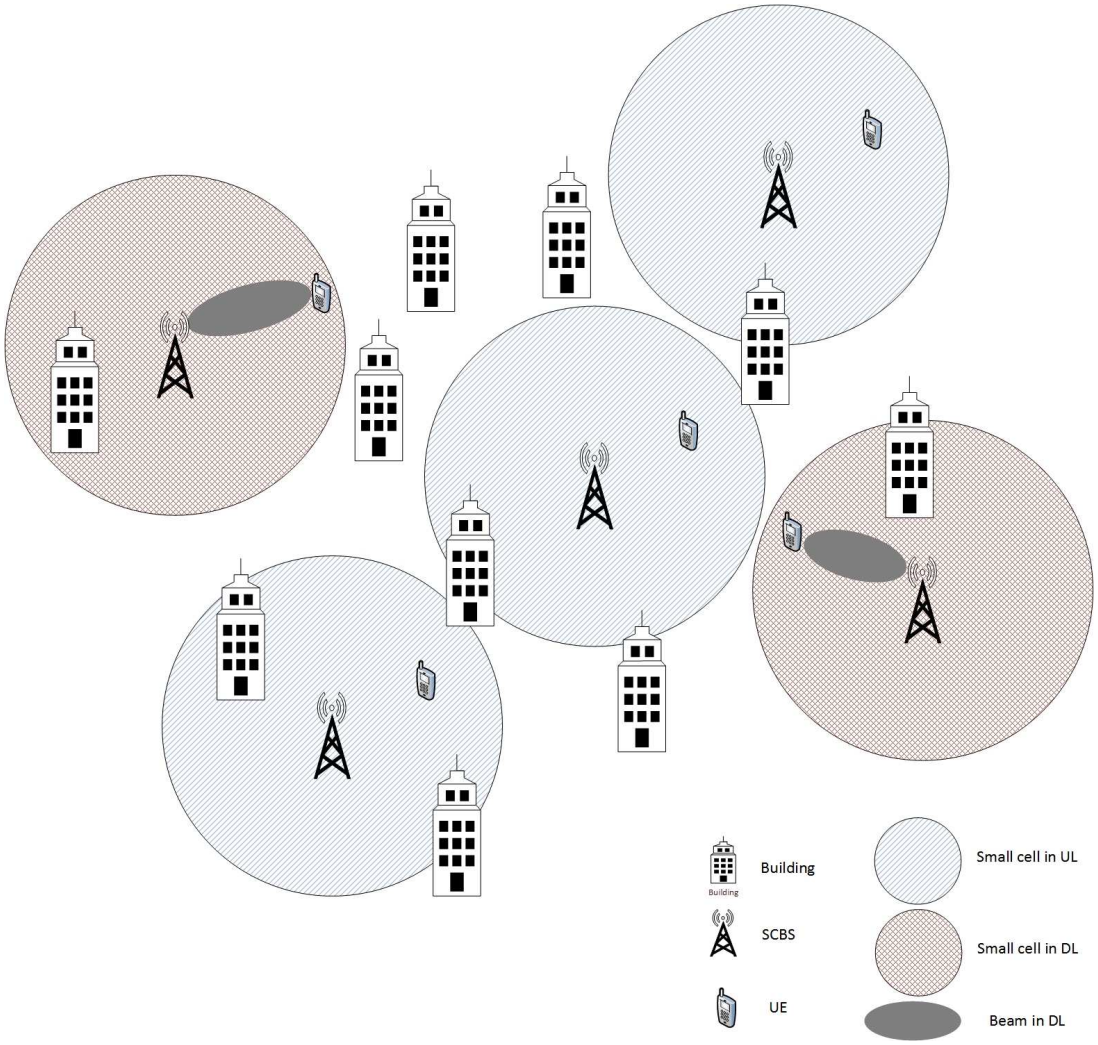

Figure 5.1: The DTDD in mm-Wave systems.

Appendix A

Appendices

Contents

A.1 Proof of Lemma 6

Given that the ith and the $(i+1)$th small cells with coverage C_i and C_{i+1} respectively are overlapped on $\mathcal{P}_0$. From Fig 3.3, the ith small cell overlaps with the $(i+1)$th small cell on $\mathcal{P}_0$ if $\bar{y}_i$ and $\bar{y}_{i+1}$ are at distance $\bar{C}_i$ or less. Thus, any overlap coverage can be expressed as:

$$\mathfrak{C}_i = \begin{cases} \bar{C}_i - \parallel \bar{y}_{i+1} - \bar{y}_i \parallel, & \parallel \bar{y}_{i+1} - \bar{y}_i \parallel < \bar{C}_i \\ 0, & \text{otherwise} \end{cases} \tag{A.1.1}$$

The PDF of $\bar{C}_i$ is the convolution of the PDFs of C_i and C_{i+1}. Since C_i and C_{i+1} are independent random variables, the joint PDF of both C_i and C_{i+1} can be expressed as

$f_{C_iC_{i+1}}(c_i, c_{i+1}) = f_{C_i}(c_i) f_{C_{i+1}}(c_{i+1})$. Therefore the PDF of $\bar{C}_i$ is obtained as:

$$\begin{aligned} f_{\bar{C}_i}(\bar{c}) &= \int_{-\infty}^{\infty} \Big(\frac{d}{d\bar{c}} \int_0^{\bar{c}-c_i} f_{C_iC_{i+1}}(c_i, c_{i+1}) dc_{i+1} \Big) dc_i \\ &= \int_{-\infty}^{\infty} f_{C_iC_{i+1}}(c_i, \bar{c} - c_i) dc_i \\ &\overset{(a)}{=} \int_0^{\bar{c}} \frac{\bar{c}c_i(\bar{c} - c_i)\, dc_i}{32 r_i^2 r_{i+1}^2 \sqrt{1 - \frac{c_i^2}{4r_i^2}} \sqrt{1 - \frac{(\bar{c}-c_i)^2}{4r_{i+1}^2}}} \\ &\overset{(b)}{=} \int_0^{\bar{c}} \frac{\bar{c}c_i(\bar{c} - c_i)\, dc_i}{16 r^3 \sqrt{8r^2 - c_i^2 - (\bar{c} - c_i)^2}} \end{aligned} \tag{A.1.2}$$

where (a) follows from Lemma 5 and from the fact that all small cells have the same distribution around $\mathcal{P}_0$, and (b) follows from $r_i = r, \forall i$. The expected value of $\bar{C}_i$ can be obtained as:

$$\mathbb{E}[\bar{C}_i] = \int_0^{4r} \bar{c}\, f_{\bar{C}_i}(\bar{c})\, d\bar{c} \tag{A.1.3}$$

where the integral limits follow from C_i and C_{i+1} being independent and from the fact that the maximum summation of both small cells coverages can be $2r_i + 2r_{i+1} = 4r$ when both are maximum $C_i = 2r_i$ and $C_{i+1} = 2r_{i+1}$, and the minimum summation of both small cells coverages can be 0 when both are minimum $C_i = C_{i+1} = 0$ as shown in Lemma 5. Given that the ith and the $(i+1)$th small cells are overlapped on $\mathcal{P}_0$, the distance between $\bar{y}_i$ and $\bar{y}_{i+1}$ is uniformly distributed in the range $[0, \bar{C}_i]$. Therefore, the expectation of one overlap becomes:

$$\mathbb{E}[\mathfrak{C}_i] = \begin{cases} \frac{\mathbb{E}[\bar{C}_i]}{2}, & \| \bar{y}_{i+1} - \bar{y}_i \| < \bar{C}_i \\ 0, & \text{otherwise} \end{cases} \tag{A.1.4}$$

The desired results in Eq. (3.19) is reached after solving Eq. (A.1.3).

A.2 Proof of Lemma 7

Since the overlap between the ith and the $(i+1)$th small cells occurs when the distance between $\bar{y}_i$ and $\bar{y}_{i+1}$ is equal or less than $\bar{C}_i$, the number of overlaps can be expressed as:

$$N_{OL} = \sum_{i=2}^{N_0+1} \mathbf{1}(\| \bar{y}_i - \bar{y}_{i-1} \| \leq \bar{C}_{i-1}) \tag{A.2.1}$$

the expected number of overlaps can be expressed as:

$$\mathbb{E}[N_{OL}] = \mathbb{E}[N_{OL,max}]\mathbb{P}_{OL} \tag{A.2.2}$$

where $\mathbb{P}_{OL}$ is defined as the probability of two consecutive small cells with coverage C_i and C_{i+1} overlapping on $\mathcal{P}_0$ and $\mathbb{E}[N_{OL,max}]$ represents the maximum number of overlaps that can occur on $\mathcal{P}_0$. Given that the number of small cells crossed by $\mathcal{U}_0$ is N_0, the maximum overlaps can take different values, for instance when W_1 is not located in the small cells coverage, the maximum number of overlaps occurring on the path will be N_0-1. However, when W_1 is located in the small cells coverage the maximum number of overlaps that can take place on $\mathcal{P}_0$ is either N_0 when W_1 is located in the coverage of small cell whose SCBS is not located in $\mathscr{A}_m$ as shown in Fig. 3.1, or $N_0 - 1$ when W_0 is located in the small cell whose SCBS belongs to $\mathscr{A}_m$. Therefore the expected maximum number of overlaps that can occur on the path can be expressed as

$$\mathbb{E}[N_{OL,max}] = \mathcal{A}_1\Big(\frac{\bar{\lambda}}{2\sqrt{\lambda_w}} - 1\Big) + \frac{\mathcal{A}_{\bar{K}}}{2}\Big(\frac{\bar{\lambda}}{\sqrt{\lambda_w}} - 1\Big) \tag{A.2.3}$$

Since the locations of the path points follow a PPP, the probability of the overlap occurring is obtained from the null probability as shown:

$$\begin{aligned}\mathbb{P}_{OL} &= 1 - \mathbb{P}\big[\text{No Overlap}\big] \\ &= 1 - \mathbb{P}\big[\parallel \bar{y}_{i+1} - \bar{y}_i \parallel > \int_0^{4r} \bar{c}\, f_{\bar{C}_i}(\bar{c})\, d\bar{c}\big] \\ &= 1 - \exp\big(-\bar{\lambda}\int_0^{4r} \bar{c}\, f_{\bar{C}_i}(\bar{c})\, d\bar{c}\big)\end{aligned} \tag{A.2.4}$$

where $\exp\big(-\bar{\lambda}\int_0^{4r} \bar{c}\, f_{\bar{C}_i}(\bar{c})\, d\bar{c}\big)$ represents the probability of no overlap occurring or the probability that $\bar{y}_{i+1}$ is at a distance greater than $\bar{C}_i$ from $\bar{y}_i$. The desired result in Eq. (3.20) is reached after substituting Eq. (A.2.4) and Eq. (A.2.3) in Eq. (A.2.2).

A.3 Proof of Lemma 8

Given that the ith and the $(i+1)$th small cells overlapped on $\mathcal{P}_0$, the distance between the ith path point and the $(i+1)$th path point is uniformly distributed in the range $[0, \bar{C}_{mn}]$.

Similar to Lemma 6, one overlap becomes:

$$\mathbb{E}[\mathfrak{C}_{mn}] = \begin{cases} \frac{\mathbb{E}[\bar{C}_{mn}]}{2}, & \parallel \bar{z}_{i+1} - \bar{z}_i \parallel < \bar{C}_{mn} \\ 0, & \text{otherwise} \end{cases} \tag{A.3.1}$$

$\mathbb{E}[\bar{C}_{mn}]$ can be obtained from Definition 3 and similar to Lemma 6 as shown:

$$\mathbb{E}[\bar{C}_{mn}] = \int_0^{2r_m+2r_n} \bar{c}\, f_{\bar{C}_{mn}}(\bar{c})\, d\bar{c} \tag{A.3.2}$$

where the integral limits follow from the fact that the maximum and the minimum summations are $2r_m + 2r_n$ and 0 respectively, and $f_{\bar{C}_{mn}}(\bar{c})$ is the PDF of $\bar{C}_{mn}$ and can be obtained as:

$$\begin{aligned} f_{\bar{C}_{mn}}(\bar{c}) &= \int_{-\infty}^{\infty} \Big(\frac{d}{d\bar{c}} \int_0^{\bar{c}-c_m} f_{C_m C_n}(c_m, c_n)\, dc_n \Big) dc_m \\ &= \int_0^{\bar{c}} f_{C_m C_n}(c_m, \bar{c} - c_m) dc_m \\ &\overset{(a)}{=} \int_0^{\bar{c}} \frac{\bar{c} c_m (\bar{c} - c_m)\, dc_m}{16 r_m^2 r_n^2 \sqrt{8 - \frac{c_m^2}{r_m^2} - \frac{(\bar{c}-c_m)^2}{r_n^2}}} \end{aligned} \tag{A.3.3}$$

where (a) follows from C_m and C_n being independent, from the fact that all small cells have the same distribution around $\mathcal{P}_0$, and from the fact that $f_{C_m C_n}(c_m, c_n) = f_{C_m}(c_m) f_{C_n}(c_n)$. Given that the ith small cell is from the mth tier, the probability that the $(i+1)$th small cell is from the nth tier is $\frac{\bar{\lambda}_n}{\lambda_{\bar{K}}}$. After solving Eq. (A.3.3), the desired results in Eq. (3.24) is reached.

A.4 Proof of Lemma 9

Assume that the point $\bar{O}$ is located on $\mathcal{P}_0$ where the received power from both the ith and the $(i+1)$th small cells are equal as shown in Fig. (3.3). Since the cell association among small cells based on the maximum received power, the average received power at $\bar{O}$ can be expressed as:

$$\frac{p_{2,m,rs}\mathscr{L}_2}{\left(\sqrt{\tau_i^2 + \Psi_{m,i}^2}\right)^{\alpha_m}} = \frac{p_{2,n,rs}\mathscr{L}_2}{\left(\sqrt{\tau_{i+1}^2 + \Psi_{n,i+1}^2}\right)^{\alpha_n}} \tag{A.4.1}$$

where $\Psi_{m,i} = \parallel \bar{z}_i - \bar{O} \parallel$ and $\Psi_{n,i+1} = \parallel \bar{z}_{i+1} - \bar{O} \parallel$ represent one side coverage served by the ith small cell and the $(i+1)$th small cell on $\mathcal{P}_0$ respectively. Since the small cells from

different tiers can be located at any distance from $\mathcal{P}_0$ and they have different transmit powers and path-loss exponents, the point $\bar{O}$ can be located either between z_i and z_{i+1}, before z_i or after z_{i+1}. Without loss of generality, assuming that $\tau_i = \tau_{i+1} = 0$, the one side coverage of the ith small cell of the mth tier can be obtained as:

$$\begin{aligned} \Psi_{m,i} &= \left(\frac{p_{2,n,rs}}{p_{2,m,rs}}\right)^{\frac{-1}{\alpha_m}} \Psi_{n,i+1}^{\frac{\alpha_n}{\alpha_m}} \\ \Psi_{m,i} &\overset{(a)}{=} \frac{\left(\frac{p_{2,n,rs}}{p_{2,m,rs}}\right)^{\frac{-1}{\alpha_m}}}{1+\left(\frac{p_{2,n,rs}}{p_{2,m,rs}}\right)^{\frac{-1}{\alpha_m}}} \parallel \bar{z}_i - \bar{z}_{i+1} \parallel \end{aligned} \tag{A.4.2}$$

Note that $\Psi_{m,i} = r_m$ and $\Psi_{n,i+1} = r_n$ when both the ith and the $(i+1)$th do not overlap on $\mathcal{P}_0$. (a) follows from $\parallel \bar{z}_i - \bar{z}_{i+1} \parallel = \Psi_{m,i} + \Psi_{n,i+1}$ and $\alpha_m = \alpha_n$. The ith small cell's footage served by the $(i+1)$th small cell can be obtained as:

$$\begin{aligned} \chi_{n\mapsto m} &= r_m - \Psi_{m,i} \\ &\overset{(b)}{=} r_m - \frac{\left(\frac{p_{2,n,rs}}{p_{2,m,rs}}\right)^{\frac{-1}{\alpha_m}} (r_m + r_n - \mathfrak{C}_{mn})}{1+\left(\frac{p_{2,n,rs}}{p_{2,m,rs}}\right)^{\frac{-1}{\alpha_m}}} \\ &\overset{(c)}{=} \frac{\mathfrak{C}_{mn}\left(\frac{p_{2,n,rs}}{p_{2,m,rs}}\right)^{\frac{-1}{\alpha_m}}}{1+\left(\frac{p_{2,n,rs}}{p_{2,m,rs}}\right)^{\frac{-1}{\alpha_m}}} \end{aligned} \tag{A.4.3}$$

where (b) follows from Eq. (A.4.2) and $\parallel \bar{z}_i - \bar{z}_{i+1} \parallel = r_m + r_n - \mathfrak{C}_{mn}$, and (c) follows from $r_m = r_n\left(\frac{p_{2,n,rs}}{p_{2,m,rs}}\right)^{\frac{-1}{\alpha_m}}$. Given that the ith small cell and the $(i+1)$th small cell overlap on $\mathcal{P}_0$, $\mathfrak{C}_{mn}$ is a random variable and its expectation is obtained in Lemma 8. Therefore the expected value of $\chi_{n\mapsto m}$ can be expressed as in Eq. (3.28).

A.5 Proof of Lemma 10

Given that a small cell of interest is from the mth tier and crossed by $\mathcal{U}_0$. Without loss of generality, assume that the destination waypoint is located at the origin and the distance to the small cell of interest is donated by $\mathfrak{r}_0$. The probability of the destination waypoint served by the reference small cell is a conditional probability and it is expressed as:

$$
\begin{aligned}
\mathbb{P}_{\mathcal{S},m} &= \mathbb{P}\Big[\mathfrak{r}_0 < r_m \mid \rho_0 > \max_{n\in[2,3,\cdots,K]} \rho_{n,0}\Big] \\
&= \mathbb{P}\Big[\mathfrak{r}_0 < \Big(\frac{\rho_{min}}{\mathscr{L}_2 p_{2,m,rs}}\Big)^{-\frac{1}{\alpha_m}}\Big] \prod_{n=2}^{K} \mathbb{P}\Big[\frac{p_{2,m,rs}\mathscr{L}_2}{\mathfrak{r}_0^{\alpha_m}} > \frac{p_{2,n,rs}\mathscr{L}_2}{\mathfrak{r}_{n,0}^{\alpha_n}}\Big] \\
&= \Big(\frac{\pi\Big(\frac{\rho_{min}}{\mathscr{L}_2 p_{2,m,rs}}\Big)^{-\frac{2}{\alpha_m}}}{\mathscr{A}_m}\Big)\Big(\prod_{n=2}^{K} \mathbb{P}\Big[\mathfrak{r}_0 < \Big(\frac{p_{2,m,rs}\mathfrak{r}_{n,0}^{\alpha_n}}{p_{2,n,rs}}\Big)^{\frac{1}{\alpha_m}}\Big]\Big) \\
&= \Big(\frac{\pi\Big(\frac{\rho_{min}}{\mathscr{L}_2 p_{2,m,rs}}\Big)^{-\frac{2}{\alpha_m}}}{\mathscr{A}_m}\Big)\Big(\int_0^\infty \prod_{n=2}^{K} \exp\Big(-\pi\lambda_n\Big(\frac{p_{2,n,rs}}{p_{2,m,rs}}\Big)^{\frac{2}{\alpha_n}} \mathfrak{r}_{n,0}^{\frac{2\alpha_m}{\alpha_n}}\Big) f_{\mathfrak{r}_{n,0}}(\mathfrak{r}_{n,0})\Big)
\end{aligned}
\tag{A.5.1}
$$

where $\mathbb{P}\big[\mathfrak{r}_0 < r_m\big]$ is the probability that the destination waypoint is in the coverage of the small cell of interest, ρ_0 and $\rho_{n,0}$ are the received power from the small cell of interest and the received power from the nearest small cell of the nth tier respectively, $\mathbb{P}\big[\rho_0 > \max_{n\in[2,3,\cdots,K]} \rho_{n,0}\big]$ is the probability that $\mathcal{U}_0$ at the destination waypoint receives the maximum received power from the small cell of interest and $\mathfrak{r}_{n,0}$ is the distance between the nearest small cell of the nth tier to the destination waypoint. Since the locations of both waypoints and SCBSs are uncorrelated and randomly distributed in the network, the variable $\mathfrak{r}_{n,0}$ is assumed to have a Rayleigh distribution with PDF $2\pi\lambda_n\mathfrak{r}_{n,0}e^{-\pi\lambda_n\mathfrak{r}_{n,0}^2}$. Eq. (A.5.1) becomes:

$$
\begin{aligned}
\mathbb{P}_{\mathcal{S},m} &= \Big(\frac{\pi\Big(\frac{\rho_{min}}{\mathscr{L}_2 p_{2,m,rs}}\Big)^{-\frac{2}{\alpha_m}}}{\mathscr{A}_m}\Big)\Big(\int_0^\infty \prod_{n=2}^{K} \exp\Big(-\pi\lambda_n\Big(\frac{p_{2,n,rs}}{p_{2,m,rs}}\Big)^{\frac{2}{\alpha_n}} \mathfrak{r}_{n,0}^{\frac{2\alpha_m}{\alpha_n}}\Big) 2\pi\lambda_n\mathfrak{r}_{n,0}e^{-\pi\lambda_n\mathfrak{r}_{n,0}^2} d\mathfrak{r}_{n,0}\Big) \\
&= \Big(\frac{\pi\Big(\frac{\rho_{min}}{\mathscr{L}_2 p_{2,m,rs}}\Big)^{-\frac{2}{\alpha_m}}}{\mathscr{A}_m}\Big)\Big(2\pi\prod_{n=2}^{K}\lambda_n \int_0^\infty \mathfrak{r}_{n,0} \exp\Big(-\pi\lambda_n\Big(\Big(\frac{p_{2,n,rs}}{p_{2,m,rs}}\Big)^{\frac{2}{\alpha_n}} \mathfrak{r}_{n,0}^{\frac{2\alpha_m}{\alpha_n}} + \mathfrak{r}_{n,0}^2\Big)\Big) d\mathfrak{r}_{n,0}\Big)
\end{aligned}
\tag{A.5.2}
$$

when $\alpha_m = \alpha_n$, $\mathbb{P}_{\mathcal{S},m}$ is obtained after solving Eq. (A.5.2).

A.6 Proof of Lemma 12

The UL average achievable rate of $\mathcal{U}_0$ associated to the kth tier can be derived similar to [31] as:

$$\mathcal{R}_{k,\uparrow} = \frac{\Upsilon_k}{\mathbb{E}[\mathcal{T}_{t,l}]} \int_0^\infty \mathbb{E}_{SINR_{k,\uparrow}}\big[\ln(1+SINR_{k,\uparrow}(x))\big]\, f_{x_k}(x)dx \tag{A.6.1}$$

By using Eq. (2.4), the UL SINR can be expressed as:

$$SINR_{k,\uparrow} = \frac{p_c g_0 \mathscr{L}_k x_k^{\alpha_k(\epsilon-1)}}{\sigma^2 + I_{k,\uparrow}} \tag{A.1}$$

where $I_{k,\uparrow} = \sum_{j\in\Phi_k} (\hat{q}_j^{\alpha_k})^\epsilon p_c h_j \mathscr{L}_k q_j^{-\alpha_k}$ and $\hat{q}_j$ represents the distance between the jth interfering UE and its serving cell. $\mathbb{E}_{SINR_{k,\uparrow}}\big[\ln(1+SINR_{k,\uparrow})\big]$ is obtained as:

$$\begin{aligned}
\mathbb{E}_{SINR_{k,\uparrow}}\big[\ln(1+SINR_{k,\uparrow})\big] &= \int_0^\infty \mathbb{P}\big[\ln(1+SINR_{k,\uparrow}(x_k)) > \iota\big]\, d\iota \\
&= \int_0^\infty \mathbb{P}\Big[\ln\big(g_0 > \frac{x_k^{\alpha_k(1-\epsilon)}(\sigma^2 + I_{k,\uparrow})(\mathrm{e}^\iota - 1)}{\mathscr{L}_k p_c}\big)\Big] d\iota \\
&= \int_0^\infty \exp\Big(\frac{-x_k^{\alpha_k(1-\epsilon)}\sigma^2(\mathrm{e}^\iota - 1)}{p_c \mathscr{L}_k}\Big)\, \mathcal{L}_{I_{k,\uparrow}}\Big(\frac{x_k^{\alpha_k(1-\epsilon)}(\mathrm{e}^\iota - 1)}{p_c \mathscr{L}_k}\Big) d\iota
\end{aligned} \tag{A.6.2}$$

where $\mathcal{L}_{I_{k,\uparrow}}(.)$ is the Laplace transform of the cumulative interference from UEs associated to the kth tier. $\mathcal{L}_{I_{k,\uparrow}}(s) = \mathbb{E}_{I_{k,\uparrow}}\left[\mathrm{e}^{-sI_{k,\uparrow}}\right]$ can be obtained as:

$$\begin{aligned}
\mathscr{L}_{I_{k,\uparrow}}(s) &= \mathbb{E}_{I_{k,\uparrow}}\left[\mathrm{e}^{-sI_{k,\uparrow}}\right] \\
&= \mathbb{E}_{\Phi_k,\hat{q},h}\Big[\exp\big(-s\sum_{j\in\Phi_k} p_c(\hat{q}_j^{\alpha_k})^\epsilon h_j q_j^{-\alpha_k}\big)\Big] \\
&\overset{(a)}{=} \mathbb{E}_{\Phi_k,\hat{q}}\Big[\prod_{j\in\Phi_k} \frac{1}{1+s(\hat{q}_j^{\alpha_k})^\epsilon p_c q_j^{-\alpha_k}}\Big] \\
&\overset{(b)}{=} \exp\Big(-2\pi\lambda_k \int_{x_k}^\infty \big(1 - \mathbb{E}_{\hat{q}}[\frac{1}{1+s(\hat{q}^{\alpha_k})^\epsilon p_c q^{-\alpha_k}}]\big) q\, dq\Big) \\
&\overset{(c)}{=} \exp\Big(-2\pi\lambda_k\, \mathbb{E}_{\hat{q}}\big[\int_{x_k}^\infty \frac{q}{1+G^{-1}q^{\alpha_k}}\, dq\big]\Big) \\
&\overset{(d)}{=} \exp\Big(\frac{-2\pi\lambda_k}{\alpha_k}\, \mathbb{E}_{\hat{q}}\big[G_k^{\frac{2}{\alpha_k}} B\big(\frac{2}{\alpha_k}, 1-\frac{2}{\alpha_k}\big)\big]\Big)
\end{aligned} \tag{A.6.3}$$

where (a) follows from the fact that $h \sim \exp(1)$, (b) follows from the probability generating functional (PGFL) of the PPP [28] and (c) follows from changing the order of the

integration and $G_k = s(\hat{q}^{\alpha_k})^{\epsilon} p_c \mathscr{L}_k$. Since x_k is very small in comparison to the area of the system, the integration limits are assumed to be from 0 to ∞. (d) follows from [76, 3.194.3] after substituting $\partial = q^{\alpha_k}$ and $dq = \frac{q^{1-\alpha_k} d\partial}{\alpha_k}$. Thus, $\mathcal{L}_{I_{k,\uparrow}}(.)$ becomes:

$$\begin{aligned}\mathcal{L}_{I_{2,\uparrow}}(.) &= \exp\Big(\frac{-2\pi\lambda_k x_k^{\alpha_k(1-\epsilon)}(e^{\iota}-1)^{\frac{2}{\alpha_k}}}{\alpha_k} B\big(\frac{2}{\alpha_k}, 1-\frac{2}{\alpha_k}\big)\int_0^{\infty} \hat{q}^{2\epsilon} f_{\hat{q}}(\hat{q})\Big) \\ &= \exp\Big(-\frac{(2\pi\lambda_k)^2 x_k^{\alpha_k(1-\epsilon)}(e^{\iota}-1)^{\frac{2}{\alpha_k}}}{\alpha_k} B\big(\frac{2}{\alpha_k}, 1-\frac{2}{\alpha_k}\big)\int_0^{\infty} \hat{q}^{2\epsilon+1}\exp(-\pi\lambda_k\hat{q}^2)d\hat{q}\Big)\end{aligned} \tag{A.6.4}$$

where $\hat{q}$ is assumed to have a Rayleigh distribution $f_{\hat{q}}(\hat{q}) = 2\pi\lambda_k\hat{q}\mathrm{e}^{-\pi\lambda_k\hat{q}^2}$, the accuracy of this assumption was shown in [34]. After solving Eq. (A.6.4) by using [76, 3.326.2], $\mathcal{R}_{k,\uparrow}$ in (4.10) is reached when $\sigma^2 = 0$.

Bibliography

[1] A. Mahbas, H. Zhu, and J. Wang, "The Effect of Small Cells Overlapping on Mobility Management," *submitted to IEEE Transactions on Wireless Communication*, Apr. 2017.

[2] A. Mahbas, H. Zhu, and J. Wang, "Trio-Connectivity for Efficient Offloading in Future Cellular Systems," *submitted to IEEE Transactions on Vehicular Technology*, Apr. 2017.

[3] A. Mahbas, H. Zhu, and J. Wang, "The Role of Inter-Frequency Measurement in Offloading Traffic to Small Cells," *to appear in IEEE 85th Vehicular Technology Conference: VTC2017-Spring*, Jun. 2017.

[4] A. Mahbas, H. Zhu, and J. Wang, "The Optimum Rate of Inter-Frequency Scan in Inter-Frequency HetNets," *to appear in IEEE International Conference on Communications (ICC'17)*, May 2017.

[5] A. Mahbas, H. Zhu, and J. Wang, "Unsynchronized Small Cells with a Dynamic TDD System in a Two-Tier HetNet," *IEEE 83rd Vehicular Technology Conference: VTC2016-Spring*, pp. 1 – 6, May 2016.

[6] A. Mahbas, "Double Spectrum Small Cell (DSSC) for Discovering Inter-Frequency Small Cell in HetNet," *IEEE International Conference on Communications (ICC'15)*, pp. 3454–3459, Jun. 2015.

[7] J. G. Andrews, S. Buzzi, W. Choi, S. V. Hanly, A. Lozano, A. C. K. Soong, and J. C. Zhang, "What Will 5G Be?," *IEEE Journal on Selected Areas in Communications*, vol. 20, pp. 1056–1082, Jun 2014.

[8] A. Osseiran, F. Boccardi, K. K. Volker Braun, P. Marsch, M. Maternia, O. Queseth, M. Schellmann, H. Schotten, H. Taoka, H. Tullberg, M. A. Uusitalo, B. Timus, and M. Fallgren, "Scenarios for 5G Mobile and Wireless Communications: The Vision of the METIS Project," *IEEE Communications Magazine*, vol. 52, pp. 26 – 35, May 2014.

[9] J. F. Monserrat, G. Mange, V. Braun, H. Tullberg, G. Zimmermann, and Ömer Bulakci, "METIS Research Advances Towards the 5G Mobile and Wireless System Definition," *EURASIP Journal on Wireless Communications and Networking*, pp. 1 – 16, Mar. 2015.

[10] Nokia White paper, "5G Use Cases and Requirements," 2015.

[11] V. Jungnickel, K. Manolakis, W. Zirwas, B. Panzner, V. Braun, M. Lossow, M. Sternad, R. Apelfröjd, and T. Svensson, "The Role of Small Cells, Coordinated Multipoint, and Massive MIMO in 5G," *IEEE Communications Magazine*, vol. 52, pp. 44–51, May 2014.

[12] S. Chen and J. Zhao, "The Requirements, Challenges, and Technologies for 5G of Terrestrial Mobile Telecommunication," *IEEE Communications Magazine*, vol. 52, pp. 36–43, May 2014.

[13] W. H. Chin, Z. Fan, and R. Haines, "Emerging Technologies and Research Challenges for 5G Wireless Networks," *IEEE Communications Magazine*, vol. 21, pp. 106–112, Apr. 2014.

[14] T. S. Rappaport, S. Sun, R. Mayzus, H. Zhao, Y. Azar, K. Wang, G. N. Wong, J. K. Schulz, MathewSamimi, and F. Gutierrez, "Millimeter Wave Mobile Communications for 5G Cellular: It Will Work!," *IEEE Access*, vol. 1, pp. 335–349, 2013.

[15] Z. Pi and F. Khan, "An Introduction to Millimeter-Wave Mobile Broadband Systems," *IEEE Communication Magazine*, vol. 49, pp. 101–107, 2011.

[16] J. G. Andrews, "Seven Ways that HetNets Are a Cellular Paradigm Shift," *IEEE Communications Magazine*, vol. 51, pp. 136 – 144, Mar. 2013.

[17] H. Zhu, "Performance Comparison between Distributed Antenna and Microcellular Systems," *IEEE Journal on Selected Areas in Communications*, vol. 29, pp. 1151 – 1163, Jun. 2011.

[18] H. Zhu and J. Wang, "Radio Resource Allocation in Multiuser Distributed Antenna Systems," *IEEE Journal on Selected Areas in Communications*, vol. 31, pp. 2058 – 2066, Oct. 2013.

[19] A. Damnjanovic, J. Montojo, Y. Wei, T. Ji, T. Luo, M. Vajapeyam, T. Yoo, O. Song, and D. Malladi, "A Survey on 3GPP Heterogeneous Networks," *IEEE Wireless Communications*, vol. 18, pp. 10–21, June 2011.

[20] O. Onireti, A. Imran, M. A. Imran, and R. Tafazolli, "Energy Efficient Inter-Frequency Small Cell Discovery in Heterogeneous Networks," *IEEE Transactions on Vehicular Technology*, vol. 65, pp. 7122 – 7135, Sep. 2016.

[21] X. Lin, R. K. Ganti, P. J. Fleming, , and J. G. Andrews, "Towards Understanding the Fundamentals of Mobility in Cellular Networks," *IEEE Transactions on Wireless Communications*, vol. 12, pp. 1686–1698, Apr. 2013.

[22] S. Singh, H. S. Dhillon, and J. G. Andrews, "Offloading in Heterogeneous Networks: Modeling, Analysis, and Design Insights," *IEEE Transactions on Wireless Communications*, vol. 12, pp. 2484–2497, May 2013.

[23] H.-S. Jo, Y. J. Sang, P. Xia, and J. G. Andrews, "Heterogeneous Cellular Networks with Flexible Cell Association: A Comprehensive Downlink SINR Analysis," *IEEE Transactions on Wireless Communications*, vol. 11, pp. 3484–3495, Oct. 2012.

[24] A. Prasad, O. Tirkkonen, P. Lunden, O. N. Yilmaz, L. Dalsgaard, and C. Wijting, "Energy-Efficient Inter-Frequency Small Cell Discovery Techniques for LTE-Advanced Heterogeneous Network Deployments," *IEEE Communications Magazine*, vol. 51, pp. 72–81, May 2013.

[25] S. Sadr and R. S. Adve, "Handoff Rate and Coverage Analysis in Multi-Tier Heterogeneous Networks," *IEEE Transactions on Wireless Communications*, vol. 14, pp. 2626–2638, May 2015.

[26] A. Merwaday and I. Güvenç, "Handover Count Based Velocity Estimation and Mobility State Detection in Dense HetNets," *IEEE Transactions on Wireless Communications*, vol. 15, pp. 4673–4688, Jul. 2016.

[27] A. Merwaday, I. Güvenç, W. Saad, A. Mehbodniya, and F. Adachi, "Sojourn Time-Based Velocity Estimation in Small Cell Poisson Networks," *IEEE Communication Letters*, vol. 20, pp. 340 – 341, Feb. 2016.

[28] D. Stoyan, W. S. Kendall, and J. Mecke, *Stochastic Geometry and Its Applications*. John Wiley and Sons Ltd., 1995.

[29] M. Haenggi, *Stochastic Geometry for Wireless Networks*. Cambridge University Press, 2012.

[30] H. S. Dhillon, R. K. Ganti, F. Baccelli, and J. G. Andrews, "Modeling and Analysis of K-Tier Downlink Heterogeneous Cellular Networks," *IEEE Journal on Selected Areas in Communications*, vol. 30, pp. 550–560, Apr. 2012.

[31] J. G. Andrews, F. Baccelli, and R. K. Ganti, "A Tractable Approach to Coverage and Rate in Cellular Networks," *IEEE Transactions on Communications*, vol. 59, pp. 3122–3134, Nov. 2011.

[32] P. Madhusudhanan, J. G. Restrepo, Y. Liu, and T. X. Brown, "Analysis of Downlink Connectivity Models in a Heterogeneous Cellular Network via Stochastic Geometry," *IEEE Transactions on Wireless Communications*, vol. 15, pp. 3895–3907, Jun. 2016.

[33] H. Elshaer, M. N. Kulkarni, F. Boccardi, J. G. Andrews, and M. Dohler, "Downlink and Uplink Cell Association With Traditional Macrocells and Millimeter Wave Small Cells," *IEEE Transactions on Wireless Communications*, vol. 15, pp. 6244–6258, Sep. 2016.

[34] T. D. Novlan, H. S. Dhillon, and J. G. Andrews, "Analytical Modeling of Uplink Cellular Networks," *IEEE Transactions on Wireless Communications*, vol. 12, pp. 2669–2679, Jun. 2013.

[35] H. ElSawy and E. Hossain, "On Stochastic Geometry Modeling of Cellular Uplink Transmission With Truncated Channel Inversion Power Control," *IEEE Transactions on Wireless Communications*, vol. 13, pp. 4454–4469, Aug. 2014.

[36] H. Elkotby and M. Vu, "Uplink User-Assisted Relaying in Cellular Networks," *IEEE Transactions on Wireless Communications*, vol. 14, pp. 5468–5483, Oct. 2015.

[37] M. D. Renzo and P. Guan, "Stochastic Geometry Modeling and System-Level Analysis of Uplink Heterogeneous Cellular Networks With Multi-Antenna Base Stations," *IEEE Transactions on Communications*, vol. 64, pp. 2453–2476, Jun. 2016.

[38] F. J. Martin-Vega, G. Gomez, M. C. Aguayo-Torres, and M. D. Renzo, "Analytical Modeling of Interference Aware Power Control for the Uplink of Heterogeneous Cellular Networks," *IEEE Transactions on Wireless Communications*, vol. 15, pp. 6742–6757, Oct. 2016.

[39] W. Bao and B. Liang, "Stochastic Geometric Analysis of User Mobility in Heterogeneous Wireless Networks," *IEEE Journal on Selected Areas in Communications*, vol. 33, pp. 2212 – 2225, Oct. 2015.

[40] H. S. Dhillon, R. K. Ganti, and J. G. Andrews, "Load-Aware Modeling and Analysis of Heterogeneous Cellular Networks," *IEEE Transactions on Wireless Communications*, vol. 12, pp. 1666–1677, Apr. 2013.

[41] Q. Ye, B. Rong, Y. Chen, M. Al-Shalash, C. Caramanis, and J. G. Andrews, "User Association for Load Balancing in Heterogeneous Cellular Networks," *IEEE Transactions on Wireless Communications*, vol. 12, pp. 2706–2716, Jun. 2013.

[42] B. Yu, L. Yang, H. Ishii, and S. Mukherjee, "Dynamic TDD Support in Macrocell-Assisted Small Cell Architecture," *IEEE Journal on Selected Areas in Communications*, vol. 33, pp. 1201–1213, Jun. 2015.

[43] A. H. Sakr and E. Hossain, "Cognitive and Energy Harvesting-Based D2D Communication in Cellular Networks: Stochastic Geometry Modeling and Analysis," *IEEE Transactions on Communications*, vol. 63, pp. 1867–1880, May 2015.

[44] M. Afshang, H. S. Dhillon, and P. H. J. Chong, "Modeling and Performance Analysis of Clustered Device-to-Device Networks," *IEEE Transactions on Wireless Communications*, vol. 15, pp. 4957–4972, Jul. 2016.

[45] K. S. Ali, H. ElSawy, and M.-S. Alouini, "Modeling Cellular Networks With Full-Duplex D2D Communication: A Stochastic Geometry Approach," *IEEE Transactions on Communications*, vol. 64, pp. 4409–4424, Oct. 2016.

[46] H. S. Dhillon, M. Kountouris, and J. G. Andrews, "Downlink MIMO HetNets: Modeling, Ordering Results and Performance Analysis," *IEEE Transactions on Wireless Communications*, vol. 12, pp. 5208–5222, Oct. 2013.

[47] B. Nosrat-Makouei, R. K. Ganti, J. G. Andrews, and R. W. Heath, "MIMO Interference Alignment in Random Access Networks," *IEEE Transactions on Communications*, vol. 61, pp. 5042–5055, Dec. 2013.

[48] Q. Ye, O. Y. Bursalioglu, H. C. Papadopoulos, C. Caramanis, and J. G. Andrews, "User Association and Interference Management in Massive MIMO HetNets," *IEEE Transactions on Communications*, vol. 64, pp. 2049–2065, May 2016.

[49] H. H. Yang, G. Geraci, and T. Q. S. Quek, "Energy-Efficient Design of MIMO Heterogeneous Networks With Wireless Backhaul," *IEEE Transactions on Wireless Communications*, vol. 15, pp. 4914–4927, Jul. 2016.

[50] K. Hosseini, W. Yu, and R. S. Adve, "A Stochastic Analysis of Network MIMO Systems," *IEEE Transactions on Signal Processing*, vol. 46, pp. 4113–4126, Aug. 2016.

[51] M. N. Kulkarni, A. Ghosh, and J. G. Andrews, "A Comparison of MIMO Techniques in Downlink Millimeter Wave Cellular Networks With Hybrid Beamforming," *IEEE Transactions on Communications*, vol. 64, pp. 1952–1967, May 2016.

[52] N. Lee, D. Morales-Jimenez, A. Lozano, and R. W. Heath, "Spectral Efficiency of Dynamic Coordinated Beamforming: A Stochastic Geometry Approach," *IEEE Transactions on Wireless Communications*, vol. 14, pp. 230–241, Jan. 2015.

[53] 3GPP TS 36.331 ver 13.1.0 Release 13, "Technical Specification Group Radio Access Network; Evolved Universal Terrestrial Radio Access (E-UTRA)," 3 2016.

[54] 3GPP TR 36.839 V11.1.0 Release 11, "Mobility Enhancements in Heterogeneous Networks," Sep 2012.

[55] A. Prasad, P. Lunden, O. Tirkkonen, and C. Wijting, "Mobility State Based Flexible Inter-Frequency Small Cell Discovery for Heterogeneous Networks," *2013 IEEE 24th International Symposium on Personal Indoor and Mobile Radio Communications (PIMRC)*, pp. 2057 – 2061, 2013.

[56] S. Jha, M. Gupta, A. Koc, and R. Vannithamby, "On the Impact of Small Cell Discovery Mechanisms on Device Power Consumption over LTE Networks," *2013 First International Black Sea Conference on Communications and Networking (BlackSeaCom)*, pp. 116 – 120, 2013.

[57] R. Mondal, J. Turkka, T. Ristaniemi, and T. Henttonen, "Positioning in Heterogeneous Small Cell Networks using MDT RF Fingerprints," *2013 First International Black Sea Conference on Communications and Networking (BlackSeaCom)*, pp. 127 – 131, 2013.

[58] A. Prasad, P. Lunden, O. Tirkkonen, and C. Wijting, "Enhanced Small Cell Discovery in Heterogeneous Networks Using Optimized RF Fingerprints," *2013 IEEE 24th International Symposium on Personal Indoor and Mobile Radio Communications (PIMRC)*, pp. 2973 – 2977, 2013.

[59] H. Ishii, Y. Kishiyama, and H. Takahashi, "A Novel Architecture for LTE-B : C-plane/U-plane Split and Phantom Cell Concept," *2012 IEEE Globecom Workshops (GC Wkshps)*, pp. 624 – 630, 2012.

[60] A. Mohamed, O. Onireti, M. A. Imran, A. Imran, and R. Tafazolli, "Control-data separation architecture for cellular radio access networks: A survey and outlook," *IEEE Communications Surveys Tutorials*, vol. 18, pp. 446–465, Firstquarter 2016.

[61] H. Song, X. Fang, and L. Yan, "Handover Scheme for 5G C/U Plane Split Heterogeneous Network in High-Speed Railway," *IEEE Transactions on Vehicular Technology*, vol. 63, pp. 4633 – 4646, Nov. 2014.

[62] M.-S. Pan, T.-M. Lin, C.-Y. Chiu, and C.-Y. Wang, "Downlink Traffic Scheduling for LTE-A Small Cell Networks With Dual Connectivity Enhancement," *IEEE Communication Letters*, vol. 20, pp. 796 – 799, Apr. 2016.

[63] S. A. Ahmad and D. Datla, "Distributed Power Allocations in Heterogeneous Networks With Dual Connectivity Using Backhaul State Information," *IEEE Transactions on Wireless Communication*, vol. 14, pp. 4574 – 4581, Aug. 2015.

[64] D. B. Johnson and D. A. Maltz, "Dynamic Source Routing in Ad Hoc Wireless Networks," *Mobile Computing*, pp. 153 – 181, 1996.

[65] C. Bettstetter, H. Hartenstein, and X. Perez-Costa, "Stochastic Properties of the Random Waypoint Mobility Model," *Wireless Networks*, vol. 10, p. 555–567, Sep. 2004.

[66] J. Broch, D. A. Maltz, D. B. Johnson, Y.-C. Hu, and J. Jetcheva, "A Performance Comparison of Multi-Hop Wireless Ad Hoc Network Routing Protocols," *ACM International Conference on Mobile Comput. and Networking*, Oct. 1998.

[67] S. Shin, U. Lee, F. Dressler, and H. Yoon, "Analysis of Cell Sojourn Time in Heterogeneous Networks With Small Cells," *IEEE Communication Letters*, vol. 20, pp. 788 – 791, Apr. 2016.

[68] Y. Hong, X. Xu, M. Tao, J. Li, and T. Svensson, "Cross-tier Handover Analyses in Small Cell Networks: A Stochastic Geometry Approach," *IEEE International Conference on Communication (ICC)*, pp. 3429–3434, Jun. 2015.

[69] J. Wang and A. Yu, "Open-Loop Power Control Error in Cellular CDMA Overlay Systems,," *IEEE Journal on Selected Areas in Communications*, vol. 19, pp. 1246 – 1254, Jul. 2001.

[70] H. Zhu and J. Wang, "Chunk-Based Resource Allocation in OFDMA Systems - Part I: Chunk Allocation," *IEEE Transactions on Communications*, vol. 57, pp. 2734 – 2744, Sep. 2009.

[71] H. Zhu and J. Wang, "Chunk-Based Resource Allocation in OFDMA Systems - Part II: Joint Chunk, Power and Bit Allocation," *IEEE Transactions on Communications*, vol. 60, pp. 499 – 509, Feb. 2012.

[72] I. F. Akyildiz, J. S. M. Ho, and W. Wang, "Mobility Management in Next-Generation Wireless Systems," *Proc. IEEE*, vol. 87, pp. 1347 – 1384, Aug. 1999.

[73] M. M. Zonoozi and P. Dassanayake, "User Mobility Modeling and Characterization of Mobility Patterns," *IEEE Journal on Selected Areas in Communications*, vol. 15, pp. 1239 – 1252, Sep. 1997.

[74] C. Bettstetter, G. Resta, and P. Santi, "The node distribution of the random waypoint mobility model for wireless ad hoc networks," *IEEE Transactions on Mobile Computing*, vol. 2, pp. 257–269, July 2003.

[75] 3GPP TS 36.133 ver 10.6.0 Release 10, "Requirements for Support of Radio Resource Management," 04 2012.

[76] I. Gradshteyn and I. Ryzhik, *Table of Integrals, Series, and Products.* San Diego, USA: ELSEVIER, 2007.

[77] H. Ishii, Y. Kishiyama, and H. Takahashi, "A novel architecture for lte-b," in *Globecom Workshops, 2012 IEEE*, pp. 624–630, 2012.

[78] S. Vasudevan, R. N. Pupala, and K. Sivanesan, "Dynamic eICIC – A Proactive Strategy for Improving Spectral Efficiencies of Heterogeneous LTE Cellular Networks by Leveraging User Mobility and Traffic Dynamics," *IEEE Transactions on Wireless Communications*, vol. 12, pp. 4956–4969, Oct 2013.

[79] K. I. Pedersen, B. Soret, S. B. Sanchez, G. Pocovi, and H. Wang, "Dynamic Enhanced Intercell Interference Coordination for Realistic Networks," *IEEE Transactions on Vehicular Technology*, vol. 65, pp. 5551–5562, Jul. 2016.

[80] D. Lopez-Perez, I. Guvenc, G. D. L. Roche, M. Kountouris, T. Q. S. Quek, and J. Zhang, " Enhanced Intercell Interference Coordination Challenges in Heterogeneous Networks," *IEEE Wireless Communications*, vol. 18, pp. 22–30, Jun. 2011.

[81] 3GPP TS 36.211 ver 13.1.0 Release 13, "Evolved Universal Terrestrial Radio Access (E-UTRA); Physical channels and modulation," 04 2016.

[82] 3GPP TS 36.213 ver 13.0.0 Release 13, "Evolved Universal Terrestrial Radio Access (E-UTRA); Physical layer procedures," 05 2016.

[83] 3GPP TS 36.212 ver 13.1.0 Release 13, "Evolved Universal Terrestrial Radio Access (E-UTRA); Multiplexing and channel coding," 04 2016.

[84] J. Wu, Y. Zhang, M. Zukerman, and E. K. N. Yung, "Energy-efficient base-stations sleep-mode techniques in green cellular networks: A survey," *IEEE Communications Surveys Tutorials*, vol. 17, pp. 803–826, Secondquarter 2015.

[85] Z. Hasan, H. Boostanimehr, and V. K. Bhargava, "Green cellular networks: A survey, some research issues and challenges," *IEEE Communications Surveys Tutorials*, vol. 13, pp. 524–540, Fourth 2011.

[86] Z. Niu, Y. Wu, J. Gong, and Z. Yang, "Cell zooming for cost-efficient green cellular networks," *IEEE Communications Magazine*, vol. 48, pp. 74–79, November 2010.

[87] S. Y. Seidel and H. W. Arnold, "Propagation measurements at 28 ghz to investigate the performance of local multipoint distribution service (lmds)," in *Global Telecommunications Conference, 1995. GLOBECOM '95., IEEE*, vol. 1, pp. 754–757 vol.1, Nov 1995.